KATHOLISCHE UNIVERSITÄT
EICHSTÄTT-INGOLSTADT

From Leaf Traits to Canopy Signatures: A Multiscale and Multisensory Assessment of Ash Dieback in *Fraxinus excelsior* L.

A dissertation presented in partial fulfilment
of the requirements of the degree
Dr. rer. nat.

Faculty of Mathematics and Geography
Catholic University of Eichstätt-Ingolstadt

Lisa Buchner

Eichstätt, 2025

Submission date: 06.08.2025

Date of the oral exam: 17.10.2025

1st examiner: Prof. Dr. Susanne Jochner-Oette

2nd examiner: Prof. Dr. Tobias Heckmann

Abstract

Ash dieback, a disease caused by the fungal pathogen *Hymenoscyphus fraxineus*, is severely threatening the existence of the European common ash (*Fraxinus excelsior* L.). The invasive pathogen leads to progressive symptoms such as leaf loss, shoot dieback, and stem necrosis, often resulting in high mortality in affected forest stands. While these visual symptoms are well documented, finer-scale physiological and morphological leaf responses remain largely unexplored. Ash dieback symptom severity is typically assessed through time-intensive field-based ratings; however, remote sensing technologies such as Unmanned Aerial Vehicles (UAVs) offer new opportunities for large-scale, remote assessment of disease impact. Therefore, this dissertation applies a multiscale and multisensory approach to assess the effects of ash dieback.

The main research questions were:

(1) Does ash dieback, beyond visible symptoms such as leaf loss and shoot dieback, also induce fine-scale morphological and physiological alterations in the leaves of infected ash trees?
(2) Can multisensory UAV data and the thereof calculated vegetation indices detect different degrees of damage caused by ash dieback?
(3) What level of segmentation accuracy is required to ensure reliable estimation of mean vegetation index values for individual ash tree crowns?

Field investigations were carried out at four study sites in 2022 and 2023, combining visual vitality assessments with detailed analyses of leaf physiology and morphology in ash trees affected by ash dieback. The examined leaf traits included chlorophyll fluorescence, chlorophyll content, Specific Leaf Area (SLA), leaf thickness, and Fluctuating Asymmetry (FA), all of which were evaluated in relation to visually assessed damage severity. In addition, at two of the sites, repeated UAV-based aerial surveys were conducted from May to October over two consecutive years to capture the whole vegetation period of the common ash, using RGB, multispectral and thermal sensors. Complementing this, close-range multispectral images of individual tree crowns were acquired in 2023 to provide higher spatial resolution data for detailed crown analysis.

In Publication 1 of this dissertation, physiological and morphological leaf traits were investigated in relation to visually assessed disease severity. Among the measured traits, SLA exhibited the most consistent and significant correlation with increasing damage severity,

highlighting a potential link between leaf morphology and ash dieback. In Publication 2 a novel UAV-based monitoring workflow that utilizes RGB and multispectral imagery is introduced to classify ash dieback severity via vegetation index thresholds. The study demonstrated that both RGB and multispectral indices, particularly the Green-Red Vegetation Index (GRVI) and Difference Vegetation Index (DVI), can effectively distinguish between mildly and severely damaged trees. The combination of both multispectral and RGB indices achieved a combined classification accuracy of 77.2 %. Publication 3 explored the influence of ash tree crown segmentation precision on vegetation index reliability. A newly developed fine segmentation method, based on unsupervised machine learning, successfully excluded non-foliar elements such as ground pixels and canopy gaps, improving spectral data interpretation. Although mean vegetation index values per crown did not differ significantly between coarse and fine segmentation, vegetation index heterogeneity increased with disease severity, emphasizing the added value of detailed crown delineation for detecting subtle stress patterns.

Collectively, these studies contribute a scalable and interdisciplinary framework that bridges leaf-level physiological and morphological measurements with crown-level spectral data and machine learning–based crown segmentation. They further demonstrate how UAV-based remote sensing can be effectively integrated into long-term conservation strategies for *Fraxinus excelsior* L. This work underscores the importance of combining plant physiology, remote sensing, and machine learning to advance forest health monitoring and offers practical insights for the conservation of *Fraxinus excelsior* L. under ongoing disease pressure.

Zusammenfassung

Das Eschentriebsterben, hervorgerufen durch den invasiven Pilz *Hymenoscyphus fraxineus*, bedroht derzeit die Existenz der Gemeinen Europäischen Esche (*Fraxinus excelsior* L.). Der Krankheitserreger führt zu fortschreitenden Symptomen wie Blattverlust, dem Absterben von Trieben und Ästen sowie Stammfußnekrosen, die häufig zu einer hohen Mortalität in betroffenen Populationen führen. Während diese visuell sichtbaren Symptome gut dokumentiert sind, bleiben feinmaßstäbliche physiologische und morphologische Reaktionen der Blätter weitgehend unerforscht. Die Schwere der Krankheitssymptome wird üblicherweise durch zeitaufwendige Feldbeobachtungen eingestuft; Fernerkundungstechnologien wie Drohnen (UAVs) bieten jedoch neue Möglichkeiten für eine flächendeckende, fernerkundliche Erfassung des Krankheitsausmaßes. Diese Dissertation verfolgt daher einen multisensorischen und multiskaligen Ansatz zur Untersuchung der Auswirkungen des Eschentriebsterbens.

Die zentralen Forschungsfragen lauteten:

(1) Verursacht das Eschentriebsterben neben sichtbaren Symptomen wie Blattverlust und Triebsterben auch feinmaßstäbliche morphologische und physiologische Veränderungen in den Blättern infizierter Eschen?
(2) Können multisensorische UAV-Daten und daraus berechnete Vegetationsindizes unterschiedliche Schweregrade der Schädigung durch das Eschentriebsterben detektieren?
(3) Welche Segmentierungsgenauigkeit ist erforderlich, um eine verlässliche Einschätzung mittlerer Vegetationsindexwerte einzelner Eschenkronen zu gewährleisten?

Felduntersuchungen wurden im Jahr 2022 und 2023 an vier Untersuchungsstandorten durchgeführt und kombinierten visuelle Vitalitätsbewertungen mit detaillierten Analysen der Blattphysiologie und -morphologie bei von Eschentriebsterben betroffenen Bäumen. Die untersuchten Blattmerkmale umfassten Chlorophyllfluoreszenz, Chlorophyllgehalt, spezifische Blattfläche (SLA), Blattdicke und Fluktuierende Asymmetrie (FA), welche in Bezug zur visuell erfassten Bonitur gesetzt wurden. Zusätzlich wurden an zwei Untersuchungsgebieten im Zeitraum von Mai bis Oktober über zwei Vegetationsperioden hinweg wiederholte UAV-basierte Befliegungen mit RGB-, multispektralen und thermalen Sensoren durchgeführt. Ergänzend dazu wurden im Jahr 2023 Nahaufnahmen einzelner Eschenkronen mit dem multispektralen UAV-Sensor erstellt, um hochaufgelöste Daten zur detaillierten Kronenanalyse zu erhalten.

Publikation 1 dieser Dissertation untersucht physiologische und morphologische Blattmerkmale in Bezug auf visuell bewertete Krankheitsintensität. Unter den gemessenen Merkmalen zeigte die spezifische Blattfläche die deutlichste und konsistenteste Korrelation mit zunehmender Schwere der Krankheitssymptome, was auf einen möglichen Zusammenhang zwischen Blattmorphologie und dem Eschentriebsterben hinweist. Publikation 2 stellt ein neuartiges, UAV-basiertes Monitoringverfahren vor, das RGB- und multispektrale Bilddaten nutzt, um den Schweregrad des Eschentriebsterbens mittels Schwellenwerten von Vegetationsindizes zu klassifizieren. Die Ergebnisse zeigen, dass sowohl RGB- als auch multispektrale Indizes, insbesondere der Green-Red Vegetation Index (GRVI) und der Difference Vegetation Index (DVI), effektiv zwischen schwach und stark geschädigten Bäumen unterscheiden können. Die Kombination von RGB und multispektralen Indizes erzielte eine Klassifikationsgenauigkeit von 77,2 %. Publikation 3 untersucht den Einfluss der Segmentierungsgenauigkeit von Baumkronen auf die Aussagekraft von Vegetationsindizes. Eine neu entwickelte, auf maschinellen Lernen basierende, Feinsegmentierungsmethode konnte erfolgreich Elemente wie Bodenpixel und Kronenlücken ausschließen und verbesserte dadurch die Interpretation der spektralen Daten. Obwohl sich die durchschnittlichen Vegetationsindexwerte pro Krone zwischen grober und feiner Segmentierung nicht signifikant unterschieden, nahm die Vegetationsindex-Heterogenität mit zunehmender Schädigung durch das Eschentriebserben zu, ein Hinweis auf den Mehrwert detaillierter Kronenabgrenzung zur Erkennung subtiler Stressmuster.

Insgesamt liefern diese Studien ein skalierbares und interdisziplinäres Framework, das physiologische Messungen auf Blattebene mit spektralen Daten auf Kronenebene sowie maschinellem Lernen zur Kronensegmentierung verknüpft. Die Studien zeigen zudem, wie UAV-gestützte Fernerkundung effektiv in langfristige Erhaltungsstrategien für *Fraxinus excelsior* L. integriert werden kann. Diese Arbeit unterstreicht die Relevanz der Kombination von Pflanzenphysiologie und Fernerkundung für die Überwachung der Waldgesundheit und liefert praxisnahe Erkenntnisse für den Schutz von *Fraxinus excelsior* L. unter dem anhaltenden Infektionsdruck.

Contents

List of abbreviations

AWG	Bavarian Office of Forest Genetics
BMEL	German Federal Ministry of Food and Agriculture
BMUV	Federal Ministry for the Environment, Nature Conservation, Nuclear Safety and Consumer Protection
DVI	Difference Vegetation Index
ExG	Excess Green Index
FA	Fluctuating Asymmetry
FNR	Agency for Renewable Resources
GNDVI	Green Normalized Difference Vegetation Index
GRVI	Green-Red Vegetation Index
IoU	Intersection-over-Union
Mavic 2 EA	DJI Mavic 2 Enterprise Advanced
Mavic 3 M	DJI Mavic 3 Multispectral
NDVI	Normalised Difference Vegetation Index
PCA	Principal Component Analysis
RGRI	Red-Green Ratio Index
SAM	Segment Anything Model
SLA	Specific Leaf Area
UAV	Unmanned Aerial Vehicle
WKF	Waldklimafonds

List of figures

List of tables

Individual contributions

This publication-based cumulative PhD thesis is comprised of three scientific articles, included as Chapters 4.1 to 4.3. Each article was submitted to a different peer-reviewed journal. All three publications have been published.

1. **Buchner, L**; Eisen, A-K; Jochner-Oette, S (2024): Effects of ash dieback on leaf physiology and leaf morphology of *Fraxinus excelsior* L. Trees, 38. DOI: 10.1007/s00468-024-02546-1.

   Susanne Jochner-Oette contributed suggestions for the framework of the study. Anna-Katharina Eisen helped with fieldwork on a few days. All co-authors contributed with corrections and proofreading. I did most of the work (**90 %**), including data collection in the field, lab work, statistical analyses and the writing of the manuscript myself.

2. **Buchner, L**; Eisen, A-K; Jochner-Oette, S (2025): Identification of damage severity in *Fraxinus excelsior* L. trees caused by ash dieback using multisensory and multitemporal UAV imagery. Forest Ecology and Management, 585. DOI: 10.1016/j.foreco.2025.122660

   Susanne Jochner-Oette contributed suggestions to the study design, Anna-Katharina Eisen assisted with fieldwork on several days. All co-authors contributed with corrections and proofreading. I did the majority of the work (**90 %**), including data collection and UAV surveys in the field, post-processing of the UAV data, statistical analyses and the writing of the manuscript myself.

3. **Buchner, L**; Eisen, A-K; Jochner-Oette, S (2025): How precise is precise enough? Tree crown segmentation using high resolution close-up multispectral UAV images and its effect on NDVI accuracy in *Fraxinus excelsior* L. trees. Journal of Forestry Research, 36. DOI: 10.1007/s11676-025-01929-5

   The study design was developed by Susanne Jochner-Oette and me. All co-authors contributed with corrections and proofreading. I did the majority of the work (**90 %**), including data collection and UAV surveys in the field, post-processing of the UAV data, development of the machine learning algorithm, statistical analyses and the writing of the manuscript myself.

All articles were written at the Professorship of Physical Geography / Landscape Ecology and Sustainable Ecosystem Development at the Catholic University of Eichstätt-Ingolstadt.

The research presented in this dissertation was conducted as part of the project FraxVir "Detection, characterisation and analyses of the occurrence of viruses and ash dieback in special stands of *Fraxinus excelsior* – a supplementary study to the FraxForFuture demonstration project" and received funding via the Waldklimafonds (WKF) funded by the German Federal Ministry of Food and Agriculture (BMEL) and Federal Ministry for the Environment, Nature Conservation, Nuclear Safety and Consumer Protection (BMUV) administrated by the Agency for Renewable Resources (FNR).

1 Introduction

1.1 Ash dieback

The European common ash (*Fraxinus excelsior* L.) is under critical threat from ash dieback, a disease caused by the invasive fungal pathogen *Hymenoscyphus fraxineus* (T. Kowalski) Baral, Queloz, Hosoya (Baral et al. 2014) (synonyms: *Hymenoscyphus pseudoalbidus* (Gross et al. 2014) and its asexual stage *Chalara fraxinea* (Kowalski 2006)). Initially detected in Poland in the 1990s and likely of East Asian origin (Kowalski 2006, Timmermann et al. 2011, Gross et al. 2014, Enderle et al. 2019), this ascomycete fungus has infected ash populations, affecting the European common ash as well as the narrow-leafed ash (*Fraxinus angustifolia* Vahl) (Kirisits et al. 2010, Nielsen et al. 2017), throughout Europe, causing high mortality rates among the affected trees (Coker et al. 2019).

The disease cycle begins with the production of wind-borne ascospores from fruiting fungal bodies on infected ash leaf litter. These spores infect living ash leaves, initiating the disease (Timmermann et al. 2011). The fungus invades through the leaf petiole, spreading into twigs and shoots. Initial symptoms include necrotic lesions on rachises and leaflets, which progress to wilted shoots and dieback of small branches, leading to increased leaf loss, thinning of the crown and the formation of epicormic shoots (Gross et al. 2014, Timmermann et al. 2017, Fuchs et al. 2024). Over time, necroses can extend into larger branches and even the stem base, compromising structural integrity (Langer 2017). While the development of symptoms and disease severity is influenced by environmental conditions (Klesse et al. 2021), tree age (McKinney et al. 2011), and genetic predisposition (Pliura et al. 2016, Wohlmuth et al. 2018), an infection with ash dieback typically leads to a high mortality rate within a few years after visible symptoms appear (Pautasso et al. 2013).

Fraxinus excelsior L. is a foundational species in many forest ecosystems, especially in floodplain and mixed deciduous forests, where it contributes to canopy structure and habitat complexity. Its loss would have significant ecological consequences, as the species supports a range of associated organisms, including insects, fungi, and lichens that are functionally or obligately linked to ash (Pautasso et al. 2013, Mitchell et al. 2017), potentially leading to the extinction of dependent organisms (Hultberg et al. 2020). Economically, ash wood is valued for its durability and versatility, used in a wide range of applications (Dobrowolska et al. 2011). Beyond ecological and economic impacts, the decline of ash trees in urban and roadside environments also

increases the risk of falling limbs or trees, posing danger to people and infrastructure (Metzler and Herbstritt 2014, Enderle et al. 2017b, Skovsgaard et al. 2017).

In Germany, *Fraxinus excelsior* L. is the sole native ash species and plays a prominent role in both forest and non-forest environments, including riparian forests, urban spaces, and managed woodlands (Langer et al. 2022). According to the Fourth National Forest Inventory (2022), the common ash now covers approximately 201,000 hectares, accounting for 1.8 % of Germany's forest area. Compared to 2012, this represents a loss of around 56,000 hectares, primarily attributed to ash dieback (BMEL 2024). Ash dieback has been documented in all regions in Germany where common ash is present, highlighting the nationwide extent of the disease (Langer et al. 2022, Fuchs et al. 2024). Ash dieback was first identified in Germany in the early 2000s and has since then resulted in extensive damage, including high mortality of the affected trees (Fuchs et al. 2024). Observations from German monitoring plots have shown that mortality and disease severity symptoms are continuously increasing, affecting forest structure and regeneration capacity (Enderle et al. 2017a, Fuchs et al. 2024).

Despite widespread high mortality rates, recent studies across Europe have highlighted the presence of less susceptible individuals within natural ash populations. Although complete resistance has not been observed, certain trees display reduced symptom severity after infection (Stener 2013, Lobo et al. 2015, Adamčíková et al. 2023). These different disease responses are strongly associated with heritable genetic traits (McKinney et al. 2011, McKinney et al. 2014, Enderle et al. 2015). Some genotypes have been proven to present high resistance to the fungal pathogen even under high infection pressure (Seidel et al. 2025). However, such resistant individuals constitute only a small fraction of the ash population (Wohlmuth et al. 2018), potentially less than 1 % (Kjær et al. 2012), underscoring the urgency of active conservation strategies and long-term genetic monitoring.

The long-term prognosis for *Fraxinus excelsior* L. in Europe remains uncertain. Projections indicate that ash populations may decline by 50 – 75 % over the next few decades due to continued spread and persistence of *Hymenoscyphus fraxineus* (Coker et al. 2019). Climate change may influence ash trees and the fungal pathogen in different ways, potentially causing a mismatch in their interactions and thereby possibly reducing the overall impact of the disease (Goberville et al. 2016). Nevertheless, ash tree mortality is expected to remain high, particularly in forests and plantations lacking resistant genotypes. The identification of heritable partial resistance within natural populations presents a potential pathway toward future restoration. Therefore, detailed analyses of physiological and morphological tree responses, combined with

the development of UAV-based monitoring techniques, are essential for assessing local disease impacts and facilitating large-scale population surveillance. Given the pervasive and ongoing nature of ash dieback, scalable, high-resolution approaches are critical for guiding adaptive, continent-wide conservation and forest management strategies.

1.2 Current state of research

The early detection and monitoring of tree health and disease progression are increasingly supported by advancements in remote sensing technologies. Unmanned aerial vehicles (UAVs) equipped with various sensors have emerged as powerful tools in forestry applications, offering non-invasive, high-resolution methods to assess tree vitality over large areas (Torresan et al. 2017, Barbedo 2019).

Vegetation indices, integrating reflectance values from distinct spectral bands, have been widely employed to identify plant stress and early disease symptoms based on spectral reflectance patterns (Huete 2012). RGB-based indices, while limited to visible wavelengths, offer affordable and accessible insights into plant canopy structure, greenness, and stress response, often revealing early signs of disease through subtle changes in colour (Bhandari et al. 2020, Garza et al. 2020). Multispectral and hyperspectral sensors extend this capacity by capturing reflectance data in near-infrared and red-edge bands, allowing for improved classification of disease severity and early physiological decline (Albetis et al. 2017, Dash et al. 2017). Thermal imaging represents another relevant sensor, as it is sensitive to physiological stress responses such as stomatal closure and reduced transpiration, which can result in elevated canopy temperatures (Chaerle et al. 1999, Hashim et al. 2020). Thermal sensors measure surface temperatures, including those of plant canopies, offering a non-invasive means to detect stress often before visible symptoms appear. UAV-mounted thermal sensors have shown promise in capturing early disease signals, prior to the onset of structural damage, by identifying subtle changes in leaf temperature. Although thermal imaging can be more susceptible to environmental interference, thermal sensors have shown potential, that complements spectral data and can enhance early detection frameworks in forest health monitoring (Jafari et al. 2017, Ortiz-Bustos et al. 2017). Combined, these technologies offer a multi-dimensional approach to monitoring plant health in a scalable manner.

In the context of *Fraxinus excelsior* L., remote sensing applications targeting ash dieback remain relatively sparse. However, several recent studies have demonstrated the utility of diverse

remote sensing applications for assessing ash dieback. Hyperspectral imaging has been effectively used to detect crown-level damage in ash trees, as shown by Chan et al. (2021) and Polk et al. (2022), who demonstrated that affected individuals can be distinguished based on subtle spectral reflectance patterns. Similarly, Waser et al. (2014) employed WorldView-2 multispectral data and vegetation indices to classify four distinct levels of crown damage in ash trees. Kampen et al. (2019) used UAV-based multispectral imagery to segment individual ash tree crowns and assess disease severity, highlighting the method's potential for forest-scale monitoring. Aerial laser scanning was applied by Kamińska et al. (2025) to examine ash mortality across extensive forest landscapes, linking structural degradation to spatial tree distribution. At finer spatial resolution, Flynn et al. (2024) also illustrated how within-crown greenness patterns derived from RGB 3D point cloud data can reflect varying degrees of disease impact. Complementing these canopy-level approaches, Bates et al. (2025) introduced a novel synthetic image dataset to train a deep learning model for classifying ash leaf infection stages, achieving robust results on real UAV-acquired video footage. These studies demonstrate that remote sensing-based imaging can differentiate different degrees of crown dieback. Nonetheless, limitations remain in integrating multiple sensor types, achieving satisfactory classification accuracy and translating such approaches into operational workflows for forest managers due to methodological complexity.

For detailed ash tree crown analysis from remote sensing imagery, the segmentation accuracy of the tree crowns from their surroundings is highly relevant. As ash tree crowns get increasingly fragmented with increased disease severity, excluding ground pixels in crown gaps is necessary for accurate tree crown analysis. While no studies in the context of ash dieback focused on detailed crown segmentation, various studies were able to generate fine-scale crown segmentation utilizing a variety of data types (Dalponte et al. 2015, Argamosa et al. 2016, Mohan et al. 2017, Qiu et al. 2020, Lassalle et al. 2022) and delineation methods, spanning from classical approaches like valley following and region growing to advanced machine and deep learning techniques (Ke and Quackenbush 2011, Kestur et al. 2018, Freudenberg et al. 2022).

Complementary to spectral analysis, physiological and morphological traits of leaves offer critical insight into the expression of ash dieback at the individual tree level. Fungal pathogens, such as *Hymenoscyphus fraxineus,* can alter photosynthesis, nutrient uptake, and water transport, often resulting in reductions of photosynthetic performance and physiological and morphological changes (Barón et al. 2012, Kumari and Kumar 2015, Lamalakshmi Devi et al. 2017, Rodrigues et al. 2018). Chlorophyll fluorescence and chlorophyll content have proven to

be effective indicators of plant stress, reflecting photochemical efficiency and pigment content (Murchie and Lawson 2013, Khaled et al. 2018, Arafat et al. 2021). Likewise, morphological traits such as leaf thickness, Specific Leaf Area (SLA), and Fluctuating Asymmetry (FA) are recognized as sensitive proxies for both abiotic and biotic stressors (Palmer and Strobeck 1986, Ahn et al. 2020, McIntire 2023), although FA has shown mixed results depending on species, leaf type, and stressor (Hochwender and Fritz 1999, Klisarić et al. 2014, Ambo-Rappe et al. 2008).

Despite the ecological urgency posed by ash dieback, little is known about how the disease affects leaf-level physiological and morphological responses or whether UAV-based approaches utilizing vegetation indices can reliably scale from individual trees to population-level assessments. Moreover, detailed crown segmentation, an essential step in accurate spectral analysis, has often been addressed through general tree detection models (Ke and Quackenbush 2011), rather than in the context of disease-induced crown structural degradation.

The growing need to monitor ash dieback across broad geographic ranges makes the integration of UAV-derived and automated crown-level analysis increasingly important. Fine-scale physiological and morphological investigations can offer deeper insights into the implication of an infection with ash dieback. An in-depth understanding of how physiological and morphological changes of ash leaves and spectral patterns correlate with disease severity will be crucial for developing operational tools for forest health assessment and management.

1.3 Research gaps and research questions

As Chapter 1.1 demonstrates, ash dieback can induce a wide range of symptoms in *Fraxinus excelsior* L., including crown thinning, epicormic shoot formation, and stem necrosis. While these visible indicators are well-documented, the finer-scale, less apparent consequences of the disease remain comparatively underexplored.

Recent studies have begun to investigate these subtler effects. For instance, Eisen et al. (2024) examined the reproductive ecology of infected trees and found that while pollen viability and seed quality were largely unaffected by ash dieback, flowering rates declined in trees with severe symptoms. Similarly, Semizer-Cuming et al. (2019) reported significantly reduced seed production in heavily damaged female trees. In addition, Przybylski et al. (2025) demonstrated a correlation between earlier bud burst and lower disease severity, highlighting the role of phenology in disease response. These findings suggest that ash dieback influences affected trees in

complex ways that go well beyond externally visible symptoms. However, it remains uncertain whether these observed patterns represent responses to infection or whether they reflect pre-existing traits that influence susceptibility and therefore the severity of the disease.

Despite these advances, there remains a notable gap in understanding how ash dieback affects trees at a functional, leaf-level scale. In particular, fine-scale responses in leaf physiology and morphology, such as changes in photosynthetic efficiency and leaf structure have not been addressed so far. This lack of detailed insight limits our ability to fully understand the mechanisms underlying disease progression and tree decline. This research gap therefore leads to Research question 1:

Research question 1

Does ash dieback, beyond visible symptoms such as leaf loss and shoot dieback, also induce fine-scale morphological and physiological alterations in the leaves of infected ash trees?

This research question seeks to determine whether ash dieback causes subtle yet functionally significant changes in leaf tissue, such as alterations in leaf thickness, specific leaf area, leaf asymmetry or photosynthetic capacity. Understanding these fine-scale changes is essential for comprehensively assessing the relationship between physiological responses and disease progression, and may inform future assessments of tree health, resilience, and breeding priorities.

Research Question 1 focuses on uncovering physiologically and morphologically significant changes in infected leaf tissue. These insights are crucial for understanding the disease's functional impact, but such investigations are time-intensive and resource-demanding. More generally, traditional field-based assessments of ash dieback severity are also laborious and limited in scale, as each tree must be evaluated individually by trained experts. Recent advancements in remote sensing technologies offer promising tools for assessing tree health through multi-sensory imaging and the application of vegetation indices. Nevertheless, only a limited number of studies have explored remote sensing approaches to detect and classify ash dieback symptoms across larger spatial scales. While some studies investigated various sensor types with varying success in characterising ash dieback impact (Waser et al. 2014, Kampen et al. 2019, Chan et al. 2021, Polk et al. 2022, Kamińska et al. 2025), several limitations persist. Many studies focus on high-resolution but less frequently available hyperspectral or airborne laser scanning data, limiting operational scalability. Additionally, usually the suitability of only one sensor type is evaluated. To date, no study has systematically investigated the potential of

thermal data in assessing ash dieback severity. Thermal sensors offer a unique opportunity for disease detection by capturing physiological stress responses (Hashim et al. 2020). While RGB and multispectral data are more commonly used in plant disease detection, no study has yet been conducted to evaluate which sensor type is most effective for assessing ash dieback severity. Vegetation indices are frequently employed in this context; however, their effectiveness can vary significantly depending on the plant species and the specific disease being investigated (Cai et al. 2018, Garza et al. 2020, Ye et al. 2020). As such, identifying the most suitable sensor and vegetation index combination for detecting varying damage severity levels of ash dieback remains an important and unresolved research need. Therefore, this dissertation addresses the following research question:

Research question 2

Can multisensory UAV data and the thereof calculated vegetation indices detect different degrees of damage caused by ash dieback?

This research question aims to identify the most suitable sensor type (RGB, multispectral, or thermal) for detecting ash dieback damage severity across different stages of the vegetation period in *Fraxinus excelsior* L. A key focus is also placed on determining the most effective RGB and/or multispectral vegetation indices for assessing disease severity. In addition, this research questions seeks to define vegetation index thresholds that enable the differentiation between mildly and severely affected ash trees using UAV-derived remote sensing data. Ultimately, the goal is to develop a practical and transferable workflow that can support forest practitioners in efficiently monitoring ash dieback in the field.

Accurate disease detection using UAV-derived vegetation indices relies not only on selecting appropriate sensors and indices but also on the precision of crown-level segmentation. Misclassification or imprecise delineation of individual trees might affect the accuracy of vegetation index values and, in turn, compromise the reliability of disease severity assessments. While a variety of automatic tree crown delineation methods have been developed (Zheng et al. 2025), most focus on outlining the general shape of the crown (e.g. Miraki et al. 2021, Tahar et al. 2021) and often neglect internal structural complexity such as crown gaps. This is particularly problematic in the case of *Fraxinus excelsior* L., where ash dieback frequently results in irregular crown shapes, thinning, and large internal gaps that challenge conventional segmentation approaches. As disease severity progresses, leaf loss intensifies, leading to substantial crown

openings. Inaccurate segmentation may either introduce background elements (e.g., soil or understory) or exclude symptomatic foliage, both of which can distort vegetation index calculations. Yet, to date no study has evaluated how the inclusion of such crown gaps in tree crown segmentation affects the accuracy of mean vegetation index values. This gap in knowledge leads to the following research question:

Research question 3

What level of segmentation accuracy is required to ensure reliable estimation of mean vegetation index values for individual ash tree crowns?

This research question aims to evaluate the impact of crown segmentation accuracy on the calculation of mean vegetation index values by comparing a detailed, newly developed automatic tree crown segmentation method with a coarser segmentation approach. Specifically, it investigates how the inclusion or exclusion of crown gaps influences vegetation index values across varying levels of ash dieback severity. Assessing the relationship between segmentation precision and disease level is critical, particularly given the irregular crown structures. Additionally, this research question addresses how vegetation index variability within individual crowns correlates with disease severity, offering insights into the reliability of mean vegetation index values at different stages of infection.

Building on the insights gained from Research questions 2 and 3, specifically the ability to detect varying levels of ash dieback severity and the importance of accurate crown segmentation, the question remains, how UAV-based remote sensing can be effectively integrated into long-term conservation strategies for *Fraxinus excelsior* L. This involves examining how UAV-based monitoring can be translated into practical forest management applications, including the use of remote sensing data to monitor disease progression and support informed decision-making in conservation planning. A particular focus lies on evaluating the potential of UAV-derived indicators and newly developed analytical workflows for their realistic implementation in the work of forest practitioners. By integrating high-resolution, scalable monitoring tools into long-term strategies, UAV-based remote sensing holds promise as a critical asset in mitigating the ecological impacts of ash dieback on *Fraxinus excelsior* L. populations.

2 Data and methods

2.1 Study sites

Four study sites located in the south of Germany, in the federal states of Baden-Wuerttemberg and Bavaria, were selected for investigation (Figure 1). Two ash seed orchards, the study sites hereafter named Emmendingen and Schorndorf based on their location, are located in the German federal state of Baden-Wuerttemberg, whereas the mixed forest stand Kaisheim and the ash clone area Grabenstätt are located in the federal state of Bavaria. Both ash seed plantations have previously been investigated in the context of ash dieback research, providing well established site-specific knowledge (Enderle et al. 2015, Buchner et al. 2022, Eisen et al. 2022, 2023, 2024).

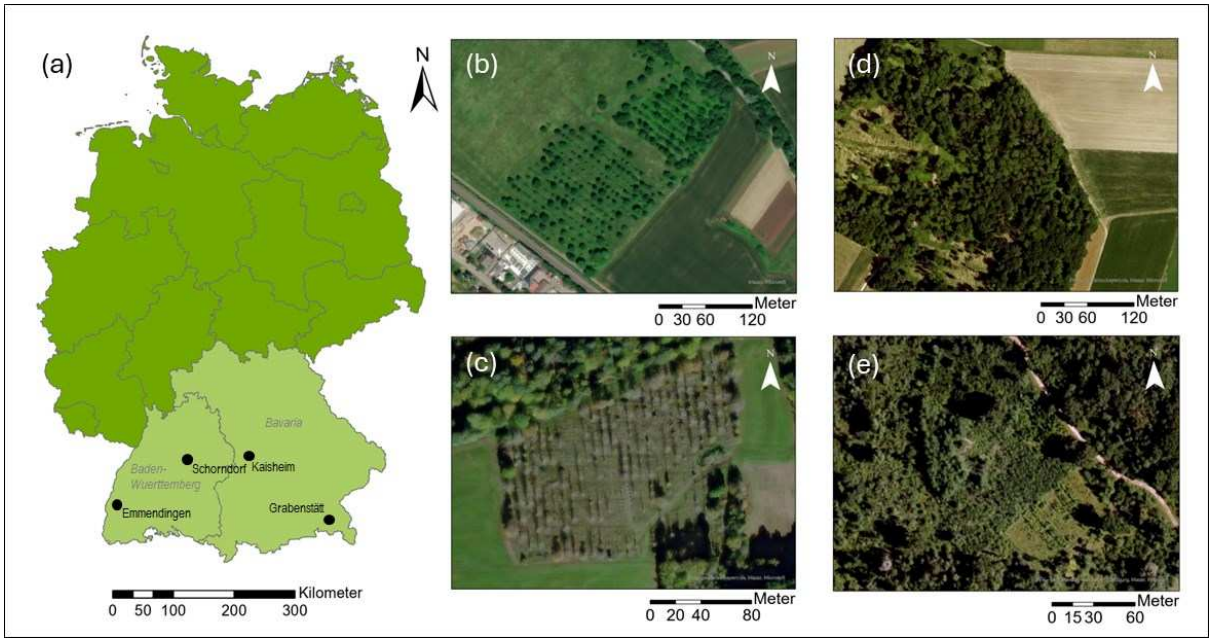

Figure 1: Investigated study sites in Germany (a, dark green): Emmendingen (b) and Schorndorf (c) in the federal state of Baden-Wuerttemberg (a, light green) and Kaisheim (d) and Grabenstätt (e) in the federal state of Bavaria (a, light green). Data source: Esri Base Map, BKG 2025 dl-de/by-2-0

Emmendingen

The Emmendingen ash seed orchard is located approximately 15 kilometres north of the city Freiburg, between the Black Forest foothills and the Kaiserstuhl region in the Upper Rhine Valley (Table 1). Established in 1995 as an afforestation project on former agricultural grassland, the plantation covers an area of 2.7 hectares planted with 228 grafted ash trees

representing 49 genotypes, arranged in a grid spacing of 10 x 10 meters. Despite the absence of formal thinning, the orchard has been heavily impacted by ash dieback, resulting in the removal of 142 trees by 2023. Crown pruning accompanied some of these removals. As of the most recent assessments in July 2023, 86 ash trees remain. The genetic material originates from Southern German hill and mountain regions. The site is surrounded by mixed land uses: a stream forms the northern and eastern borders, agricultural fields lie to the west and east, and residential development marks the southern edge.

Schorndorf

The Schorndorf ash seed orchard is located in the Rems valley near Stuttgart in Baden-Wuerttemberg and covers approximately 2.3 ha (Table 1). Established in 1992 with a 7 × 7 m spacing, the orchard was originally planted in 25 rows with 416 *Fraxinus excelsior* L. trees from 68 clones originating from southern Germany and the Alpine region. Ash trees predominate in the plantation itself, but there are also occasional other tree species such as cherry trees, especially at the edge of the plantation. The site is surrounded by meadows and mixed forest. Due to thinning measures and severe ash dieback, about 70 % of the original trees have been lost. As of 2023, only 119 living mature trees remained, representing 30 genotypes.

Grabenstätt

The clone area Grabenstätt is located near Lake Chiemsee in Bavaria, about 2.5 km south of the mouth of the Tiroler Achen River (Table 1). Located in the Inn-Chiemsee Hill Country of the Alpine foothills, the site covers 0.1 ha and lies within a mixed forest but is enclosed and distinctly separated by a surrounding fence. In 2014, the Bavarian Office of Forest Genetics (AWG) established 319 ramets from 36 visually healthy ash trees from severely infected stands in a randomized block design to account for small-scale site variability and local infection pressure. As of summer 2023, 212 ash trees remained, ranging in height from less than 1 m up to 8 m.

Kaisheim

The Kaisheim study site is located in the Southern Franconian Alb, about 1 km northeast of Sulzdorf (Markt Kaisheim) in the Donau-Ries district of Bavaria (Table 1). The monitoring site covers 1 ha of state forest that has not been thinned and is not subject to public safety interventions. The mixed forest site is dominated by *Fraxinus excelsior* L., *Carpinus betulus* (hornbeam), and *Quercus* spp. (oak). The approximately 80-year-old and up to 30 m tall ash trees are officially approved as seed harvest stock (“Selected Propagation Material”), and about 30 % of

the stand consists of natural regeneration, clearly linked to older trees. In recent years, ash dieback has caused extensive damage.

Table 1: Site specific characteristics, mean temperature and precipitation for the period 1981-2010 (DWD Climate Data Center (CDC), multi-annual grids)

	Coordinates	Site size	Mean temperature	Mean precipation	Soil type	Number of trees in 2023
Emmendingen	48°6′38.50″N, 7°52′20.49″E	2.7 ha	10.6 °C	951 mm	Sandy silt	86
Schorndorf	48°46′35.59″ N, 9°25′31.00″E	2.3 ha	9.7 °C	837 mm	Moderately silty sand	119
Grabenstätt	47°50′28.62″N, 12°30′41.87″E	0.1 ha	8.6 °C	1374 mm	Silty sand	212
Kaisheim	48°48′20.83″N, 10°47′33.34″E	1.0 ha	8.2 °C	838 mm	Silty sand	202

2.2 Field measurements

In the summer months July and August in 2022 and 2023 field measurements were conducted at all four study sites. For each study site 30 individual ash trees were selected, affected in varying degrees by ash dieback, for further analysis.

2.2.1 Vitality assessment

The vitality of *Fraxinus excelsior* L. trees affected by ash dieback was assessed in the field using a standardized scoring system, developed by Peters et al. (2021) for all trees present on the study sites. This assessment was conducted during the late growing season at the end of July/beginning of August in 2022 and 2023. Each tree was individually evaluated based on visible symptoms, including crown condition, the extent of leaf loss, the presence of dead shoots and branches, and additional indicators such as epicormic shoots, insect infestation and stem necrosis. Based on these criteria, trees were assigned to one of six vitality classes (Figure 2), ranging from healthy (class 0) to dead (class 5).

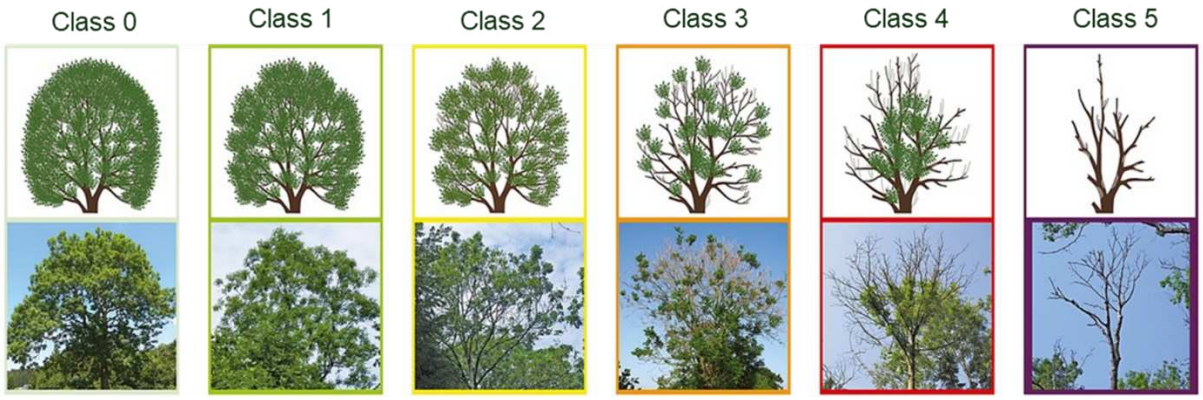

Figure 2: Vitality assessment score (image modified after Peters et al. 2021)

Class 0 represented trees with no visible symptoms typical of ash dieback. Classes 1 and 2 were associated with mild damage: class 1 showed moderate leaf loss (up to 25 %) and slightly reduced crown density, while class 2 displayed more pronounced thinning of the foliage (up to 60 %) and early signs of shoot dieback. Severely affected trees were assigned to classes 3 and 4. Class 3 included individuals with substantial crown thinning (leaf loss up to 75 %) and dead branches visible mainly on the outer parts of the crown. Class 4 represented trees with extreme crown deterioration, with only residual foliage remaining near the trunk and multiple dead large branches. Class 5 was used for completely dead trees with total leaf loss and no green foliage remaining.

Due to the widespread occurrence of ash dieback in Germany (Fuchs et al. 2024), symptom-free trees were absent from all study areas. Consequently, the assessment focused exclusively on trees exhibiting mild to severe damage, while dead trees were excluded from further analysis as they were not relevant to the research objectives.

Figure 3 displays the distribution of vitality classes across all four study sites for the years 2022 and 2023. All trees present on the study sites were considered; however, trees that had already been removed prior to this investigation were not included. While Emmendingen and Grabenstätt still exhibited a high proportion of only mildly damaged trees, Schorndorf and especially Kaisheim showed a markedly higher percentage of trees with severe damage caused by ash dieback. A general decline in tree health is evident at all sites from 2022 to 2023, with Grabenstätt experiencing the most pronounced reduction in trees classified as vitality class 1.

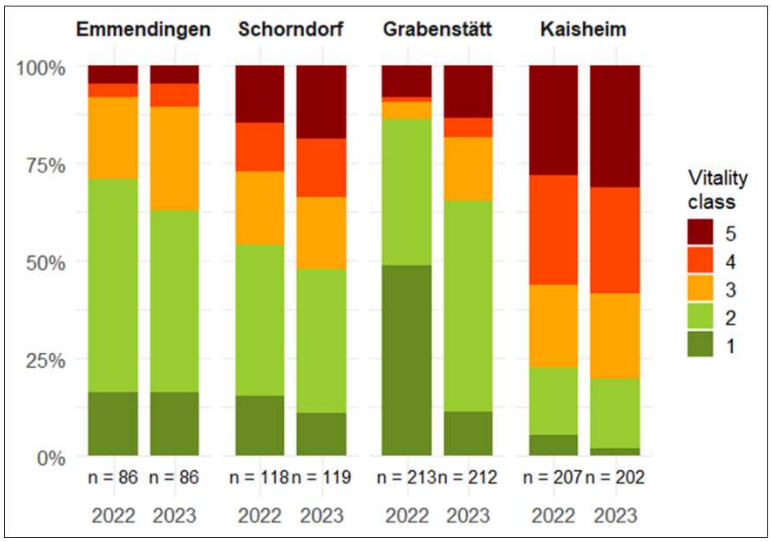

Figure 3: Percentage of the five vitality classes for the existing ash trees on the four study sites for 2022 and 2023.

2.2.2 Leaf physiology

For each of the 30 selected ash trees per study site, chlorophyll content and chlorophyll fluorescence measurements were conducted. Chlorophyll content was assessed using a SPAD-502Plus meter (Konica Minolta, Japan) (Figure 4a), which estimates chlorophyll by measuring red and infrared light transmittance through the leaf (Uddling et al. 2007, Konica Minolta Optics, Inc. 2009). For each individual tree, 30 sun leaves were measured across the crown, and one mean SPAD value per tree was determined.

Chlorophyll fluorescence (F_v/F_m) was measured using the F_v/F_m meter of the Plant Stress Kit (Opti-Sciences, Inc., USA) (Figure 4b). Three sun leaves per tree were selected, each partially covered with a dark-adaptation clip (Figure 4c) for at least 40 minutes before measurement (Mevy et al. 2020). Clips were placed consistently on the second leaflet from the top on the right side of the rachis. The dark-adapted test measures the maximum potential quantum efficiency of photosystem II, assessed under conditions where all reaction centers are fully open (Murchie and Lawson 2013). The F_v/F_m ratio indicates the maximum quantum efficiency of PSII, with values between 0.79 and 0.85 considered typical for healthy plants, while lower values indicate stress (Maxwell and Johnson 2000, Murchie and Lawson 2013).

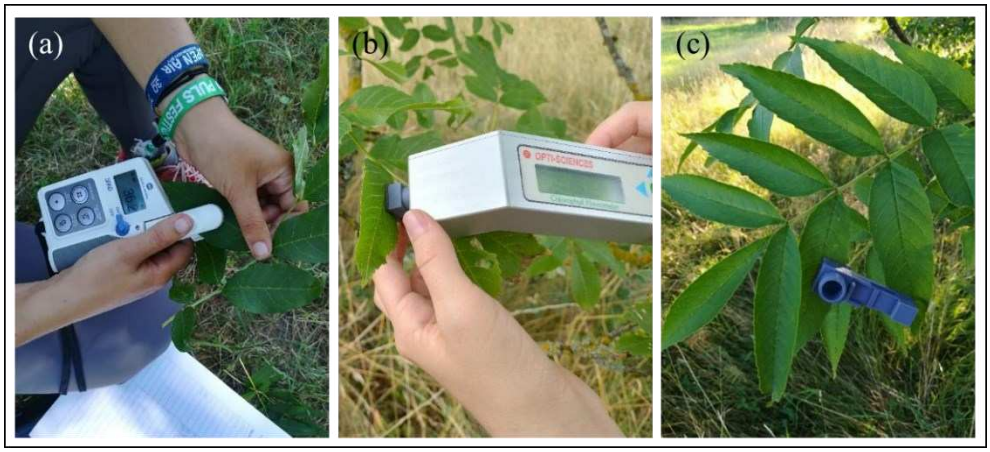

Figure 4: Leaf physiology measurements, (a) SPAD-502Plus meter, (b) F_v/F_m meter, (c) dark adaption of the leaf

2.2.3 Leaf morphology

Up to 20 fully expanded sun leaves were collected from each of the 30 selected ash tree in both 2022 and 2023 to assess SLA. Samples were stored in sealed plastic bags with moist tissue paper and refrigerated until analysis, which took place shortly after sampling. Leaves were scanned at 300 dpi, then dried for 48 hours at 70 °C and weighed. Leaf area was determined using the R package LeafArea (Katabuchi 2015), and SLA was calculated for each leaf based on the following equation. An average SLA value and standard deviation were calculated per tree.

$$SLA = \frac{Leaf\ area\ (cm^2)}{Leaf\ dry\ weight\ (g)}$$

Leaf thickness was measured on the same set of leaves using a digital thickness gauge (Käfer Messuhrenfabrik GmbH & Co. KG, Germany) (Figure 5a). Measurements were taken at a consistent position on each leaf, avoiding the central midvein to ensure consistency and comparability (White and Montes-R 2005). Mean thickness and standard deviation were calculated per tree.

FA was assessed from scanned images of three randomly selected compound leaves per tree (Figure 5b). On each leaf, four opposing leaflets were measured at standardized positions to calculate the difference between left and right sides (Graham 2021). To account for variation in leaf size, asymmetry was expressed as the absolute log-transformed difference ($|\ln R - \ln L|$) (Graham et al. 2003, Palmer and Strobeck 2003). A subset of measurements was repeated to check for consistency, and a principal component analysis (PCA) was used to summarize the

variation across all measured traits. These values were then compared between mildly and severely damaged trees to explore potential differences in FA.

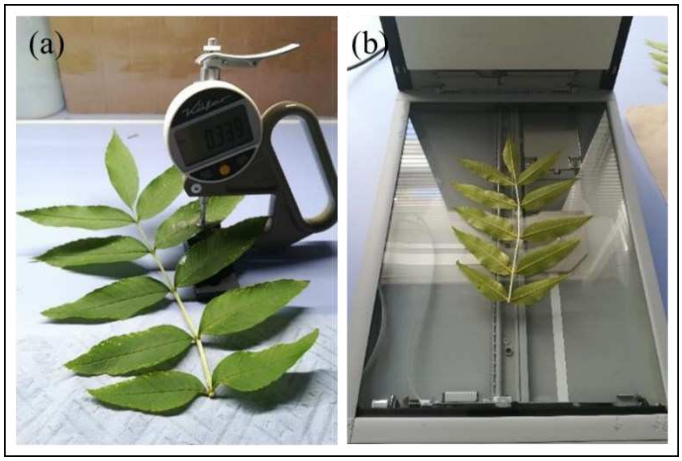

Figure 5: Leaf morphology analysis, (a) digital thickness gauge, (b) scanning of an ash leaf

2.3 UAV data

Due to the presence of isolated trees with minimal crown overlap, UAV surveys were carried out exclusively at the Emmendingen and Schorndorf ash seed orchards. Over the course of the 2022 and 2023 growing seasons (May to October), multiple UAV surveys were carried out using the DJI Mavic 2 Enterprise Advanced (Mavic 2 EA) and DJI Mavic 3 Multispectral (Mavic 3 M) systems, capturing RGB, thermal, and multispectral data. The multispectral sensor captured images in near-infrared (860nm ±26nm), red edge (730nm ±16nm), red (650nm ±16nm), and green (560nm ±16nm) wavelengths. All UAV surveys were taken at a flight height of 80 m with a front and side overlap of 85 %. After post-processing and the generation of orthophotos for each survey, a set of 20 vegetation indices was derived from the RGB and multispectral imagery. Vegetation index thresholding analysis was conducted to determine suitable vegetation index thresholds to estimate the damage severity caused by ash dieback. Furthermore, a mean crown temperature value per tree crown was calculated and set in relation to the damage severity.

Additionally, in June, July, and October 2023, high-resolution close-up UAV images were captured for a selection of 30 tree crowns across both ash seed orchards using the Mavic 3 M. These images were taken from approximately 8 meters above the crowns, allowing for detailed analysis of individual tree crowns (Figure 6). A novel machine learning algorithm was developed to segment only the leaf mass of each crown, excluding surrounding vegetation. Mean

NDVI accuracy was then compared between fine and coarse crown segmentations, and NDVI heterogeneity within individual tree crowns was examined in relation to damage severity.

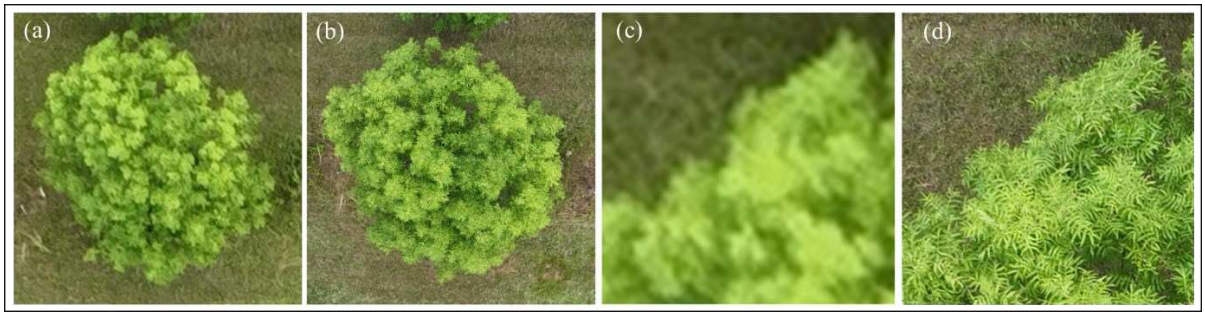

Figure 6: Images of a tree crown at different spatial resolutions: (a) UAV image taken from 80 m flight altitude, (b) close-up image from 8 m above the crown, (c) detailed section of the crown from the UAV survey, (d) detailed section of the crown 8 m above the tree

3 Summary of publications

Publicaton 1: Effects of ash dieback on leaf physiology and leaf morphology of *Fraxinus excelsior* L.

Authors: Lisa Buchner, Anna-Katharina Eisen, Susanne Jochner-Oette
Year: 2024
Journal: Trees: Structure and Function
Publisher: Springer
DOI: 10.1007/s00468-024-02546-1
Status: published

Summary:

This study examined the effects of ash dieback on leaf-level physiological and morphological traits in *Fraxinus excelsior* L. trees and assessed the potential of these traits to serve as indicators of tree vitality. A total of 123 trees with varying levels of ash dieback-related damage were sampled across four sites in southern Germany during the summer months of 2022 and 2023. Five traits were investigated: chlorophyll content, chlorophyll fluorescence (F_v/F_m), SLA, leaf thickness, and FA. Field and laboratory measurements were used to evaluate differences between mildly and severely damaged trees. Among the traits examined, SLA exhibited the clearest and most consistent relationship with damage severity, showing significantly lower values in more severely affected trees. Leaf thickness showed a non-significant trend toward higher values with increasing damage, while chlorophyll content and F_v/F_m were influenced by site-specific and temporal variation. FA did not differ significantly between damage classes. The findings suggest that ash dieback is related to measurable alterations in leaf morphology and physiology, with SLA emerging as a promising trait for assessing tree vitality under disease pressure.

Publication 2: Identification of damage severity in *Fraxinus excelsior* L. trees caused by ash dieback using multisensory and multitemporal UAV imagery

Authors: Lisa Buchner, Anna-Katharina Eisen, Susanne Jochner-Oette
Year: 2025
Journal: Forest Ecology and Management
Publisher: Elsevier
DOI: 10.1016/j.foreco.2025.122660
Status: published

Summary:

This study explored the use of multisensory and multitemporal UAV imagery to classify damage severity in *Fraxinus excelsior* L. trees affected by ash dieback. UAV surveys were conducted across two growing seasons (2022–2023) at two ash seed orchards in southern Germany, using RGB, multispectral, and thermal sensors. Tree vitality was assessed in the field and compared to remotely sensed vegetation indices derived from UAV imagery. A total of 20 vegetation indices were tested for their ability to differentiate between mild and severe damage, and thresholds were developed for each index to classify tree health. Among the tested indices, the multispectral DVI and RGB-based GRVI performed best, achieving classification accuracies of up to 74.9 % and 73.0 %, respectively. Combining RGB and multispectral indices further improved classification accuracy to 77.2 %. Thermal imagery, in contrast, showed limited diagnostic value. The study demonstrates that vegetation indices obtained from UAV surveys can reliably estimate ash dieback severity and presents a practical workflow for forest monitoring and early detection of resilient individuals, supporting conservation and management of declining ash populations.

Publication 3: How precise is precise enough? Tree crown segmentation using high resolution close-up multispectral UAV images and its effect on NDVI accuracy in *Fraxinus excelsior* L. trees

Authors: Lisa Buchner, Anna-Katharina Eisen, Susanne Jochner-Oette
Year: 2025
Journal: Journal of Forestry Research
Publisher: Springer
DOI: 10.1007/s11676-025-01929-5
Status: published

Summary:

This study examined how the precision of tree crown segmentation affects the accuracy of vegetation index measurements in ash trees impacted by ash dieback. Given that advanced disease stages often lead to substantial crown gaps, the inclusion of non-foliar elements like ground pixels can distort vegetation indices. A newly developed unsupervised machine learning algorithm, using a blended NDVI-NIR image, enabled detailed crown segmentation that effectively excluded these gaps. This fine segmentation was compared to a coarser approach using the Segment Anything Model (SAM). Both methods produced similar mean NDVI values per tree crown with no significant differences. However, the fine segmentation revealed greater heterogeneity in NDVI values in severely damaged trees, highlighting its advantage for capturing subtle structural variation. These findings suggest that while coarse segmentation may suffice for general index calculation, fine segmentation offers critical benefits for detailed crown condition assessments.

4 Publications

4.1 Effects of ash dieback on leaf physiology and leaf morphology of *Fraxinus excelsior* L.

Trees
https://doi.org/10.1007/s00468-024-02546-1

ORIGINAL ARTICLE

Effects of ash dieback on leaf physiology and leaf morphology of *Fraxinus excelsior* L.

Lisa Buchner[1] · Anna-Katharina Eisen[1] · Susanne Jochner-Oette[1]

Received: 21 February 2024 / Accepted: 12 July 2024

Abstract

Key message **Ash dieback causes alterations in leaf physiology and morphology, particularly affecting the specific leaf area, which can be used to discriminate between different degrees of damage.**

Abstract Since the introduction of the invasive fungal pathogen *Hymenoscyphus fraxineus* in Europe, the European common ash (*Fraxinus excelsior* L.) has been threatened by ash dieback. An infection leads, for example, to typical symptoms of dying shoots, but changes of leaf physiology and morphology are still largely unexplored. Therefore, five physiological and morphological traits, chlorophyll content, chlorophyll fluorescence, specific leaf area, leaf thickness, and fluctuating asymmetry, were investigated in four different study sites in southern Germany regarding possible changes due to ash dieback and their relationship to different degrees of damage. Both higher and lower levels of chlorophyll with increasing damage due to ash dieback were observed. Chlorophyll fluorescence and fluctuating asymmetry proved to be less suitable indicators of damage. Leaf thickness showed the tendency (however not significant) of an increase in more severely damaged trees. The specific leaf area was identified as a suitable indicator of the damage severity, with significant smaller values in less healthy trees. Therefore, ash dieback can also result in notable alterations in leaf physiology and morphology.

Keywords Chlorophyll content · Chlorophyll fluorescence · Specific leaf area · Fluctuating asymmetry · Leaf thickness

Introduction

Ash dieback has become increasingly widespread in Europe since the first documentation of symptoms caused by the fungal pathogen *Hymenoscyphus fraxineus* (T. Kowalski) Baral, Queloz, Hosoyain (Baral et al. 2014) in the 1990s in Poland (Kowalski 2006; Timmermann et al. 2011) affecting the European common ash (*Fraxinus excelsior* L.) as well as the narrow-leafed ash (*Fraxinus angustifolia* Vahl) (Kirisits et al. 2010; Nielsen et al. 2017). Wind-dispersed ascospores of *Hymenoscyphus fraxineus* primarily infect leaves, further spreading into the woody shoots through the leaf petiole (Gross et al. 2014; Haňáčková et al. 2017; Nielsen et al. 2022). The infection leads to a thinning of ash crowns and often ultimately to the death of the affected trees (Enderle et al. 2019). High mortality rates of up to 70 and 85% in woodland and ash plantations have been observed. Over the next 30 years, ash populations in Europe are expected to decline between 50 and 75% (Coker et al. 2019). However, *Fraxinus excelsior* L. plays an important role in Europe, from both an economic and ecological perspective (Enderle et al. 2019). Numerous species are dependent on ash trees and a decline in *Fraxinus excelsior* L. will have negative effects on other species (Hultberg et al. 2020; Agostinelli et al. 2021). Not all common ash trees react to an infection with *Hymenoscyphus fraxineus* in the same way, and differences in susceptibility to ash dieback have been documented in various studies across Europe (McKinney et al. 2011; Stener 2013; Lobo et al. 2015; Havrdová et al. 2016; Stocks et al. 2017; Wohlmuth et al. 2018; Adamčíková et al. 2023).

Plants often present physiological changes as a result of disease infestation (Berger et al. 2007; Kumari and Kumar 2015; Rodrigues et al. 2018). However, it is yet unknown how the disease progression of ash dieback is manifesting in leaf physiology and morphology of *Fraxinus excelsior* L. Plant stress arises from a deviation from an ideal and

Communicated by Varone.

✉ Lisa Buchner
LBuchner@ku.de

[1] Physical Geography/Landscape Ecology and Sustainable Ecosystem Development, Catholic University of Eichstätt-Ingolstadt, 85072 Eichstätt, Germany

Published online: 27 July 2024

tolerable range of environmental conditions. This includes both biotic (biological origin such as fungal diseases induced by, e.g., *Hymenoscyphus fraxineus* or insects) and abiotic (physical or chemical attributes such as ambient temperature or nutrient availability) factors (Hopkins and Hüner 2009). When a plant experiences stress conditions exceeding its tolerance threshold, it is prone to undergo physiological and morphological alterations (Lamalakshmi Devi et al. 2017). Pathogens have been proven to negatively influence water transport, carbon flow processes, nutrient uptake, plant growth, and lead to a reduction of photosynthetic pigments and a reduced photosynthetic performance within the affected plant (Kumari and Kumar 2015). Photosynthesis, a vital part of a plant's physiology, can be heavily affected after an infection with fungal pathogens, where the degeneration of chloroplasts is coupled with a reduction in photosynthetic rates (Barón et al. 2012).

The loss of photosynthetic pigments leads to a reduced photochemical efficiency of photosystem II (PSII), which can be interpreted as an indicator for plant stress by measuring chlorophyll fluorescence. Chlorophyll fluorescence is sensitive to both biotic and abiotic stress and measures the reemitted light of PSII, assessing the impact of stressors on photosynthetic processes (Murchie and Lawson 2013; Banks 2017). Chlorophyll fluorescence has been found as a suitable indicator among others for waterlogging and salinity stress (Zeng et al. 2013), water stress, high-light stress, and temperature stress (Ibaraki and Murakami 2007) as well as leaf diseases (Duraes et al. 2001). As an important photosynthetic pigment, chlorophyll content can represent the photosynthetic energy efficiency available in the measured plant. There are various methods used to determine chlorophyll content; however, the utilization of SPAD values, representative of the chlorophyll content in the leaves, enables fast real-time measurements (Uddling et al. 2007; Li et al. 2020). SPAD values can also be influenced when a plant experiences stress, e.g., induced by diseases (Zhao et al. 2011; Khaled et al. 2018; Arafat et al. 2021).

Besides, the analysis of leaf morphology is also a suitable tool for identifying possible stress reactions. The specific leaf area (SLA), the ratio of leaf area to leaf dry mass, is commonly used to determine whether plants are experiencing stress (Garnier et al. 2001). It has been reported that SLA can change due to a number of environmental factors such as light and temperature (Awal et al. 2004), radiation (Liu et al. 2022), elevation (Hulshof et al. 2013), heavy metal load (Pleijel et al. 2021), water stress (Chaimala et al. 2023) or salt stress (Said et al. 2022). The thickness of leaves is also reported to be sensitive to stress associated with disease infection (Ahn et al. 2020; España-Guechá et al. 2020; McIntire 2023). Fluctuating asymmetry (FA) focusses on the symmetry of leaves and is characterized as a non-directional deviation from perfect symmetry in a bilateral trait, which is sensitive to stress, mainly from environmental and/or genetic origin (Palmer and Strobeck 1986). Environmental stress, in the context of FA analysis, is a broad term including many factors such as water stress, nutrient limitation, pollutants, extreme climatic conditions, herbivory, and infection (Graham et al. 2010). Various studies focused on the importance of FA as an indicator for the severity of stress such as induced by electromagnetic fields (Freeman et al. 1999), elevation stress in mountain birch (*Betula pubescens*) (Hagen et al. 2008), industrial pollution effects for *Betula pendula* (Turmukhametova et al. 2021), pollution stress in *Robinia pseudoacacia* leaves (Klisarić et al. 2014), and climatic factors (Shadrina et al. 2023). However, FA also often proved to be an unsuitable indicator, e.g., for environmental stress in fragmented habitats in the case of *Quercus deserticola* (García-Jain et al. 2022) or for investigations on the influence of the heavy metals copper and nickel on cucumber (*Cucumis sativus*), sweet pepper (*Capsicum annuum*), and common bean (*Phaseolus vulgaris*) (Gavrikov et al. 2023). In the case of *Salix alba*, neither air pollution, shading, air temperature, humidity nor herbivory had an influence on leaf FA (Wuytack et al. 2011). The informative value of FA as an indicator for environmental stress is, therefore, varying, depending on the investigated environmental factor and the studied plants. For plant diseases, such as ash dieback, caused by a fungal pathogen, very few studies have yet been conducted addressing FA, none in the case of *Fraxinus excelsior* L. Hochwender and Fritz (1999) studied the impact of *Melampsora epitea*, a leaf rust pathogen on FA of *Salix* hybrids. While variations were observed between plants exposed to the pathogen and those protected against leaf rust, these differences did not reach statistical significance.

The leaves of *Fraxinus excelsior* L. are compound leaves and, therefore, add complexity to the analysis of FA, due to the presence of multiple leaflets. Compound leaves are less frequently studied with respect to FA. Various studies focused on different species, each with characteristic leaf shapes such as horse chestnut (*Aesculus hippocastanum*) (Velickovic 2008), soybean (*Glycine max*) (Freeman et al. 1999), *Rhus copallinum* (Freeman et al. 2004), honey locust (*Gleditsia triacanthos*) (Murphy and Lovett-Doust 2004) or parsley (*Petroselinum crispum*) (Rakutko et al. 2017), using different methods in determining FA. No exclusive studies of FA in *Fraxinus excelsior* L. compound leaves, focusing on the impact of ash dieback, have been conducted to date.

This study, therefore, investigates the effects of ash dieback on the physiology and morphology of *Fraxinus excelsior* L. leaves and assesses the suitability of various biomarkers and plant traits, such as chlorophyll content, chlorophyll fluorescence, specific leaf area, leaf thickness, and fluctuating asymmetry, as indicators for the damage severity caused by ash dieback.

Materials and methods

Study sites

This study was conducted at four different study sites, located in the south of Germany in the federal states of Bavaria and Baden-Wuerttemberg (Fig. 1).

The seed plantation, in close proximity to the city Emmendingen (48°6′38.50″N, 7°52′20.49″E, 209 m NHN), located in Baden-Wuerttemberg, was established in 1995 on an area of 2.7 ha. Ash trees were planted with a spacing of 10 m × 10 m. Originally, 228 trees were planted, but due to the extensive damage caused by ash dieback, only 86 ash trees remained on the plantation in the summer of 2023.

Another seed plantation (48° 46′ 35.59″ N, 9° 25′ 31.00″ E, 420 m NHN) is located near the city Schorndorf in Baden-Wuerttemberg. The plantation was established in 1992 in a 7 m × 7 m planting unit and has an area of 2 ha. In 2023, from initially 416 individuals, only 120 living ash trees remained on the plantation. Both ash seed plantations have already been the subject of ash dieback research in other studies (Enderle et al. 2015; Buchner et al. 2022; Eisen et al. 2022, 2023, 2024).

The third study site is a younger plantation densely stocked with ash clones (here referred as clone area) close to Grabenstätt near the lake Chiemsee in Bavaria (47° 50′ 28.62″ N, 12° 30′ 41.87″ E). In 2014, clones of 36 visually healthy trees from heavily infested stands with a total of 319 ramets were established in a randomized block design by the Bavarian Office of Forest Genetics (Fussi 2020). 213 ash trees still existed in the summer of 2023, varying in height from less than 1 m to 8 m.

The mixed forest stand, Kaisheim (48° 48′ 20.83″ N, 10° 47′ 33.34″ E), is located about 1 km northeast of Sulzdorf in Bavaria. The approx. 80 years old and 30 m tall ash trees are approved as seed harvest stock ("Selected Propagation Material"). The stand is part of the intensive monitoring plots of the project FraxForFuture (Langer et al. 2022). Especially in the last 4 years, ash dieback has caused severe damage.

Assessment of vitality

For each study site, 30 ash trees with various degrees of damage due to ash dieback were selected (exception: 33 in Kaisheim 2022) resulting in 123 studied trees in total. We assessed their vitality in the field, using the vitality scoring system developed by Peters et al. (2021). Vitality was assessed in the months July and August of 2022 and 2023 by taking the condition of the crown and overall leaf loss into consideration. The trees were divided into six categories, ranging from class 0 (no damage) to class five (dead). Only trees in class 0 can be classified as healthy, without typical ash dieback symptoms. Classes 1 and 2 are linked to mild damage symptoms (reduced foliage in class 1 and 2, few young dead shouts in class 2). Classes 3 and 4, with different degrees of advanced leaf loss, increased thinning of the crown, and multiple dead branches, represent severe damage due to ash dieback.

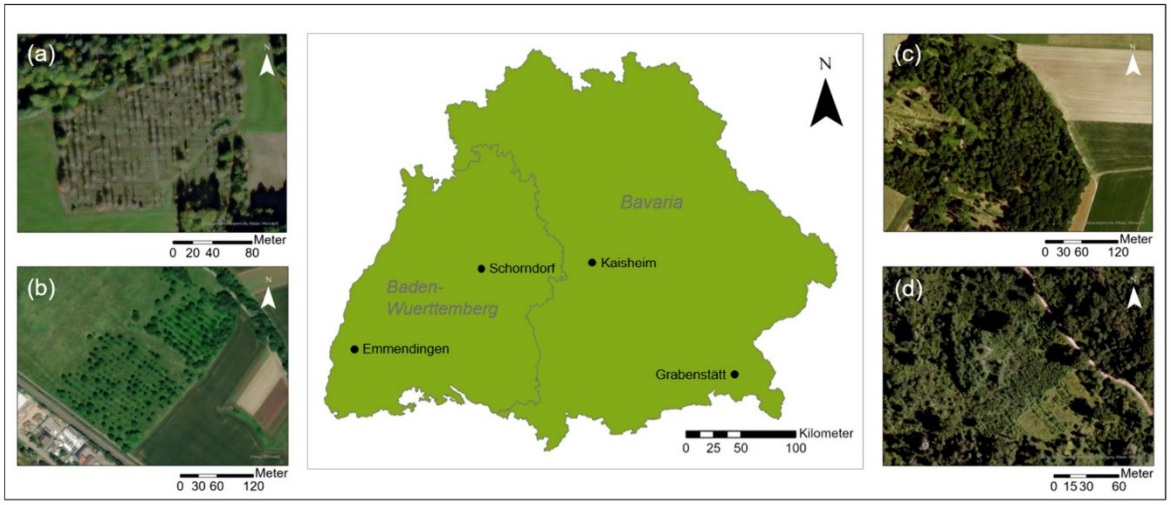

Fig. 1 Location of the four study sites in the German federal states Baden-Wuerttemberg and Bavaria; **a** seed plantation Schorndorf, **b** seed plantation Emmendingen, **c** forest site Kaisheim, **d** clone area Grabenstätt (Map Source: ESRI Data and Maps)

Chlorophyll content and chlorophyll fluorescence

Measurements of chlorophyll content and chlorophyll fluorescence were conducted in the field in the period of end of July until the beginning of August in 2022 and 2023. The chlorophyll content was determined using the SPAD-502Plus (Konica Minolta Optics, Inc., Japan). Recorded SPAD values correspond to the chlorophyll present in the leaf by measuring the transmittance of red and infrared radiation through the leaf (Uddling et al. 2007, Konica Minolta Optics, Inc. 2009). For each of the selected 30 trees per study site, measurements of 30 leaves were taken from various sun leaves throughout the tree crown. An average value was calculated to generate one SPAD value per tree. In addition, the standard deviation was assessed to infer on the variability of SPAD values from one tree.

Furthermore, chlorophyll fluorescence was investigated using the F_v/F_m meter, which is part of the Plant Stress Kit (Opti-Sciences, Inc., USA). The F_v/F_m meter uses dark adaptation clips for reliable measurements. The dark-adapted test is a measurement ratio indicative of the maximal potential quantum efficiency of PSII under the condition wherein all reaction centers are simultaneously in an open state (Murchie and Lawson 2013). Three clips were attached to each tree on three different leaves (Mevy et al. 2020), each time on the same position of the leaf, on the second leaflet from the top on the right side of the rachis. The leaves were then dark adapted for at least 40 min, until the chlorophyll fluorescence measurements were taken. Since the F_v/F_m ratio can differ between sun and shade leaves (Lichtenthaler and Babani 2004), attention was paid to exclusively select sun leaves. Healthy plants should exhibit F_v/F_m values in the range of 0.79 and 0.85 and lower values are indicative of plant stress (Maxwell and Johnson 2000). The standard deviation was calculated for each tree to infer on the variability of F_v/F_m measurements. Due to organizational and technical reasons, SPAD measurements for Kaisheim were only available in 2023, and no chlorophyll fluorescence measurements were possible in both years.

Specific leaf area

For SLA, up to 20 fully expanded leaves from the light crown of the selected 123 trees were sampled and processed to calculate an average SLA value per tree for both 2022 and 2023. The standard deviation was assessed to infer on the variability of SLA values from the individual trees. Leaves with obvious damage caused by insects were avoided (Cornelissen et al. 2003). The sampled leaves were placed on moist tissue paper within sealed plastic bags and refrigerated. To prevent desiccation or decay of the leaves, the SLA analysis was performed in the laboratory in the days immediately following sampling. Since the rachis of compound leaves is considered part of standardized SLA analysis (Cornelissen et al. 2003), the leaflets were not treated separately. Each sampled leaf was scanned in color with 300 dpi resolution using a scanner (CanoScan Lide 200, Canon Deutschland GmbH, Germany). Due to the size of the scanner and the sampling method in the field, the petiole of each leaf was cut below the last set of leaflets to ensure comparability. Subsequently, the leaves were dried for 48 h at 70 °C in an oven and the weight of each leaf was determined. The area of the leaves was then specified using the scanned image and the R package LeafArea (Katabuchi 2015) in R Studio (version 2021.09.0). This package implements the software ImageJ (version 1.53) and transforms the scanned color image into a black and white image. In the next steps, the area of the black leaf can be determined, and the SLA is calculated using the formula:

$$SLA = \frac{Leaf\ area\ (cm^2)}{Leaf\ dry\ weight\ (g)}$$

Leaf thickness

Leaf thickness was measured on the same leaves analyzed for SLA, using a digital thickness gauge (Käfer Messuhrenfabrik GmbH & Co. KG, Germany). Every measurement was taken on the same position on the leaf, i.e., on the second leaflet from the top on the right side of the rachis. Close attention was paid to avoid the dense tissue of the leaflet midvein (White and Montes-R 2005). For each tree, we calculated the standard deviation and the average leaf thickness value out of the measurements of the 20 individual leaves.

Statistical analysis

Leaf physiological and morphological data were tested for statistically significant differences between the vitality classes using a *t* test or Mann–Whitney *U* test depending on the condition of a normal distribution, which was tested using the Shapiro–Wilk test. Homogeneous variances were tested using the Levene's test. For correlation analyses, we calculated the Spearman correlation coefficient and associated *p* values.

All statistical analyses were carried out using the software R Studio (version 2021.09.0).

Fluctuating asymmetry

The workflow for the determination of FA also builds on the images of the scanned leaves. For each tree, three scanned leaves were randomly selected (number of investigated leaves in total: 729). Since the leaves of *Fraxinus excelsior* L. are compound leaves, four leaflets per leaf were measured

and examined. These leaflets were the two youngest mature leaflets on both sides of the rachis. The software ImageJ (version 1.53) was used for the 12 measurements per leaf displayed in Fig. 2.

FA in general is calculated as the difference between the right (R) and left (L) side of the object under investigation (Palmer and Strobeck 1986; Graham 2021). The differences between these sides often are very small and the results of FA can be heavily affected by measurement error (Kozlov 2015; Kozlov et al. 2017); thus, the effect of measurement error has to be tested. A randomly chosen subset containing 5% of the 8,748 original individual lengths was measured a second time by a different researcher. The two series of measurements were then statistically compared to each other using a *t* test. It is necessary to discriminate FA from other forms of asymmetry (Palmer and Strobeck 2003). Besides FA, there are two other forms of asymmetry whose possible presence must be tested: antisymmetry and directional asymmetry. FA exists when the variances between R and L adhere to a normal distribution centered around zero. Directional asymmetry occurs when these R − L differences exhibit a normal distribution, yet with a mean value significantly deviating from zero. Antisymmetry is identified by a platykurtic or bimodal distribution of R − L differences, converging around a mean value of zero, indicating that a left- or right-biased asymmetry exists (Palmer and Strobeck 1986; Palmer 1994; Klingenberg 2015; Maldonado-López et al. 2019). To determine the possible presence of directional asymmetry, a two-tailed *t* test against a mean of zero was applied (Mabrouk et al. 2020). Antisymmetry was evaluated using the Kolmogorov–Smirnov test, which tests for deviation from normality, a requirement for FA (Ambo-Rappe et al. 2008; Mabrouk et al. 2020).

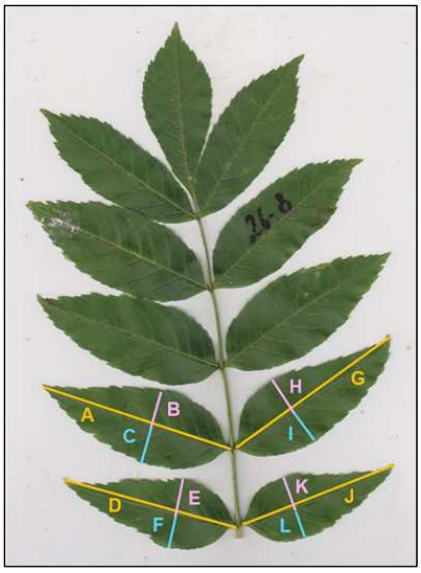

Fig. 2 Measurements made on each leaf; for each leaflet, the right and left side was measured from the main vein at the widest point of the leaflet. The length of each leaflet was measured from the tip of the leaflet to the rachis of the leaf, independent of the main vain. A–L denote the different measured lengths

Since larger leaves have had more time to develop more distinct FA than smaller leaves, the effect of size dependency was addressed. The traditional way of addressing size dependency is dividing R − L by (R + L)/2 or R + L. Even if R and L are lognormally distributed, a log-transformation is a more elegant approach, since log R − log L is normally distributed. This method is especially suitable if the measurement error is small (Graham et al. 2003; Graham 2021). The transformation can be performed either using natural or base 10 logarithms (Palmer and Strobeck 2003). In this study, the absolute values of the right and left side were used for |lnR − lnL|, according to the trait calculations in Table 1.

While it is possible to simply averaging the deviations of multiple traits from symmetry after a log-transformation (Palmer and Strobeck 2003) or using a median leaflet as a representation of the entire leaf (Boeger et al. 2018), more precise methods exist. Leung et al. (2000) developed

Table 1 Leaf traits and calculations for asymmetry and the trait level (leaf or leaflet level) based on |R−L|, measured parameters shown in Fig. 2

Trait level	Trait	Asymmetry
Asymmetry of the individual leaflets, ratio between the right and left side of the main vein for four individual leaflets	Lateral leaflet width (LLW)	B–C
		H–I
		E–F
		K–L
Asymmetry of the leaf, ratio between the right and left top side of the leaf of two pairs of leaflets	Lateral leaflet top (LLT)	E–K
		B–H
Asymmetry of the leaf, ratio between the right and left bottom side of the leaf of two pairs of leaflets	Lateral leaflet bottom (LLB)	F–L
		C–I
Asymmetry of the leaf, ratio between the right and left length of the leaflet of two pairs of leaflets	Lateral leaflet length (LLL)	A–G
		F–J

multiple Composite Fluctuating Asymmetry Indices, each taking into account multiple measured traits. In this study, however, individual traits might be dependent on each other and, thus, contain the same informative value. Therefore, a principal component analysis (PCA) was conducted to reduce the number of individual dependent values, resulting in a more compact dataset with fewer independent variables, while retaining the most significant variance present in the data. This approach highlights similarities and differences between leaf trait measurements by transforming the original variables into a new set of uncorrelated variables, known as principal components (PC) (Greenacre et al. 2022). The reduced dataset was then set in relation to the vitality assessment (mild or severe damage) of the individual ash trees. Two-factor ANOVA and MANOVA analyses were used to test whether trees with more severe damage due to ash dieback exhibit a significantly different FA compared to the trees with only mild damage. The application of the PCA and the further statistical analyses were carried out using the software R Studio (version 2021.09.0).

Results

Vitality assessment of ash trees

The vitality assessment showed a differentiated picture with regard to the distribution of the damage classes (Fig. 3), as the severity of the damage due to ash dieback varied for the four study sites. Especially the site Kaisheim was generally heavily affected with a large number of severely damaged trees. While for Emmendingen, Schorndorf, and Grabenstätt, the same trees were selected in both years, in Kaisheim, several trees had to be removed in 2023 due to the extensive damage of ash dieback and alternative trees were selected. A direct comparison of both years is, therefore, not possible for Kaisheim. Schorndorf and Grabenstätt showed a decline of trees sorted into class 1 from 2022 to 2023, indicating a decrease in only mildly affected trees in accordance with an increase of more severely affected trees. However, trees can also partially recover from one year to the next. In Emmendingen in 2023, less trees were grouped to class 3 than in the previous year. For all four study sites, no healthy trees (class 0) could be observed in both 2022 and 2023.

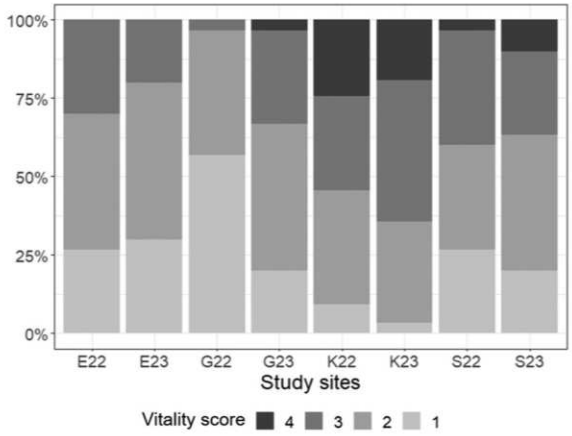

Fig. 3 Vitality scores of the selected ashes in the four study sites Emmendingen (E), Grabenstätt (G), Kaisheim (K), and Schorndorf (S) in 2022 and 2023. A vitality score of 1 and 2 accounts for mild damage due to ash dieback and vitality scores of 3 and 4 for severe damage. Note that the trees in Kaisheim were not all identical in 2022 and 2023 and 33 trees were selected in 2022

Chlorophyll fluorescence and chlorophyll content of ash leaves

The results of the F_v/F_m meter measurements displayed in Fig. 4 present the distribution of the F_v/F_m values for each study site for mildly and severely damaged trees by ash dieback. F_v/F_m values < 0.79 indicate stress; however, trees affected more severely by ash dieback demonstrated not always lower F_v/F_m values than mildly damaged trees. There were no significant differences in F_v/F_m values between the classes mild and severe damage for any of the study sites. The standard deviation of F_v/F_m values per tree ranged from a minimum of < 0.001 to a maximum of 0.11 with a mean standard deviation for all measured trees of 0.02.

Only for Emmendingen 2022 and Schorndorf 2023, the percentage of stressed trees was higher for the more severely affected than mildly damaged ashes (Table 2). However, this was not the case for Emmendingen 2023, Schorndorf 2022, and for both years in Grabenstätt. For the study site Grabenstätt, the results differed greatly from the other two study sites with very high numbers of stressed trees, independent of their vitality status. Especially in 2023, all trees were linked to very low F_v/F_m values, and no unstressed trees could be detected.

For the two plantation sites Emmendingen and Schorndorf, SPAD values tended to be lower with severely affected trees. This, however, did not apply to the ash trees in Grabenstätt. Here, SPAD values in 2023 were slightly but non-significantly higher for severely damaged trees. Only for Emmendingen in 2023 (t test, p value = 0.005) and Schorndorf 2022 (Mann–Whitney U test, p value = 0.021) (Fig. 5), the differences for mildly and severely damaged ash trees were statistically significant. Overall SPAD values also differed between the different study sites: higher values were recorded for Emmendingen, Grabenstätt, and Kaisheim, whereas the trees displayed an on average lower chlorophyll content in Schorndorf. Note that the standard deviation of

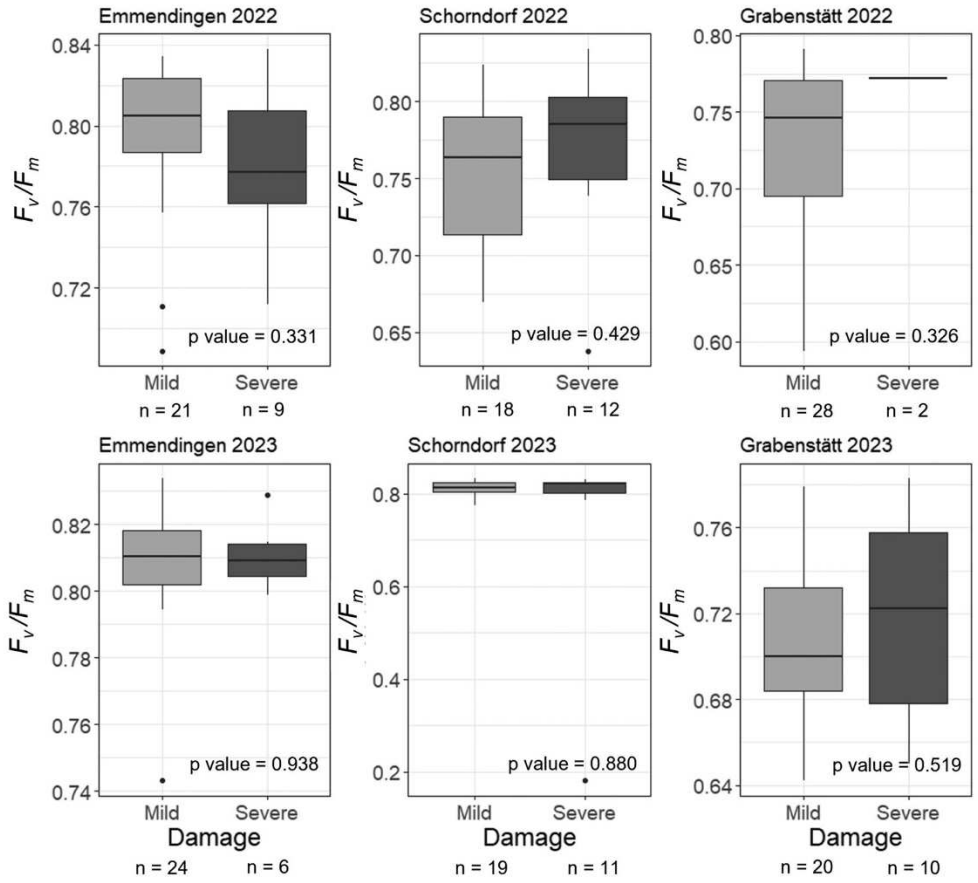

Fig. 4 Boxplots of F_v/F_m values differentiated for mildly and severely affected ash trees for three study sites in 2022 and 2023. Interquartile range (IQR) represented by height of boxes, median by bold horizontal lines, upper (lower) whiskers indicate minimum of maximum (minimum) of metric and 1.5 times IQR, dots represent observations exceeding or falling below 1.5 times IQR. A different y-axis was applied for each plot

Table 2 Percentage of stressed trees (low F_v/F_m values < 0.79 indicate stress, high F_v/F_m values from 0.79 to 0.85 indicate no stress) in mildly and severely damaged ash trees for the three study sites in 2022 and 2023

	Mild damage		Severe damage	
	Number of trees (*n*)	Percentage of stressed trees	Number of trees (*n*)	Percentage of stressed trees
Emmendingen 2022	21	28.6%	9	55.6%
Emmendingen 2023	24	20.8%	6	16.7%
Schorndorf 2022	18	66.7%	12	58.3%
Schorndorf 2023	19	10.5%	8	37.5%
Grabenstätt 2022	28	85.7%	2	100.0%
Grabenstätt 2023	20	100.0%	10	100.0%

the 30 SPAD measurements per tree ranged from a minimum of 0.90 to a maximum of 5.28, with a mean standard deviation for all measured trees of 2.27 pointing to a reasonable sample size.

Specific leaf area

The standard deviation of the SLA measurements ranged from a minimum of 3.0 to a maximum of 81.6, with a mean standard deviation for all measured trees of 15.5, demonstrating an overall suitable sample size, while also

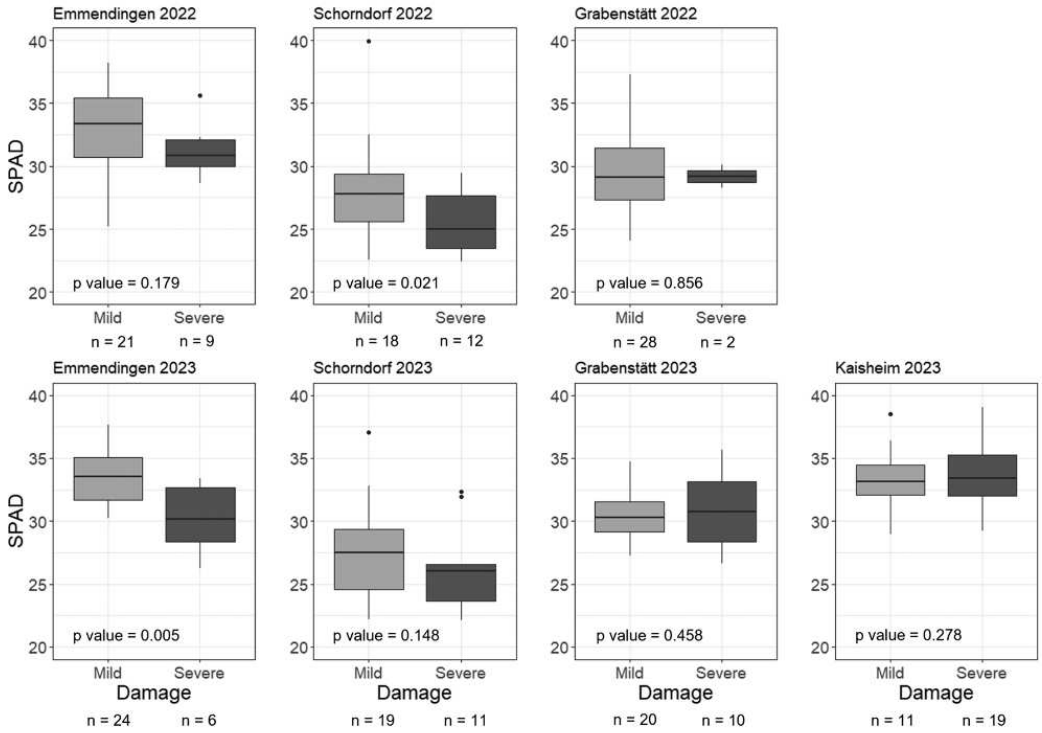

Fig. 5 Boxplots of chlorophyll content (SPAD) differentiated for mildly and severely affected ash trees for four study sites in 2022 and 2023. Interquartile range (IQR) represented by height of boxes, median by bold horizontal lines, upper (lower) whiskers indicate minimum of maximum (minimum) of metric and 1.5 times IQR, dots represent observations exceeding or falling below 1.5 times IQR

representing the variability of the SLA of leaves within individual trees. In general, smaller SLA for severely affected ash trees were observed for all study sites for both investigated years. The difference in SLA was significant for Schorndorf in 2022 and for Schorndorf and Kaisheim in 2023, though Emmendingen and Kaisheim in 2022 were marginally significant (Fig. 6).

Leaf thickness

Leaf thickness tended to be slightly higher in more severely damaged trees. However, the difference was only statistically significant for Schorndorf in 2022 (p value = 0.043) and Kaisheim 2023 (p value = 0.022). While the mean leaf thickness was similar across years, there were differences between the four areas. Leaf thickness was slightly higher in Schorndorf and Kaisheim, whereas ashes from Grabenstätt had overall thinner leaves (Fig. 7). The standard deviation of the 20 leaf thickness measurements per tree ranged from a minimum of 0.01 cm to a maximum of 0.12 cm, with a mean standard deviation for all measured trees of 0.04 cm; thus, many leaves are rather uniform in thickness, but some also exhibit a different pattern.

Correlations of leaf traits

Leaf thickness correlated significantly (Table 3) with SLA, demonstrating that leaves with a lower SLA are related to thicker leaves than leaves with a high SLA. A significant negative correlation between SLA and chlorophyll content is shown in Table 3: trees with a smaller SLA were linked to a higher chlorophyll value. High F_v/F_m values, indicative of a non-stressed plant, corresponded to both thicker leaves and leaves with a high SLA. No significant correlations between chlorophyll content and leaf thickness or F_v/F_m were found.

Fluctuating asymmetry

Related to the analysis of FA, the paired t test conducted to assess measurement error yielded a statistically highly significant result (p value < 0.001), and a strong correlation between the two sets of measurements was observed. Consequently, the measurement error was determined to be negligible. Given the significance of the Kolmogorov–Smirnov test for normal distribution (p value < 0.001) and the t test results indicating no significant deviation of recorded values from zero (p value = 0.745), both antisymmetry and directional asymmetry were rejected. Consequently, the

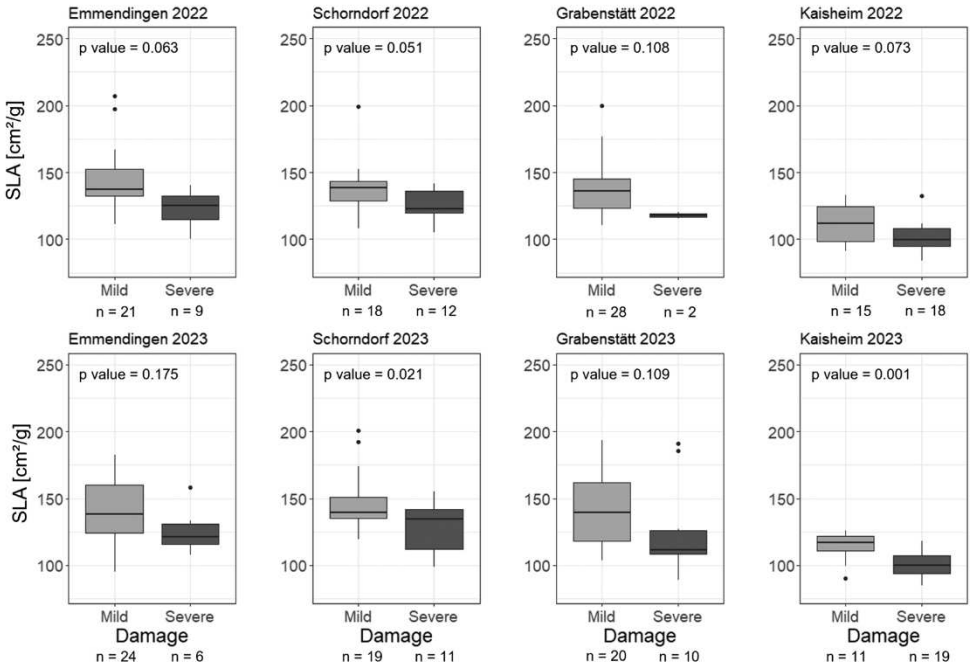

Fig. 6 Boxplots of the impact of different degrees of damage due to ash dieback on SLA (specific leaf area) differentiated for mildly and severely affected ash trees for the four study sites in 2022 and 2023. IQR represented by height of boxes, median by bold horizontal lines, upper (lower) whiskers indicate minimum of maximum (minimum) of metric and 1.5 times IQR, dots represent observations exceeding or falling below 1.5 times IQR

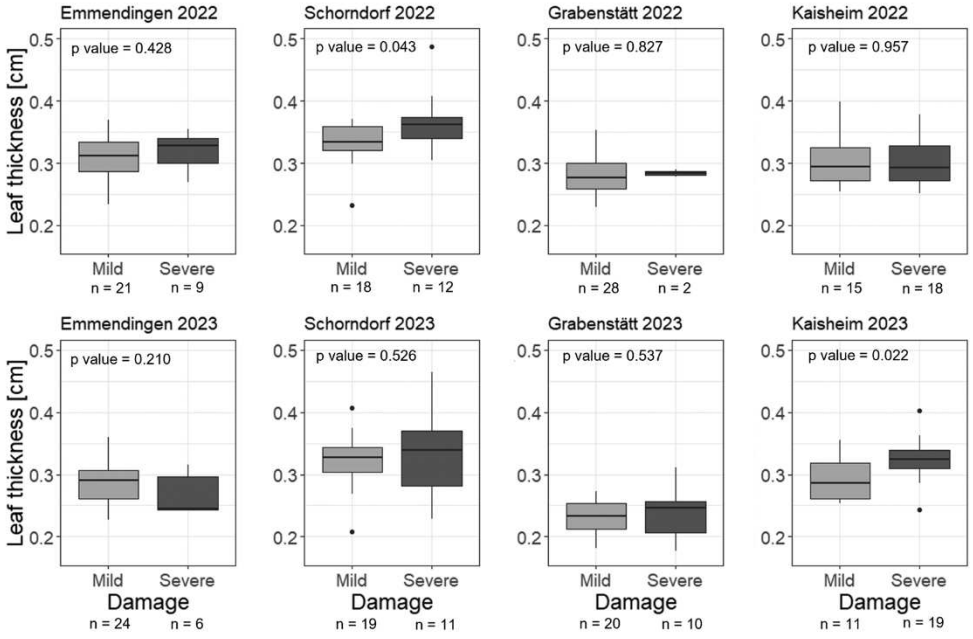

Fig. 7 Boxplots of leaf thickness for trees differentiated for mildly and severely affected ash trees for the four study sites in 2022 and 2023. IQR represented by height of boxes, median by bold horizontal lines, upper (lower) whiskers indicate minimum of maximum (minimum) of metric and 1.5 times IQR, dots represent observations exceeding or falling below 1.5 times IQR

Table 3 Spearman correlations between the investigated leaf traits (leaf thickness and SLA $n=243$, SPAD $n=210$, F_v/F_m $n=180$)

	Leaf thickness	SLA	F_v/F_m
SPAD	r: −0.120	r: −0.171	r: 0.079
	p value: 0.081	p value: 0.012*	p value: 0.291
F_v/F_m	r: 0.254	r: 0.216	–
	p value: <0.001*	p value: 0.003*	
SLA	r: −0.314	–	–
	p value: <0.001*		

*Significant correlation with $p<0.05$

Table 6 p values of two-way ANOVA analysis, testing the difference between mild and severely damaged trees for the four principal components (PC) and four study sites

	Emmendingen	Schorndorf	Grabenstätt	Kaisheim
PC 1	0.398	0.190	0.757	0.066
PC 2	0.338	0.737	0.975	0.485
PC 3	0.098	0.509	0.440	0.191
PC 4	0.023*	0.828	0.338	0.604

*Significant difference with $p<0.05$

measurements were deemed to accurately represent FA. The PCA identified four principal components with eigenvalues > 1, each merging two to three traits (Table 4). Higher eigenvalues indicate a higher explanatory value of the respective PC. The traits included in PC 1 and PC 2, focusing on the FA of the entire leaf, therefore, exhibited a higher informative value than PC 3 and PC 4, which measured the FA of the individual leaflets. The higher the loading value, the better the observation is represented by the PC, as shown in Table 5. Our results show a clear distribution of the traits with none of them being loaded on more than one PC. In total, 67% of the variance of the dataset was retained by the application of the PCA (Table 4).

Each of the four principal components was set in relation to the four study sites and tested for significant difference between mildly and severely damaged ash trees regarding FA. However, only for Emmendingen and PC 4, the result was significant (Table 6), demonstrating increased FA in more severely damaged trees. All other principal components showed no significant difference between disease severity for any of the study sites. A scatterplot of PC 1 and PC 2 for all study sites (Fig. 8) shows that leaves from both mildly and severely damaged trees are densely clustered near the origin [around (0,0)]. This suggests that the majority of leaves, regardless of damage severity, have similar PC scores. The lack of a clear separation between mild and severe damage along the two PCs implies that damage severity does not drastically alter the overall pattern of asymmetry, although individual leaves may still show differences. As there are some leaves demonstrating increased FA for both mildly and severely affected trees, changes in FA cannot be attributed to damage caused by ash dieback. A MANOVA analysis using the combined data of all four study sites revealed no significant difference between the four principal components and the damage severity (p value = 0.304).

Table 4 Eigenvalue, proportion variance, and the respective included traits for the four PCs from the FA analysis of the sampled ash leaves

Factor	Eigenvalue	Proportion variance	Included traits
PC 1	2.03	0.21	First leaflet set from the bottom: LLL (D–J), LLB (F–L), LLT (E–K)
PC 2	2.05	0.20	Second leaflet set from the bottom: LLL (A–G), LLB (C–I), LLT (B–H)
PC 3	1.36	0.14	First leaflet set from the bottom: LLW (K–L), LLW (E–F)
PC 4	1.18	0.12	Second leaflet set from the bottom: LLW (B–C), LLW (H–I)

Table 5 Loadings of the individual traits for the respective PCs from the FA analysis of the sampled ash leaves

Traits	Asymmetry	PC 1	PC 2	PC 3	PC 4
First leaflet set from the bottom: LLL	D–J	0.84	–	–	–
First leaflet set from the bottom: LLB	F–L	0.79	–	–	–
First leaflet set from the bottom: LLT	E–K	0.76	–	–	–
Second leaflet set from the bottom: LLL	A–G	–	0.83	–	–
Second leaflet set from the bottom: LLB	C–I	–	0.79	–	–
Second leaflet set from the bottom: LLT	B–H	–	0.75	–	–
First right leaflet from the bottom: LLW	K–L	–	–	0.81	–
First left leaflet from the bottom: LLW	E–F	–	–	0.75	–
Second left leaflet from the bottom: LLW	B–C	–	–	–	0.88
Second right leaflet from the bottom: LLW	H–I	–	–	–	0.58

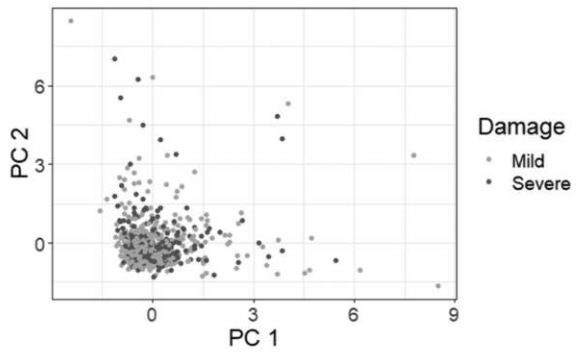

Fig. 8 Scatterplot displaying the values of FA of PC 1 and PC 2 of all four study sites, colored in the two damage classes "mildly affected" (light grey) and "severely affected" (dark grey)

Discussion

Five different leaf physiology and morphology traits were tested within the scope of this study; however, only some were associated with significant differences between mildly and severely affected ash trees.

Using F_v/F_m values for the assessment of plant stress is a quick way of obtaining information; however, this method does not delineate the cause of stress. While for Emmendingen 2022 and Schorndorf in 2023, more stressed trees were observed in more severely damaged trees, this could neither be confirmed for the other year nor for the third study site Grabenstätt. For this study site, we recorded very high numbers of stressed trees, especially in 2023. It has to be noted that we observed visible symptoms presumable caused by drought stress during the measurements in early August. This highlights the difficulty of interpreting F_v/F_m values in the context of ash dieback. In general, F_v/F_m has been proven as a reliable indicator for diseases in multiple species. For *Plantago ovata*, affected by downy mildew disease, maximum quantum yield of PSII differed significantly between healthy and chlorotic leaves (Mandal et al. 2009). In the case of wheat (*Triticum aestivum*) affected by spot blotch, diseased plants presented reduced chlorophyll fluorescence variables, negatively correlated with severity (Rosyara et al. 2010). Chlorophyll fluorescence differences of white root rot in avocado stands, caused by the fungus *Rosellinia necatrix*, might even be suitable for identifying susceptible genotypes (Martínez-Ferri et al. 2016). For ash trees that were infested with emerald ash borer and treated with stem injections, chlorophyll fluorescence values improved, thus proving the general suitability of F_v/F_m as a measure of the photosynthetic capacity for this species (Hanavan and Heuss 2019).

Fungal pathogens can be differentiated in biotrophs (utilization of living host tissue) or necrotrophs (utilization of nutrients obtained from dead host tissue), or classified as hemibiotrophic if they are able to switch from a biotrophic to a necrotrophic phase (Perfect and Green 2001). *Hymenoscyphus fraxineus* has been characterized as hemibiotroph, with an extended biotrophic phase in the stem tissue (Mansfield et al. 2019). Ajigboye et al. (2016) suggest that fungal pathogens, once switched to necrotrophic phase, are damaging the chloroplasts inside the leaves, thus changing the efficiency of PSII photochemistry. Therefore, we suggest that leaf infestation might not be detectable using F_v/F_m values as long as *Hymenoscyphus fraxineus* is in its biotroph phase. Thus, we conclude that further studies should focus on F_v/F_m measurements while taking a larger number of leaves into account and measuring other environmental factors such as air temperature and edaphic conditions of the soil to assess the influence of other stressors. Extended time series are necessary to establish dependable relationships between F_v/F_m values and these stress factors.

The results of the analysis of chlorophyll content present two different dynamics. While there was a noticeable distinction between mildly and severely damaged trees at the two seed plantation sites, characterized by lower SPAD values for severely affected ashes, the clone area Grabenstätt exhibited the opposite pattern, with severely damaged trees showing higher SPAD values. Various studies in the context of plant diseases reported lower SPAD values for affected plants (Rosyara et al. 2010; Zhao et al. 2011; Yahya et al. 2020; Arafat et al. 2021). However, in the case of oil palm, affected by basal stem rot disease caused by *Ganoderma boninense* fungus, SPAD value differences were only recorded between healthy and diseased plants, without variation based on disease severity (Khaled et al. 2018). It has to be noted that it was not possible to include completely unaffected ash trees in this study due to the extended spread of ash dieback in Germany. The expected decrease of SPAD values associated with increased damage severity was only observed for the two ash seed plantations. Differences between the sites imply the presence of potential additional environmental factors influencing chlorophyll content.

A negative relationship between SPAD values and SLA was found, indicating a higher chlorophyll content in leaves with smaller SLA. This negative chlorophyll content–SLA relationship was also documented in six Amazonian tree species (Marenco et al. 2009), for groundnut (*Arachis hypogaea*) (Nageswara Rao et al. 2001; Nigam and Aruna 2008) and green gram (*Vigna radiata*) (Basu et al. 2019). This can be explained by the fact that elevated chlorophyll concentrations in a reduced leaf surface area facilitate enhanced absorption of solar radiation per unit leaf area by the plant (Basu et al. 2019) and, thus, counteract the possible negative effects of a reduced SLA.

In this study, SLA is significantly reduced in ash trees severely damaged by ash dieback. Plant diseases can have a high impact on SLA as demonstrated for American beech

(*Fagus grandifolia*) associated with a decreased SLA on leaves with severe symptoms caused by beech leaf disease. A clear difference in SLA between healthy trees and different degrees of damage was observed (McIntire 2023). A very similar result was reported for oil palms (*Elaeis guineensis*) affected by the plumero disorder (España-Guechá et al. 2020). Both studies are consistent with our findings of a decreased SLA for plants affected by varying degrees of a disease. However, an increased SLA was demonstrated for willow (*Salix* sp.) leaves damaged by leaf rust (*Melampsora epitea*) (Toome et al. 2010), illustrating species- and disease-specific reactions. SLA possibly demonstrates a high variability based on the position of the sampled leaves in the crown (Eriksson et al. 2005). Shade can have a crucial influence on leaves, with SLA increasing as a consequence of shadow (Wuytack et al. 2011). This was also documented for *Fraxinus excelsior* L., where SLA increased from top to bottom leaves (Petriţan et al. 2009) and shadowed leaves had a higher SLA (Legner et al. 2014). While in our study, close attention was paid to only collect leaves with exposure to direct sunlight, a possible variability in SLA due to the position of the leaf in the crown cannot be ruled out entirely. This fact may also be related to the variability of the measurements from different leaves of one tree: a relatively high standard deviation for some trees point to a possible high variability in SLA within individual trees. The SLA links the carbon and water cycle of a plant as it describes the distribution of leaf biomass in relation to leaf area, and thus changes in SLA also indicate changes in the latter (Pierce et al. 1994). It is yet unclear, if the reduction in SLA for severely damaged trees is a reaction to the infection with *Hymenoscyphus fraxineus* or leaves with a smaller SLA are more easily infected. However, the answer to this question would be highly interesting and further investigations are necessary.

Leaf thickness tends to be higher with advanced damage symptoms associated with a reduced SLA. The leaves of severely damaged ash trees, therefore, have a smaller area but exhibit an increased thickness. Changes in leaf thickness following stressors have been documented for various species. *Platanus acerifolia* growing under air-polluted conditions demonstrated higher leaf thickness than a non-polluted control group. The strengthened anatomic xeromorphic characteristics of the leaves were regarded as an adaptive strategy to air pollution (Dineva 2004). The cell wall of plants is dynamic and can change, when a disease occurs as a result of activated defense mechanisms (Zhao and Dixon 2014). Ahn et al. (2020) reported an increased thickness in the midribs of the leaves of Johnson grass as a response to the infection with *Colletotrichum sublineola*. Based on the presence of a thicker spongy mesophyll observed in highly susceptible clones, conclusions regarding the susceptibility of *Vitis vinifera* to downy mildew were possible; however, the differences were not statistically significant (Alonso-Villaverde et al. 2011). Increases of the thickness of the epidermis and hypodermis cell layer of grape berries were positively correlated with resistance to the disease *Botrytis cinerea*; however, the thickness of the leaves was not investigated in this study (Gabler et al. 2003). Jarosz et al. (1982) found no significant correlation between the thickness of the leaf cuticle and resistance to an infection with powdery mildew *Erysiphe cichoracearum*, demonstrating the species-specific different dynamics. In the context of the evaluation of leaf thickness, leaf hydration may play an important role. McIntire (2023) concluded that the increased leaf thickness found in diseased leaves is caused by a higher water content in the leaves which leads to more hydrated leaves. White and Montes-R (2005) also emphasized the need to include leaf water content to minimize the effects of varying environmental conditions. The simple and fast measurements of leaf thickness applied in this study yielded promising results; however, reliable statements regarding the leaf thickness of trees under the influence of ash dieback cannot be concluded at this point. For future investigations on leaf thickness of *Fraxinus excelsior* L., it is recommended to take multiple measurements per leaf and additionally measure leaf water content. This study did not differentiate between the individual components in the leaves; however, this would be recommended for future studies, especially with regard to possible conclusions on susceptibility.

Fluctuating asymmetry is proved to be an unsuitable indicator for stress caused by ash dieback. Only for one principal component, one study site was linked to significant differences between FA values and the two different damage classes. This may indicate that stress caused by ash dieback does not lead to increased FA in the leaves. Many studies also reported difficulties in proving FA as a reliable indicator, e.g., to detect stress due to insect herbivory (García-Jain et al. 2022), heavy metal stress (Gavrikov et al. 2023), stress caused by air pollution (Ambo-Rappe et al. 2008), environmental and genetic stress in fragmented populations (Murphy and Lovett-Doust 2004) or stress caused by landfill leachate (Dimitriou et al. 2006). FA is a controversial concept as it is linked to uncertainties regarding sample size (Mogie and Cousins 2001), the lacking reproducibility of measurements (Kozlov 2015; Dodonov et al. 2024), and the high impact of measurement error (Kozlov et al. 2017; Dodonov et al. 2024).

Due to the widespread impact of ash dieback, it is now very rare to find completely healthy ash trees in Germany (Fuchs et al. 2024). Therefore, it was not possible to include healthy trees in this study and our results only highlight the differences between mildly and severely damaged trees. The observed tendencies of a reduction in photosynthetic pigments and the changes in leaf morphology in terms of SLA and leaf thickness are indicative of

the significant changes that *Hymenoscyphus fraxineus* can cause on *Fraxinus excelsior* L. leaves. A decline of photosynthetic activity suggests changes in energy conversion with possible additional implications further affecting the overall fitness of the infected trees (Berger et al. 2007). The noted effects may potentially lead to additional health disadvantages, exacerbating the overall well-being of the ash trees.

Conclusion

The general health status of ash trees, infected by *Hymenoscyphus fraxineus*, can be easily recognized by the typically observed dieback of the shoots. In this study, we demonstrated that ash dieback has an influence on leaf physiology and morphology of *Fraxinus excelsior* L. Especially SLA enables a clear differentiation between the different degrees of damage by ash dieback. A reduced SLA of the leaves, in conjunction with alterations in leaf thickness and chlorophyll, may potentially contribute to additional adverse consequences, further impacting the overall health of the ash trees. Long-term data are needed for understanding the development of the observed physiological and morphological changes. Further studies on leaf physiology and morphology of *Fraxinus excelsior* L. affected by ash dieback are, therefore, highly recommended.

Acknowledgements We thank the Forestry Baden-Wuerttemberg, the Forest Research Institute Baden-Wuerttemberg, and the Bavarian Office for Forest Genetics for providing the seed orchards and the ash clone area as study sites. We thank Tobias Heckmann for valuable discussions, and Georgia Kahlenberg, Simone Perzl, Anna-Lena Dupois, and Alfred Buchner for technical assistance.

Author contributions Conceptualization: Susanne Jochner-Oette; methodology: Lisa Buchner, Anna-Katharina Eisen; formal analysis and investigation: Lisa Buchner; writing—original draft preparation: Lisa Buchner; writing—review and editing: Susanne Jochner-Oette, Anna-Katharina Eisen; funding acquisition: Susanne Jochner-Oette; supervision: Susanne Jochner-Oette.

Funding Open Access funding enabled and organized by Projekt DEAL. This study was conducted within the project FraxVir "Detection, characterisation and analyses of the occurrence of viruses and ash dieback in special stands of*Fraxinus excelsior—a supplementary study to the FraxForFuture demonstration project" and receives funding via the Waldklimafonds (WKF) funded by the German Federal Ministry of Food and Agriculture (BMEL) and Federal Ministry for the Environment, Nature Conservation, Nuclear Safety and Consumer Protection (BMUV) administrated by the Agency for Renewable Resources (FNR) under grant agreement 2220WK40A4.*

Data availability The data supporting the findings of this study are not publicly available, as the project in which the study was conducted is still ongoing.

Declarations

Conflict of interest The authors have no relevant financial or non-financial interests to disclose.

References

Adamčíková K, Pažitný J, Pastirčáková K (2023) Individual resistance of *Fraxinus angustifolia* and *F. excelsior* clones to *Hymenoscyphus fraxineus*. J Plant Prot Res 58(3):227–233. https://doi.org/10.24425/122937

Agostinelli M, Nguyen D, Witzell J, Cleary M (2021) Mycobiome of *Fraxinus excelsior* with different phenotypic susceptibility to ash dieback. Front for Glob Change. https://doi.org/10.3389/ffgc.2021.580514

Ahn E, Odvody G, Prom LK, Magill C (2020) Leaf angle distribution in Johnsongrass, leaf thickness in sorghum and Johnsongrass, and association with response to *Colletotrichum sublineola*. Sci Rep 10:22320. https://doi.org/10.1038/s41598-020-79473-x

Ajigboye OO, Bousquet L, Murchie EH, Ray RV (2016) Chlorophyll fluorescence parameters allow the rapid detection and differentiation of plant responses in three different wheat pathosystems. Funct Plant Biol 43(4):356–369. https://doi.org/10.1071/FP15280

Alonso-Villaverde V, Gago P, Rodríguez-García MI, Martínez MC (2011) Leaf thickness and structure of *Vitis Vinifera* L. CV. Albariño clones and its possible relation with susceptibility to downy mildew (*Plasmopara Vitivola*) infection. J Int Sci Vigne Vin 45:161–169. https://doi.org/10.20870/oeno-one.2011.45.3.1492

Ambo-Rappe R, Lajus DL, Schreider MJ (2008) Increased heavy metal and nutrient contamination does not increase fluctuating asymmetry in the seagrass *Halophila ovalis*. Ecol Ind 8(1):100–103. https://doi.org/10.1016/j.ecolind.2006.12.004

Arafat KH, Hassan M, Hussein EA (2021) Detection, disease severity and chlorophyll prediction of date palm leaf spot fungal diseases. New Val J Agric Sci 1(2):98–110. https://doi.org/10.21608/nvjas.2022.110022.1027

Awal MA, Ishak W, Endan J, Haniff M (2004) Determination of specific leaf area and leaf area-leaf mass relationship in oil palm plantation. Asian J Plant Sci 3(3):264–286

Banks JM (2017) Continuous excitation chlorophyll fluorescence parameters: a review for practitioners. Tree Physiol 37(8):1128–1136. https://doi.org/10.1093/treephys/tpx059

Baral H-O, Queloz V, Hosoya T (2014) *Hymenoscyphus fraxineus*, the correct scientific name for the fungus causing ash dieback in Europe. IMA Fungus 5:79–80. https://doi.org/10.5598/imafungus.2014.05.01.09

Barón M, Flexas J, Delucia EH (2012) Photosynthetic responses to biotic stress. In: Flexas J, Loreto F, Medrano H (eds) Terrestrial photosynthesis in a changing environment: a molecular,

physiological and ecological approach. Cambridge University Press, Cambridge, pp 331–350
Basu PS, Pratap A, Gupta S, Sharma K, Tomar R, Singh NP (2019) Physiological traits for shortening crop duration and improving productivity of greengram (*Vigna radiata* L. Wilczek) under high temperature. Front Plant Sci. https://doi.org/10.3389/fpls.2019.01508
Berger S, Sinha AK, Roitsch T (2007) Plant physiology meets phytopathology: plant primary metabolism and plant-pathogen interactions. J Exp Bot 58(15/16):4019–4026. https://doi.org/10.1093/jxb/erm298
Boeger MRT, Pilatti DM, de Lima CS, de Alvarenga AMSB, Da Pereto SCAS (2018) Leaf architecture and symmetry of understory tree species of an Araucaria forest. Acta Sci Biol Sci 40(1):43118. https://doi.org/10.4025/actascibiolsci.v40i1.43118
Buchner L, Eisen A-K, Šikoparija B, Jochner-Oette S (2022) Pollen viability of *Fraxinus excelsior* in storage experiments and investigations on the potential effect of long-range transport. Forests. https://doi.org/10.3390/f13040600
Chaimala A, Jogloy S, Vorasoot N, Holbrook C, Kvien CK, Laohasiriwong S (2023) The variation of relative water content, SPAD chlorophyll meter reading, stomatal conductance, leaf area, and specific leaf area of Jerusalem artichoke genotypes under different durations of terminal drought in tropical region. J Agron Crop Sci 209(1):12–26. https://doi.org/10.1111/jac.12561
Coker TLR, Rozsypálek J, Edwards A, Harwood TP, Butfoy L, Buggs RJA (2019) Estimating mortality rates of European ash (*Fraxinus excelsior*) under the ash dieback (*Hymenoscyphus fraxineus*) epidemic. Plants People Planet 1(1):48–58. https://doi.org/10.1002/ppp3.11
Cornelissen JHC, Lavorel S, Garnier E, Díaz S, Buchmann N, Gurvich DE, Reich PB, ter Steege H, Morgan HD, van der Heijden MGA, Pausas JG, Poorter H (2003) A handbook of protocols for standardised and easy measurement of plant functional traits worldwide. Aust J Bot 51(4):335–380. https://doi.org/10.1071/BT02124
Dimitriou I, Aronsson P, Weih M (2006) Stress tolerance of five willow clones after irrigation with different amounts of landfill leachate. Biores Technol 97(1):150–157. https://doi.org/10.1016/j.biortech.2005.02.004
Dineva SB (2004) Comparative studies of the leaf morphology and structure of white ash *Fraxinus americana* L. and London plante tree *Platanus acerifolia* Willd growing in polluted area. Dendrobiology 52:3–8
Dodonov P, Braga AL, Arruda LH, Alves-Ferreira G, Silva-Matos DM (2024) Is leaf fluctuating asymmetry related to plant and leaf size in *Miconia albicans*, a common Melastomataceae species? Braz J Biol 84:e260884. https://doi.org/10.1590/1519-6984.260884
Duraes F, Gama E, Malgalhaes PC, Marriel IE, Casela CR, Oliveira AC, Luchiari Junior A, Shanahan JF (2001) The usefulness of chlorophyll fluorescence in screening for disease resistance, water stress tolerance, aluminium toxicity tolerance, and n use efficiency in maize. In: Seventh Eastern and Southern Africa Regional Maize Conference, pp 356–360
Eisen A-K, Buchner L, Fussi B, Jochner-Oette S (2024) Does ash dieback affect the reproductive ecology of *Fraxinus excelsior* L.? J for Res. https://doi.org/10.1007/s11676-023-01670-x
Eisen A-K, Fussi B, Šikoparija B, Jochner-Oette S (2022) Aerobiological pollen deposition and transport of *Fraxinus excelsior* L. at a small spatial scale. Forests 13(3):424. https://doi.org/10.3390/f13030424
Eisen A-K, Semizer-Cuming D, Jochner-Oette S, Fussi B (2023) Pollination success of *Fraxinus excelsior* L. in the context of ash dieback. Ann for Sci. https://doi.org/10.1186/s13595-023-01189-5
Enderle R, Nakou A, Thomas K, Metzler B (2015) Susceptibility of autochthonous German *Fraxinus excelsior* clones to *Hymenoscyphus pseudoalbidus* is genetically determined. Ann for Sci 72:183–193. https://doi.org/10.1007/s13595-014-0413-1
Enderle R, Stenlid J, Vasaitis R (2019) An overview of ash (*Fraxinus* spp.) and the ash dieback disease in Europe. CABI Reviews. https://doi.org/10.1079/PAVSNNR201914025
Eriksson H, Eklundh L, Hall K, Lindroth A (2005) Estimating LAI in deciduous forest stands. Agric Meteorol 129:27–37. https://doi.org/10.1016/j.agrformet.2004.12.003
España-Guechá MS, Cayón-Salinas DG, Darghan-Contreras AE, Ochoa-Cadavid I (2020) Leaf area, chlorophyll content, and root dry mass in oil palms (*Elaeis guineensis* Jacq.) affected by the plumero disorder. Agron Colomb 38(3):335–341. https://doi.org/10.15446/agron.colomb.v38n3.85309
Freeman DC, Brown ML, Duda JJ, Graham JH, Emlen JM, Krzysik AJ, Balbach HE, Kovacic DA, Zak JC (2004) Photosynthesis and fluctuating asymmetry as indicators of plant response to soil disturbance in the fall-line sandhills of Georgia: a case study using *Rhus copallinum* and *Ipomoea pandurata*. Int J Plant Sci 165(5):805–816. https://doi.org/10.1086/421478
Freeman DC, Graham JH, Tracy M, Emlen JM, Alados CL (1999) Developmental instability as a means of assessing stress in plants: a case study using electromagnetic fields and soybeans. Int J Plant Sci 160(6):157–166. https://doi.org/10.1086/314213
Fuchs S, Häuser H, Peters S, Knauf L, Rentschler F, Kahlenberg G, Kätzel R, Evers J, Paar U, Langer GJ (2024) Ash dieback assessments on intensive monitoring plots in Germany: influence of stand, site and time on disease progression. J Plant Dis Prot. https://doi.org/10.1007/s41348-024-00889-y
Fussi B (2020) So hat die Esche eine Chance! LWF aktuell:60–61
Gabler FM, Smilanick JL, Mansour M, Ramming DW, Mackey BE (2003) Correlations of morphological, anatomical, and chemical features of grape berries with resistance to *Botrytis cinerea*. Phytopathology 93:1263–1273. https://doi.org/10.1094/PHYTO.2003.93.10.1263
García-Jain SE, Maldonado-López Y, Oyama K, Fagundes M, de Faria ML, Espírito-Santo MM, Cuevas-Reyes P (2022) Effects of forest fragmentation on plant quality, leaf morphology and herbivory of *Quercus deserticola*: is fluctuating asymmetry a good indicator of environmental stress? Trees 36(2):553–567. https://doi.org/10.1007/s00468-021-02228-2
Garnier E, Shipley B, Roumet C, Laurent G (2001) A standardized protocol for the determination of specific leaf area and leaf dry matter content. Funct Ecol 15(5):688–695. https://doi.org/10.1046/j.0269-8463.2001.00563.x
Gavrikov DE, Zverev V, Rachenko MA, Pristavka AA, Kozlov MV (2023) Experimental evidence questions the relationship between stress and fluctuating asymmetry in plants. Symmetry 15(2):339. https://doi.org/10.3390/sym15020339
Graham JH (2021) Fluctuating asymmetry and developmental instability, a guide to best practice. Symmetry. https://doi.org/10.3390/sym13010009
Graham JH, Raz S, Hel-Or H, Nevo E (2010) Fluctuating asymmetry: methods, theory, and applications. Symmetry 2(2):466–540. https://doi.org/10.3390/sym2020466
Graham JH, Shimizu K, Emlen JM, Freeman DC, Merkel J (2003) Growth models and the expected distribution of fluctuating asymmetry. Biol J Linn Soc 80:57–65. https://doi.org/10.1046/j.1095-8312.2003.00220.x
Greenacre M, Groenen PJF, Hastie T, D'Enza AI, Markos A, Tuzhilina E (2022) Principal component analysis. Nat Rev Methods Prim. https://doi.org/10.1038/s43586-022-00184-w
Gross A, Holdenrieder O, Pautasso M, Queloz V, Sieber TN (2014) *Hymenoscyphus pseudoalbidus*, the causal agent of European ash

dieback. Mol Plant Pathol 15(1):5–21. https://doi.org/10.1111/mpp.12073
Hagen SB, Ims RA, Yoccoz NG, Sørlibråten O (2008) Fluctuating asymmetry as an indicator of elevation stress and distribution limits in mountain birch (*Betula pubescens*). Plant Ecol 195:157–163. https://doi.org/10.1007/s11258-007-9312-y
Haňáčková Z, Koukol O, Čmoková A, Zahradník D, Havrdová L (2017) Direct evidence of *Hymenoscyphus fraxineus* infection pathway through the petiole-shoot junction. For Pathol. https://doi.org/10.1111/efp.12370
Hanavan RP, Heuss M (2019) Physiological response of ash trees, *Fraxinus* spp., infested with emerald ash borer, Agrilus planipennis Fairmaire (Coleoptera: Buprestidae), to Emamectin Benzoate (Tree-Äge) stem injections. Arboric Urban for 45:132–138. https://doi.org/10.48044/jauf.2019.012
Havrdová L, Novotná K, Zahradník D, Buriánek V, Pešková V, Šrůtka P, Černý K (2016) Differences in susceptibility to ash dieback in Czech provenances of *Fraxinus excelsior*. Forest Pathol 46(4):281–288. https://doi.org/10.1111/efp.12265
Hochwender C, Fritz R (1999) Fluctuating asymmetry in *Salix* hybrid system: the importance of genetic versus environmental causes. Evolution 53:408–416. https://doi.org/10.1111/j.1558-5646.1999.tb03776.x
Hopkins WG, Hüner NPA (2009) Introduction to plant physiology, 4th edn. Wiley, Hoboken
Hulshof CM, Violle C, Spasojevic MJ, McGill B, Damschen E, Harrison S, Enquist BJ (2013) Intra-specific and inter-specific variation in specific leaf area reveal the importance of abiotic and biotic drivers of species diversity across elevation and latitude. J Veg Sci 24:921–931. https://doi.org/10.1111/jvs.12041
Hultberg T, Sandström J, Felton A, Öhman K, Rönnberg J, Witzell J, Cleary M (2020) Ash dieback risks an extinction cascade. Biol Cons 244:108516. https://doi.org/10.1016/j.biocon.2020.108516
Ibaraki Y, Murakami J (2007) Distribution of chlorophyll fluorescence parameter Fv/Fm within individual plants under various stress conditions. Acta Hort 761:255–260. https://doi.org/10.17660/ActaHortic.2007.761.33
Jarosz AM, Sheets M, Levy M (1982) Cuticle thickness in Phlox and resistance to powdery mildew: an unreliable line of defense. Am J Bot 69:824–828. https://doi.org/10.1002/j.1537-2197.1982.tb13325.x
Katabuchi M (2015) *LeafArea*: an R package for rapid digital image analysis of leaf area. Ecol Res 30(6):1073–1077. https://doi.org/10.1007/s11284-015-1307-x
Khaled AY, Aziz SA, Bejo SK, Nawi NM, Seman IA, Izzuddin MA (2018) Dielectric constant and chlorophyll content measurements for basal stem tor (BSR) disease detection. In: The 2018 international conference on signals and systems, pp 69–72. https://doi.org/10.1109/ICSIGSYS.2018.8373570
Kirisits T, Matlakova M, Mottinger-Kroupa S, Halmschlager E, Lakatos F (2010) *Chalara fraxinea* associated with dieback of narrow-leafed ash (*Fraxinus angustifolia*). Plant Pathol 59:411. https://doi.org/10.1111/j.1365-3059.2009.02162.x
Klingenberg C (2015) Analyzing fluctuating asymmetry with geometric morphometrics: concepts, methods, and applications. Symmetry 7:843–934. https://doi.org/10.3390/sym7020843
Klisarić NB, Miljković D, Avramov S, Zivković U, Tarasjev A (2014) Fluctuating asymmetry in *Robinia pseudoacacia* leaves—possible in situ biomarker? Environ Sci Pollut Res Int 21:12928–12940. https://doi.org/10.1007/s11356-014-3211-2
Konica Minolta Optics, Inc. (2009) Chlorophyll Meter SPAD-502Plus
Kowalski T (2006) *Chalara fraxinea* sp. nov. associated with dieback of ash (*Fraxinus excelsior*) in Poland. For Pathol 36:264–270. https://doi.org/10.1111/j.1439-0329.2006.00453.x
Kozlov MV (2015) How reproducible are the measurements of leaf fluctuating asymmetry? PeerJ 3:e1027. https://doi.org/10.7717/peerj.1027
Kozlov MV, Cornelissen T, Gavrikov DE, Kunavin MA, Lama AD, Milligan JR, Zverev V, Zvereva EL (2017) Reproducibility of fluctuating asymmetry measurements in plants: Sources of variation and implications for study design. Ecol Ind 73:733–740. https://doi.org/10.1016/j.ecolind.2016.10.033
Kumari A, Kumar M (2015) Physiology of diseased plants and plant response against pathogen attack. In: Sinha A, Srivastava S, Kumar R (eds) Microbial biodiversity: a boon for agriculture sustainability. Biotech books, New Delhi, pp 525–536
Lamalakshmi Devi E, Kumar S, Basanta Singh T, Sharma SK, Beemrote A, Devi CP, Chongtham SK, Singh CH, Yumlembam RA, Haribhushan A, Prakash N, Wani SH (2017) Adaptation strategies and defence mechanisms of plants during environmental stress. In: Ghorbanpour M, Varma A (eds) Medicinal plants and environmental challenges. Springer, Cham, pp 359–413
Langer GJ, Fuchs S, Osewold J, Peters S, Schrewe F, Ridley M, Kätzel R, Bubner B, Grüner J (2022) FraxForFuture—research on European ash dieback in Germany. J Plant Dis Prot 129(6):1285–1295. https://doi.org/10.1007/s41348-022-00670-z
Legner N, Fleck S, Leuschner C (2014) Within-canopy variation in photosynthetic capacity, SLA and foliar N in temperate broad-leaved trees with contrasting shade tolerance. Trees 28(1):263–280. https://doi.org/10.1007/s00468-013-0947-0
Li J, Zhou X, Zhou J, Shang R, Wang Y, Jing P (2020) Comparative study on several determination methods of chlorophyll content in plants. IOP Conf Ser Mater Sci Eng. https://doi.org/10.1088/1757-899X/730/1/012066
Lichtenthaler HK, Babani F (2004) Light adaptation and senescence of the photosynthetic apparatus. Changes in pigment composition, chlorophyll fluorescence parameters and photosynthetic activity. In: Papageorgiou GC (ed) Chlorophyll a fluorescence. A signature of photosynthesis. Springer, Dordrecht, pp 713–736
Liu Z, Zhao M, Zhang H, Ren T, Liu C, He N (2022) Divergent response and adaptation of specific leaf area to environmental change at different spatio-temporal scales jointly improve plant survival. Glob Change Biol 29(4):1144–1159. https://doi.org/10.1111/gcb.16518
Lobo A, McKinney LV, Hansen JK, Kjær ED, Nielsen LR (2015) Genetic variation in dieback resistance in *Fraxinus excelsior* confirmed by progeny inoculation assay. Forest Pathol 45(5):379–387. https://doi.org/10.1111/efp.12179
Mabrouk L, Mabrouk W, Mansour HB (2020) High leaf fluctuating asymmetry in two native plants growing in heavy metal-contaminated soil: the case of Metlaoui phosphate mining basin (Gafsa, Tunisia). Environ Monit Assess. https://doi.org/10.1007/s10661-020-08385-0
Maldonado-López Y, Vaca-Sánchez MS, Canché-Delgado A, García-Jaín SE, González-Rodríguez A, Cornelissen T, Cuevas-Reyes P (2019) Leaf herbivory and fluctuating asymmetry as indicators of mangrove stress. Wetlands Ecol Manage 27:571–580. https://doi.org/10.1007/s11273-019-09678-z
Mandal K, Saravanan R, Maiti S, Kothari IL (2009) Effect of downy mildew disease on photosynthesis and chlorophyll fluorescence in *Plantago ovata* Forsk. J Plant Dis Prot 116:164–168
Mansfield J, Brown I, Papp-Rupar M (2019) Life at the edge—the cytology and physiology of the biotroph to necrotroph transition in *Hymenoscyphus fraxineus* during lesion formation in ash. Plant Pathol 68(5):908–920. https://doi.org/10.1111/ppa.13014
Marenco RA, Antezana-Vera SA, Nascimento H (2009) Relationship between specific leaf area, leaf thickness, leaf water content and *SPAD-502* readings in six Amazonian tree sprecies. Photosynthetica 47:184–190. https://doi.org/10.1007/s11099-009-0031-6

Martínez-Ferri E, Zumaquero A, Ariza MT, Barceló A, Pliego C (2016) Nondestructive detection of white root rot disease in avocado rootstocks by leaf chlorophyll fluorescence. Plant Dis 100(1):49–58. https://doi.org/10.1094/PDIS-01-15-0062-RE

Maxwell K, Johnson GN (2000) Chlorophyll fluorescence—a practical guide. J Exp Bot 51:659–668. https://doi.org/10.1093/jexbot/51.345.659

McIntire CD (2023) Physiological impacts of beech leaf disease across a gradient of symptom severity among understory American beech. Front for Glob Change. https://doi.org/10.3389/ffgc.2023.1146742

McKinney LV, Nielsen LR, Hansen JK, Kjær ED (2011) Presence of natural genetic resistance in *Fraxinus excelsior* (Oleraceae) to *Chalara fraxinea* (Ascomycota): an emerging infectious disease. Heredity 106(5):788–797. https://doi.org/10.1038/hdy.2010.119

Mevy JP, Guibal F, Lecareux C, Miglietta F (2020) The decline of *Fraxinus angustifolia* Vahl in a Mediterranean salt meadow: chlorophyll fluorescence measurements in long-term field experiment. Estuar Coast Shelf Sci 247:107068. https://doi.org/10.1016/j.ecss.2020.107068

Mogie M, Cousins M (2001) Are sample sizes usually at least an order of magnitude too low for reliable estimates of leaf asymmetry? J Theor Biol 211(2):181–185. https://doi.org/10.1006/jtbi.2001.2338

Murchie EH, Lawson T (2013) Chlorophyll fluorescence analysis: a guide to good practice and understanding some new applications. J Exp Bot 64(13):3983–3998. https://doi.org/10.1093/jxb/ert208

Murphy HT, Lovett-Doust J (2004) Landscape-level effects on developmental instability: fluctuating asymmetry across the range of honey locust, *Gleditsia triacanthos* (Fabaceae). Int J Plant Sci 165(5):795–803. https://doi.org/10.1086/421857

Nageswara Rao RC, Talwar HS, Wright GC (2001) Rapid assessment of specific leaf area and leaf nitrogen in peanut (*Arachis hypogaea* L.) using a chlorophyll meter. J Agron Crop Sci 186(3):175–182. https://doi.org/10.1046/j.1439-037X.2001.00472.x

Nielsen LR, McKinney LV, Hietala AM, Kjær ED (2017) The susceptibility of Asian, European and North American *Fraxinus* species to the ash dieback pathogen *Hymenoscyphus fraxineus* reflects their phylogenetic history. Eur J Forest Res 136(1):59–73. https://doi.org/10.1007/s10342-016-1009-0

Nielsen LR, Nagy NE, Piqueras S, Kosawang C, Thygesen LG, Hietala AM (2022) Host-pathogen interactions in leaf petioles of common ash and manchurian ash infected with *Hymenoscyphus fraxineus*. Microorganisms. https://doi.org/10.3390/microorganisms10020375

Nigam SN, Aruna R (2008) Stability of soil plant analytical development (SPAD) chlorophyll meter reading (SCMR) and specific leaf area (SLA) and their association across varying soil moisture stress conditions in groundnut (*Arachis hypogaea* L.). Euphytica 160(1):111–117. https://doi.org/10.1007/s10681-007-9581-5

Palmer AR (1994) Fluctuating asymmetry analyses: a primer. In: Markow TA (ed) Developmental instability. In: Proceedings of the International Conference on Developmental Instability: Its Origins and Evolutionary Implications, Tempe, Arizona, 14–15 June 1993. Springer Netherlands, Dordrecht, pp 335–364

Palmer AR, Strobeck C (1986) Fluctuating asymmetry: measurement, analysis, patterns. Ann Rev Ecol Syst 17:391–421

Palmer AR, Strobeck C (2003) Fluctuating asymmetry analyses revisited. In: Polak M (ed) Developmental instability. Causes and consequences. Oxford University Press, Oxford, pp 279–319

Perfect SE, Green JR (2001) Infection structures of biotrophic and hemibiotrophic fungal plant pathogens. Mol Plant Pathol 2(2):101–108. https://doi.org/10.1046/j.1364-3703.2001.00055.x

Peters S, Langer G, Kätzel R (eds) (2021) Eschentriebsterben. Kriterien zur Schadensbonitur an Eschen, 1. Auflage. Fachagentur Nachwachsende Rohstoffe (FNR), Gülzow-Prüzen

Petriţan AM, von Lüpke B, Petriţan IC (2009) Influence of light availability on growth, leaf morphology and plant architecture of beech (*Fagus sylvatica* L.), maple (*Acer pseudoplatanus* L.) and ash (*Fraxinus excelsior* L.) saplings. Eur J Forest Res 128(1):61–74. https://doi.org/10.1007/s10342-008-0239-1

Pierce LL, Running SW, Walker J (1994) Regional-scale relationships of leaf area index to specific leaf area and leaf nitrogen content. Ecol Appl 4(2):313–321. https://doi.org/10.2307/1941936

Pleijel H, Klingberg J, Nerentorp M, Broberg MC, Nyirambangutse B, Munthe J, Wallin G (2021) Mercury accumulation in leaves of different plant types—the significance of tissue age and specific leaf area. Biogeosciences 18:6313–6328. https://doi.org/10.5194/bg-18-6313-2021

Rakutko S, Rakutko E, Kaposhko D, Vaskin A (2017) Influence of light quality on fluctuating asymmetry of bilaterally traits of forced parsley (*Petroselinum tuberosum*) leaves. Eng Rural Develop. https://doi.org/10.22616/ERDev2017.16.N009

Rodrigues FA, Einhardt AM, Oliveira LM, Dias CS (2018) Physiological and biochemical changes in plants infected by pathogens. In: VIII Simpósio Sobre Atualidades em Fitopatologia (ed) Ferramentas Moleculares Aplicadas à Fitopatologia

Rosyara UR, Subedi S, Duveiller E, Sharma RC (2010) The effect of spot blotch and heat stress on variation of canopy temperature depression, chlorophyll fluorescence and chlorophyll content of hexaploid wheat genotypes. Euphytica 174(3):377–390. https://doi.org/10.1007/s10681-010-0136-9

Said AA, Moursi YS, Sallam A (2022) Association mapping and candidate genes for physiological non-destructive traits: chlorophyll content, canopy temperature, and specific leaf area under normal and saline conditions in wheat. Front Genet. https://doi.org/10.3389/fgene.2022.980319

Shadrina E, Soldatova V, Turmukhametova N (2023) Fluctuating asymmetry as a measure of stress in natural populations of woody plants: influence of ecological and geographical factors on developmental stability. Symmetry. https://doi.org/10.3390/sym15030700

Stener L-G (2013) Clonal differences in susceptibility to the dieback of *Fraxinus excelsior* in southern Sweden. Scand J for Res 28(3):205–216. https://doi.org/10.1080/02827581.2012.735699

Stocks JJ, Buggs RJA, Lee SJ (2017) A first assessment of *Fraxinus excelsior* (common ash) susceptibility to *Hymenoscyphus fraxineus* (ash dieback) throughout the British Isles. Sci Rep 7(1):16546. https://doi.org/10.1038/s41598-017-16706-6

Timmermann V, Børja I, Hietala AM, Kiristis T, Solheim H (2011) Ash dieback: pathogen spread and diurnal patterns of ascospore dispersal, with special emphasis on Norway. EPPO Bull 41:14–20. https://doi.org/10.1111/j.1365-2338.2010.02429.x

Toome M, Heinsoo K, Luik A (2010) Relation between leaf rust (*Melampsora epitea*) severity and the specific leaf area in short rotation coppice willows. Eur J Plant Pathol 126(4):583–588. https://doi.org/10.1007/s10658-009-9566-4

Turmukhametova NV, Shadrina EG, Soldatova VY, Ivantsova EN (2021) Fluctuating asymmetry of the lamina of *Betula pendula* Roth in the context of different cities and industrial load. IOP Conf Ser Earth Environ Sci 839(5):52011. https://doi.org/10.1088/1755-1315/839/5/052011

Uddling J, Gelang-Alfredsson J, Piikki K, Pleijel H (2007) Evaluating the relationship between leaf chlorophyll concentration and SPAD-502 chlorophyll meter readings. Photosynth Res 91(1):37–46. https://doi.org/10.1007/s11120-006-9077-5

Velickovic M (2008) A modified version of fluctuating asymmetry, potential for the analysis of *Aesculus hippocastanum* L. compound leaves. Rivista di Biologia. Biol Forum 101

White JW, Montes-R C (2005) Variation in parameters related to leaf thickness in common bean (*Phaseolus vulgaris* L.). Field Crops Res 91(1):7–21. https://doi.org/10.1016/j.fcr.2004.05.001

Wohlmuth A, Essl F, Heinze B (2018) Genetic analysis of inherited reduced susceptibility of *Fraxinus excelsior* L. seedlings in Austria to ash dieback. For Int J for Res 91(4):514–525. https://doi.org/10.1093/forestry/cpy012

Wuytack T, Wuyts K, van Dongen S, Baeten L, Kardel F, Verheyen K, Samson R (2011) The effect of air pollution and other environmental stressors on leaf fluctuating asymmetry and specific leaf area of *Salix alba* L. Environ Pollut (barking Essex: 1987) 159(10):2405–2411. https://doi.org/10.1016/j.envpol.2011.06.037

Yahya M, Saeed NA, Nadeem S, Hamed M, Saleem K (2020) Effect of leaf rust disease on photosynthetic rate, chlorophyll contents and grain yield of wheat. Arch Phytopathol Plant Prot 53(9–10):425–439. https://doi.org/10.1080/03235408.2020.1748369

Zeng F, Shabala L, Zhou M, Zhang G, Shabala S (2013) Barley responses to combined waterlogging and salinity stress: separating effects of oxygen deprivation and elemental toxicity. Front Plant Sci. https://doi.org/10.3389/fpls.2013.00313

Zhao D, Glynn NC, Glaz B, Comstock JC, Sood S (2011) Orange rust effects on leaf photosynthesis and related characters of sugarcane. Plant Dis 95:640–647. https://doi.org/10.1094/PDIS-10-10-0762

Zhao Q, Dixon RA (2014) Altering the cell wall and its impact on plant disease: from forage to bioenergy. Annu Rev Phytopathol 52:69–91. https://doi.org/10.1146/annurev-phyto-082712-102237

4.2 Identification of damage severity in *Fraxinus excelsior* L. trees caused by ash dieback using multisensory and multitemporal UAV imagery

Forest Ecology and Management 585 (2025) 122660

Contents lists available at ScienceDirect

Forest Ecology and Management

journal homepage: www.elsevier.com/locate/foreco

Identification of damage severity in *Fraxinus excelsior* L. trees caused by ash dieback using multisensory and multitemporal UAV imagery

Lisa Buchner *, Anna-Katharina Eisen, Susanne Jochner-Oette

Physical Geography / Landscape Ecology and Sustainable Ecosystem Development, Catholic University of Eichstätt-Ingolstadt, Eichstätt 85072, Germany

ARTICLE INFO

Keywords:
Common ash
Hymenoscyphus fraxineus
Multispectral
RGB
Thermal
Thresholding
Vegetation indices

ABSTRACT

The extended spread of ash dieback in Europe has far-reaching consequences for *Fraxinus excelsior* L. populations. The progression of the disease leads to characteristic symptoms, particularly within the tree crowns. To date, assessing the damage severity of each individual tree typically requires in-field inspections. However, UAVs equipped with RGB, thermal, and multispectral sensors offer cost-effective and objective possibilities. This study relied on such analyses and focused on two ash seed orchards in Baden-Wuerttemberg, Germany, where visual inspections were compared with multisensorial data obtained in spring, summer and autumn of 2022 and 2023. The calculated RGB and multispectral vegetation indices were able to significantly discriminate between different degrees of damage due to ash dieback; in contrast, thermal data were less reliable and linked to different dynamics. Novel thresholds applied to the vegetation indices enabled a classification of mild and severe damage with an overall accuracy of 74.9 % for the multispectral index DVI (Difference Vegetation Index) and 73.0 % for the RGB index GRVI (Green-Red Vegetation Index). Combining RGB and multispectral indices further improved the overall accuracy to 77.2 %. The presented workflow offers forest practitioners an accessible toolset for evaluating the health status of ash populations affected by ash dieback.

1. Introduction

The common ash (*Fraxinus excelsior* L.) in Europe is seriously threatened in its existence due to the ash dieback disease caused by the invasive fungal pathogen *Hymenoscyphus fraxineus* (T. Kowalski) Baral, Queloz, Hosoya (Baral et al., 2014). Since the first documentation of ash dieback in Poland in the 1990s (Kowalski, 2006, Timmermann et al., 2011), the disease has become increasingly widespread across Europe, causing extensive damage to ash populations. Infected trees present typical symptoms of dying shoots and increased leaf loss with thinning of the crowns. Especially in more severely damaged trees, epicormic shoots often constitute a large part of the remaining foliage. Ash dieback is linked to a high mortality rate amongst the affected trees (Enderle et al., 2019), and the European ash populations are expected to drastically decrease over the next few decades (Coker et al., 2019). In Germany, the European common ash is a common tree species both in forests and non-forest sites, such as private gardens, along rivers or in public spaces (Enderle et al., 2017a). In 2022, the forth National Forest Inventory documented that ash accounted for 1.8 % of Germany's total forest area (BMEL, 2024). As an ecologically vital tree species, with several species dependent on the existence of the common ash, its conservation is crucial in the face of ash dieback (Mitchell et al., 2017, Hultberg et al., 2020). Additionally to the high ecological impact, the common ash is also an important economic tree species, as it is also valued for its high-quality timber (Pautasso et al., 2013). However, symptoms of ash dieback can also manifest as collar and root rot, negatively influencing the stability of the affected trees. Those trees present a safety risk for humans (e.g., forest workers or visitors) and infrastructure (e.g., traffic roads) (Metzler and Herbstritt, 2014, Enderle et al., 2017b, Skovsgaard et al., 2017). The vast majority of ash trees in German forest stands has been affected by ash dieback, with only very few healthy trees remaining (Fuchs et al., 2024). To assess the damage severity and gain an estimate of the health status of ash populations, usually each individual tree has to be assessed by a trained expert in the field. Rating scales are commonly used to classify trees into classes based on their health, taking into account various factors such as foliage density or the presence of epicormic shoots (Lenz et al., 2012, Peters et al., 2021).

Remote sensing technologies offer advantageous options for forest monitoring. Unmanned aerial vehicles (UAVs) equipped with a variety

* Corresponding author.
E-mail address: LBuchner@ku.de (L. Buchner).

https://doi.org/10.1016/j.foreco.2025.122660
Received 17 December 2024; Received in revised form 6 March 2025; Accepted 9 March 2025
Available online 22 March 2025

of different sensor systems allow for the rapid assessment of large areas. UAVs have been tested in a number of forest applications, e.g., for the estimation of tree parameters, species phenotyping, phenology, drought stress, fire hazards, nutrient status, insect pests and plant diseases (Torresan et al., 2017, Barbedo, 2019, Abd El-Ghany et al., 2020, Kleinsmann et al., 2023). Plant stress caused by biotic and abiotic factors can be detected using UAV technology (Castro et al., 2021). Sensors such as RGB, thermal, as well as multi- and hyperspectral UAV systems provide valuable insights into plant disease status (Neupane and Baysal-Gurel, 2021). The foliage of each plant is linked to a specific spectral reflectance, and the analysis thereof gives indications on the plant's biochemical components and overall health. Vegetation indices (VIs), calculated by formulas that commonly incorporate multiple wavelengths are often employed to analyse the spectral reflectance (Huete, 2012).

Inexpensive RGB sensors can provide information on plant height and crown diameter (Barbosa et al., 2021), biomass (Bendig et al., 2015), phenology (Park et al., 2019), canopy area (Starý et al. 2020) or forage yield (Lussem et al., 2018). Especially in the context of plant diseases, VIs based on RGB data have been proven to be a valuable tool for the identification and characterization of damage caused by plant diseases. Diseases can cause subtle changes in leaf colour, texture, and brightness, making RGB VIs effective for identifying diseases early, even before symptoms become visually severe. For example, a significant relationship between different RGB VIs and leaf rust severity was documented for wheat (*Triticum aestivum* L.) affected by the fungus *Puccinia triticina* (Bhandari et al., 2020). Similarly investigations on diseased citrus trees also proved a connection between RGB VIs and health status (Garza et al., 2020). Using RGB VIs, it was also possible to detect disease severity in rice (*Oryza* spp.) caused by narrow leaf spot (Cai et al., 2018).

With more specific wavelengths, also extending to the red-edge and near-infrared range, multispectral sensors offer a wide range of additional information to the visible light sensors. Multispectral UAV data are widely used in various applications such as precision farming (Candiago et al., 2015) and can also effectively identify and monitor physiological stress in trees (Dash et al., 2017). Healthy and diseased trees often display distinct spectral signatures, influenced by differences in pigment composition and structural properties (Mahlein et al., 2013). Numerous multispectral VIs exist, each targeting specific wavelengths with a focus on characteristics such as biomass, greenness, or vegetation status (Xue and Su, 2017). In the context of plant diseases, multispectral data have been shown to be successful in identifying diseases. UAV multispectral data in combination with VIs were used to detect grapevine (*Vitis vinifera* L.) disease (Albetis et al., 2017), monitor sugarcane white leaf disease symptoms (Sanseechan et al., 2019) and detect banana (*Musa* spp.) plant diseases (Ye et al., 2020, Choosumrong et al., 2023).

Thermal sensors, which capture the surface temperature including those of plants, offer unique possibilities for detecting plant diseases and the overall health status of plants (Hashim et al., 2020). Disease induced stress can lead to the closure of leaf stomata, reducing the transpiration rate and resulting in higher leaf temperatures. Increased plant surface temperatures were often observed using thermal imaging techniques even before visible symptoms were documented (Chaerle et al., 1999, Jafari et al., 2017, Ortiz-Bustos et al., 2017). For instance, thermal imaging successfully identified diseases in banana plants (Anasta et al., 2021), and significant differences in leaf surface temperature were observed in oilseed rape (*Brassica napus*) infected with fungal species of the genus *Alternaria* (Baranowski et al., 2015).

In the context of plant diseases, thermal imaging has mostly been carried out under controlled indoor conditions, since thermal systems can be easily influenced by outdoor conditions, such as changing solar conditions or wind (Hashim et al., 2020). Nevertheless, UAVs equipped with thermal cameras have also proven to be valuable tools to identify plant disease status. Smigaj et al. (2015) investigated the use of a UAV-operated thermal camera to monitor the canopy temperature of diseased trees and were able to document a significant positive correlation between tree canopy temperature and disease status.

While the use of UAVs in forests or plantations to detect plant diseases is widespread (Holzwarth et al., 2023), few studies using remote sensing technologies have focused on ash tree health: The impact of the emerald ash borer (*Agrilus planipennis*), a major insect pest additionally threatening ash populations, on ash tree health has been assessed using hyperspectral data (Pontius et al., 2008) and multispectral WorldView-2 satellite data (Murfitt et al., 2016). Both data enabled an estimation of the health status of the affected ash trees. Waser et al. (2014) also used WorldView-2 data and calculated multispectral VIs for classifying four different levels of damage caused by ash dieback. Hyperspectral data facilitated the identification of individual ash trees affected by ash dieback (Chan et al., 2021, Polk et al., 2022). Further, Kampen et al. (2019) demonstrated the potential of UAV-based multispectral data to assess ash dieback severity.

However, none of the studies integrated thermal sensors or are partly only based on single seasons and years. Moreover, the results of the few studies focusing on the damage caused by ash dieback reported difficulties in detecting the damage severity and complex workflows make it difficult to implement these in practice across the board.

Therefore, this study investigates the potential of RGB, multispectral and thermal UAV surveys to determine the extent of damage to *Fraxinus excelsior* L. affected by ash dieback in two German ash seed orchards. We hypothesize that vegetation indices values derived from UAV surveys vary based on infection status. Additionally, the use of thresholds may effectively differentiate between varying degrees of damage. Multiple UAV surveys spread over the course of two years (2022–2023) provide extensive data at different times of the vegetation period. Emphasis is placed on the effectiveness of the three different camera systems. Practical applications for forest practitioners are a key focus of this study, since the fast and straightforward use of UAV systems combined with an easy-to-follow workflow can enable a quick estimate of the disease status of ash populations.

2. Materials and methods

2.1. Study sites

This study was conducted at two study sites (Fig. 1), located in the south of Germany in the federal state of Baden-Wuerttemberg. Both study sites have previously been included in research on ash dieback (Enderle et al., 2015, Buchner et al., 2022, Buchner et al., 2024, Eisen et al., 2024), thus detailed information on the health status of the planted individuals already exists.

The ash seed orchard Emmendingen (48°6′38.50"N, 7°52'20.49"E, 209 m NHN) is located approx. 15 km north of the city Freiburg. The plantation has a size of 2.7 ha and was established in 1995. Originally, 228 ash trees were planted in a grid of 10 m x 10 m. Even though there were no thinning measures, 142 trees had to be removed due to ash dieback, with only 86 ash trees consisting of 32 different genotypes remaining.

The seed orchard Schorndorf (48°46'35.59''N, 9°25'31.00''E, 420 m NHN) is located east of the state capital Stuttgart in Baden-Wuerttemberg. The plantation was established in 1992 with a spacing of 7 m x 7 m and has an area of approx. 2.27 ha. 416 ash trees were originally planted, but since then, due to thinning measures and the effect of ash dieback, 296 of the ash trees were removed and only 120 living trees, consisting of 30 different genotypes remained on the orchard.

2.2. Methods

Fig. 2 provides an overview of the applied workflow of the UAV surveys, the respective post-processing of the data and the workflow for

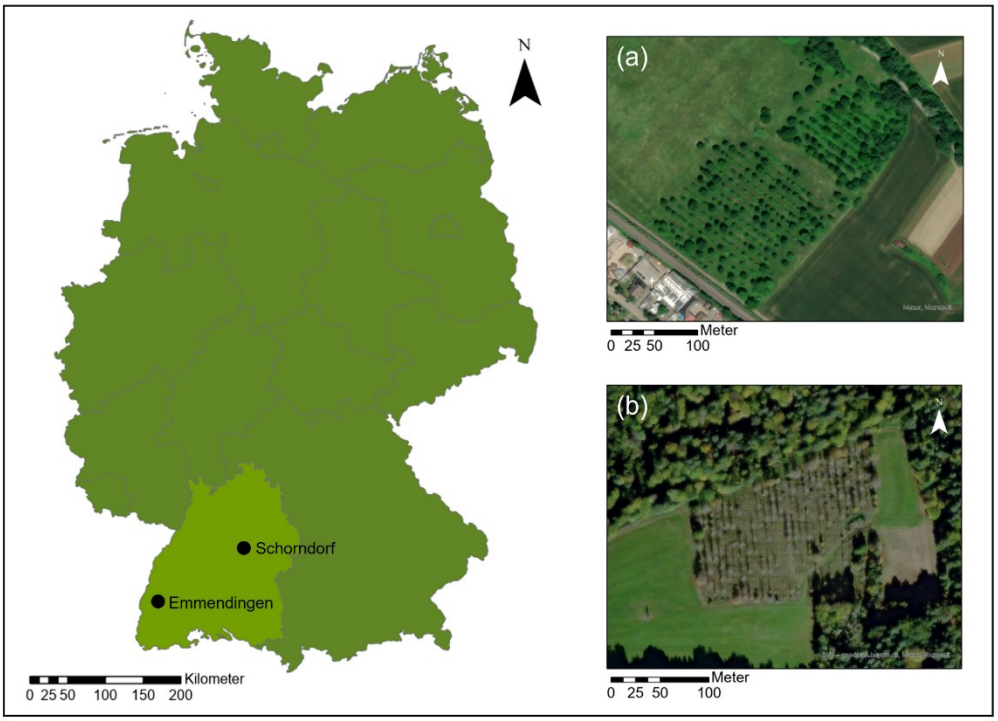

Fig. 1. Study sites Emmendingen (a) and Schorndorf (b) located in the federal state of Baden-Wuerttemberg (light green) in Germany (green), Source: Esri Base Map.

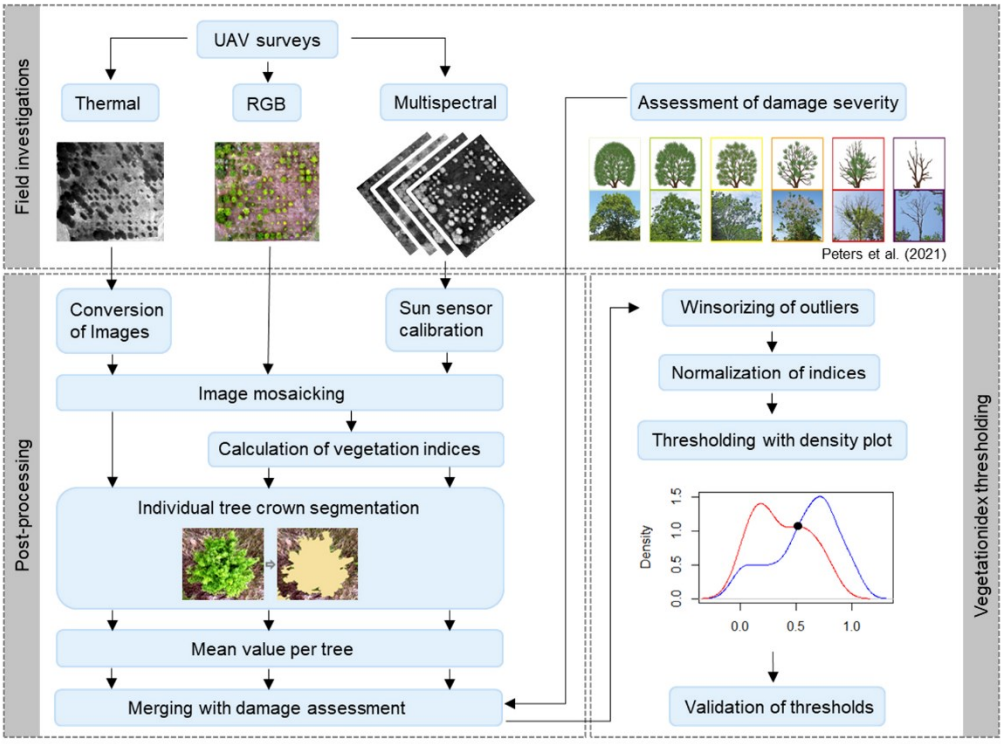

Fig. 2. Methodological framework of the field investigations, post-processing of the data and the vegetation index thresholding.

obtaining and analysing vegetation indices to index thresholding. In brief, the multisensorial vegetation indices were calculated for each tree and compared with field-based vitality assessments to evaluate the index's effectiveness in distinguishing different levels of damage. Differences across vitality classes were tested for statistical significance, using appropriate statistical methods based on data distribution and variance. This approach was used to identify suitable indices for assessing damage severity. A key advancement of this study is represented by the calculation of thresholds that can be universally used in assessing the ash tree's health based on remotely sensed data following this workflow. The individual work steps are explained in more detail in the following.

2.2.1. Assessment of vitality

Each of the ash trees on both ash seed orchards was assessed regarding their vitality, by using a standardized vitality scoring systems developed by Peters et al. (2021). The ash trees were classified into six categories, ranging from class 0, consisting of healthy trees, to mildly damaged trees (class 1 and 2), severely damaged trees (class 3 and 4) and lastly to dead trees (class 5). Each class is characterised by different degrees of thinning of the crown, leaf loss, dead shoots and branches, and the presence of epicormic shoots. The vitality assessments were conducted at both orchards in late July of 2022 and 2023.

2.2.2. UAV surveys

2.2.2.1. Image acquisition. Between spring and autumn in 2022 and 2023, two to four UAV aerial surveys were conducted at each study site (Table 1). Two UAV systems were employed: the DJI Mavic 2 Enterprise Advanced (Mavic 2 EA) and the DJI Mavic 3 Multispectral (Mavic 3 M). The Mavic 2 EA is equipped with a 48 MP RGB camera and a thermal sensor, capturing both RGB and thermal images simultaneously. The Mavic 3 M, on the other hand, features a 20 MP RGB camera and four 5 MP multispectral sensors, which record multispectral and RGB images concurrently. The multispectral sensors cover the near-infrared (860 nm ± 26 nm), red edge (730 nm ± 16 nm), red (650 nm ± 16 nm), and green (560 nm ± 16 nm) wavelengths. An integrated sun sensor measures solar radiation, enabling light compensation during image post-processing which enhances the accuracy and consistency of data over time (DJI, 2022).

All surveys were taken at a flight height of 80 m above the ground, with side and front overlaps of 85 % and a flight speed of 3 m/s for the Mavic 2 EA and 4 m/s for the Mavic 3 M. A ground sampling distance of 2.22 cm/pixel was achieved for RGB and 10.48 cm/pixel for thermal images taken by the Mavic 2 EA and 2.77 cm/pixel for the multispectral images of the Mavic 3 M.

Pre-planned flight plans were generated using the UAVs' software to ensure comprehensive coverage of the entire plantation sites. Due to the size of the plantations and the UAVs' battery limitations, each survey was divided into two flight missions at the Schorndorf seed orchard and three at the Emmendingen seed orchard. These consecutive missions were conducted back-to-back to minimize any changes in environmental conditions between flights. All surveys were carried out on sunny, cloud-free days with minimal wind to ensure optimal image quality and consistency.

The images were georeferenced using ground control points (GCPs) that were represented by red sheets with reflecting panels. The coordinates of the GCPs were recorded using the surveying system Stonex S9III (STONEX® Srl, Paderno Dugnano, Italy). The Mavic 3 M includes an RTK module, ensuring positioning with centimetre precision, and no GCPs were used for those flights.

2.2.2.2. Image processing of multispectral and RGB data. RGB and multispectral images captured by the UAV systems were processed using Agisoft Metashape Professional (version 1.8.1). After aligning the imported images, a point cloud was generated, followed by the construction of an orthophoto. For the multispectral images, data from the sun sensor were used for calibration. Georeferencing was achieved with recorded GCPs and, in the case of the Mavic 3 M, supplemented by recorded RTK data.

Subsequently, the orthophotos were imported into ArcGIS Pro (version 2.8.3) and the individual tree crowns were manually delineated. A polygon was created to represent the shape of each tree crown, capturing only leaf mass. Although several methods for automatic single tree crown segmentation exist (Dalponte et al., 2015, Panagiotidis et al., 2017, Mohan et al., 2017, Qiu et al., 2020, Miraki et al., 2021), none achieved the necessary accuracy for this study. Given the generous spacing of ash trees in both orchards, manual segmentation of the crowns was feasible. Since ash dieback causes leaf loss and crown thinning, special care was taken to segment only those areas of the crown that still contained leaves. This approach minimized the influence of extraneous pixels, particularly ground pixels. Some trees were excluded from further analyses due to crown blurring caused by movement of the tree crowns during the UAV survey.

2.2.2.3. Vegetation indices and thresholding. RGB band values were first normalized, as described in Eqs. 1 – 3, to reduce the effects of illumination (Torres-Sánchez et al., 2014, Zhang et al., 2019, Suh et al., 2020, Barbosa et al., 2021) using the raster calculator in ArcGIS Pro.

$$r = \frac{R}{R+G+B} \tag{1}$$

$$g = \frac{G}{R+G+B} \tag{2}$$

$$b = \frac{B}{R+G+B} \tag{3}$$

Ten RGB and ten multispectral VIs were selected, each in the context of plant health. The respective VIs and their definitions are listed in Table 2.

Using the raster calculator in ArcGIS Pro, the individual bands of the generated orthophotos were used to calculate the VIs. The zonal statistics tool was then applied to calculate the mean VI value per tree canopy using the segmented tree crown polygons.

The mean vegetation index value for each tree was compared with the field-based vitality assessments to evaluate each index's capability to distinguish between varying levels of ash dieback damage. Statistical differences among the four vitality classes (1−4) were formally assessed using ANOVA. In these models, vegetation index values represented the dependent variables, while the field-assessed vitality class served as the independent categorical factor. Assumptions underlying ANOVA, namely the normality of residuals and homogeneity of variances, were

Table 1
Months in which the aerial surveys were conducted in 2022 and 2023 for the two seed orchards Emmendingen and Schorndorf and the used UAVs: Mavic 2 EA (M2EA), Mavic 3 M (M3M).

	2022				2023			
Seed orchard	May	June	Juli	Oct.	May	June	July	Oct.
Emmendingen	M2EA		M2EA	M2EA		M2EA, M3M	M3M	M2EA, M3M
Schorndorf		M2EA		M2EA	M2EA	M2EA, M3M	M3M	M2EA, M3M

Table 2
Vegetation indices (VIs) selected for this study. For each index, the equation and exemplary references, where the VI was applied in the context of plant health, are displayed.

	Vegetation index	Equation	References
RGB	Green-Red Vegetation Index	$GRVI = \frac{g-r}{g+r}$	(Albetis et al. 2017, Albetis et al. 2019)
	Excess Green Index	$ExG = 2*g - r - b$	(Cai et al. 2018)
	Excess Red Index	$ExR = 1.4*r - g$	(Cai et al. 2018)
	Excess Green-Red	$ExGR = ExG - ExR$	(Cai et al. 2018)
	Green Leaf Index	$GLI = \frac{2*g-r-b}{2*g+r+b}$	(Bhandari et al. 2020)
	Red Green Blue Vegetation Index	$RGBVI = \frac{g^2 - b*r}{g^2 + b*r}$	(Bendig et al. 2015)
	Red Green Ratio Index	$RGRI = \frac{r}{g}$	(Albetis et al. 2017, Albetis et al. 2019, Cai et al. 2018)
	Green Blue Ratio Index	$GBRI = \frac{b}{g}$	(Vilela et al. 2024)
	Triangular Greenness Index	$TGI = g - 0.39*r - 0.61*b$	(Garza et al. 2020)
	Greenness Index	$GI = \frac{g}{r}$	(Sanseechan et al. 2019)
Multispectral	Normalized Difference Vegetation Index	$NDVI = \frac{NIR-R}{NIR+R}$	(Guo et al. 2021, Wu et al. 2023)
	Red Edge Normalized Difference Vegetation Index	$NDRE = \frac{NIR-RE}{NIR+RE}$	(Chang et al. 2020, Albetis et al. 2019, Wu et al. 2023)
	Green Normalized Difference Vegetation Index	$GNDVI = \frac{NIR-G}{NIR+G}$	(Sanseechan et al. 2019)
	Green Chlorophyll Index	$Clg = \frac{NIR}{G} - 1$	(Ye et al. 2020)
	Red Edge Chlorophyll Index	$Clre = \frac{NIR}{RE} - 1$	(Albetis et al. 2019, Ye et al. 2020)
	Chlorophyll Vegetation Index	$CVI = \frac{NIR}{G} * \frac{R}{G}$	(Wu et al. 2023)
	Difference Vegetation Index	$DVI = NIR - R$	(Steddom et al. 2005, Jie et al. 2015)
	Red Edge Green Index	$REGI = \frac{RE-G}{RE+G}$	(Albetis et al. 2019)
	Anthocyanin Reflectance Index	$ARI = \frac{1}{G} - \frac{1}{RE}$	(Ashourloo et al. 2014, Abdulridha et al. 2019)
	Plant Senescence reflectance Index	$PSRI = \frac{R-G}{NIR}$	(Ashourloo et al. 2014, Guo et al. 2021, Wu et al. 2023)

verified by visually inspecting residual distribution plots and performing Levene's test, respectively. If these assumptions were violated (non-normal residuals or unequal variances), the non-parametric Kruskal-Wallis test was applied instead. When significant differences were detected, post-hoc tests were applied to determine pairwise differences between vitality classes. For ANOVA, pairwise t-tests with Holm's correction were conducted. For Kruskal-Wallis, pairwise Wilcoxon rank-sum tests with Bonferroni correction were used. This approach enabled the identification of vegetation indices suitable for assessing ash dieback damage.

To establish a threshold separating the value range of a vegetation index for mild and severe damage the datasets of both seed orchards were merged to generate universal thresholds. Extreme outlier values were adjusted by limiting all values higher than the 95th percentile to the 95th percentile value, and all values lower than the 5th percentile to the 5th percentile value. Vegetation indices were then normalized using Eq. 4, scaling all indices to a range of 0–1. To simplify the vitality data, classes 1 and 2 were combined to represent mild damage, while classes 3 and 4 were combined to represent severe damage. Due to the extended spread of ash dieback in Germany (Fuchs et al., 2024), no healthy trees (class 0) were found on the two study sites. Since the focus of our study lies on the analysis of leaf mass, dead trees (class 5) were excluded from the analysis. To determine whether the index values significantly differentiate between mild and severe damage for the three best RGB and multispectral indices, we assessed the normality of the data distribution using the Shapiro-Wilk test. As for none of the indices the assumption of normality was met, the Mann-Whitney *U* test was applied.

$$VI\_normalized = \frac{VI - VI_{min}}{VI_{max} - VI_{min}} \quad (4)$$

A density plot was generated for each vegetation index in each UAV survey to display the index value range for the two damage classes, mild and severe. The intersection point of these distributions was identified as the optimal threshold for distinguishing between the two damage classes. Since each vegetation index was calculated for every UAV survey, an average threshold value was then determined across all surveys. This established average threshold was then re-evaluated across all surveys. Each threshold was verified by 10-fold cross-validation, where the original datasets were resampled into 10 sub-datasets. Overall accuracy (OA) (Eq. 6) and F1 score (Eqs. 6–8) were calculated to assess threshold performance. True positives (TP) and true negatives (TN) represented correct predictions that aligned with actual observations, while false positives (FP) and false negatives (FN) indicated incorrect predictions. OA represents the percentage of correct predictions. Precision measures the accuracy of positive predictions, while recall evaluates the ability to identify all relevant positive instances. As a measure of the optimal balance between precision and recall, the F1 score highlights the correctly identified TP and TN (Fawcett, 2006).

$$OA = \frac{TP + TN}{TP + FP + FN + TN} \quad (5)$$

$$Precision = \frac{TP}{TP + FP} \quad (6)$$

$$Recall = \frac{TP}{TP + FN} \quad (7)$$

$$F1Score = 2 * \frac{Precision * Recall}{Precision + Recall} \quad (8)$$

Additionally, due to the imbalance between the number of cases in the classes mild and severe, i.e., a higher prevalence of mildly damaged trees, the Matthews Correlation Coefficient (MCC; Eq. 9), was calculated. The MCC considers the balance of TP, TN, FP, and FN, offering a robust and unbiased evaluation metric, particularly in scenarios with class imbalance. MCC values can range from −1–1, with higher values indicating better model performance (Chicco and Jurman, 2020, Foody, 2023).

$$MCC = \frac{TP * TN - FP * FN}{\sqrt{(TP + FP) * (TP + FN) * (TN + FP) * (TN + FN)}} \quad (9)$$

All analyses were performed in R (version 4.1.1) using R Studio (version 2021.09.0).

2.2.2.4. Combination of indices. To improve damage estimation, we tested combinations of multiple VIs using binary logistic regression with 10-fold cross-validation. This method allows us to predict whether an outcome will be present or absent based on several predictor variables. The dependent variable is either 0 (mild damage) or 1 (severe damage). The model estimates the influence of each independent variable, in this case the various VIs, on the outcome, the disease severity. The dependent variable (*P*), the probability of the disease severity, was calculated according to Eq. 10 (Lee and Pradhan, 2007, Ye et al., 2020).

$$P = \frac{1}{1 + e^{-y}} \tag{10}$$

The variable y is a linear combination calculated according to Eq. 11 (Lee and Pradhan, 2007, Ye et al., 2020)

$$y = b_0 + \quad b_1 x_1 \quad + \quad b_2 x_2 + \quad b_3 x_3 + \quad b_n x_n \tag{11}$$

Here, b_0 is the intercept, b_1 are the slope coefficients, and x_1 represent the independent variables. In this study, this equation was applied to model the probability of the disease severity based on the thresholds of multiple, combined VIs. The glm() function of the R package "car" was utilized to fit the logistic regression models.

For both RGB and multispectral data, the three indices, which were most successful in discriminating the damage severity with thresholding were selected and combined in the logistic regression model to determine the efficiency of the calculated thresholds in combination with other indices.

A correlation analysis was conducted between these six indices to assess their relationships. To avoid multicollinearity, which can lead to unstable regression models, only indices with a low correlation were selected from both the RGB and multispectral data. Multicollinearity was tested for applying variance inflation factor (VIF) analysis, using the function vif() in the "car" package in R. The smallest VIF value is 1, values greater than 5 indicate multicollinearity. VIF was calculated using Eq. 12 where R^2 represents the coefficient of determination, which measures how well one independent variable can be predicted by all the other independent variables in the model. If the R^2 value is close to 1, the variable is highly related to the others (collinearity), resulting in a high VIF. In such cases, the variable does not provide much unique information to the model (James et al., 2023).

$$VIF = \frac{1}{1 - R^2} \tag{12}$$

Binary logistic regression analysis was used to determine whether combining RGB and multispectral data improves the accuracy of damage severity estimation.

The results of the logistic regression analysis were again assessed with a 10-fold cross-validation, focusing on the statistical measures of OA, F1 score and MCC.

2.2.2.5. Processing of the thermal images. Since the thermal images captured by the Mavic 2 EA were initially saved as 8-bit JPEG-files, a pre-processing of the images was necessary, converting them into 16-bit TIFF-files. An adapted R script, based on the script developed by Kattenborn (2023), was used for facilitating this image conversion. This ensured a consistent scale across all images, where each specific temperature value corresponded to the same digital number, enabling the application of structure-from-motion processing. The script is based on the DJI Thermal SDK (version 1.4) and incorporated factors such as emissivity, relative humidity, and camera-target-distance.

Relative humidity was measured on both study sites using a relative humidity logger (HOBO U23–001, Onset, Bourne, MA, USA) recording data every ten minutes. We used the mean relative humidity during the flight time and an emissivity value of 0.96 was applied for all images, based on the estimated average emissivity value for plants determined by Harrap et al. (2018).

The converted thermal images were validated randomly using the DJI Thermal Analysis Tool (version 2.1.8). Afterwards the converted images were stitched together to an orthomosaic as described for the RGB and multispectral images.

In the final thermal orthophoto, individual ash tree crowns were segmented manually in ArcGIS Pro. Using the tool "zonal statistics", the mean temperature per segmented tree crown was calculated. To determine statistically significant differences in mean crown temperatures across vitality classes, we followed the statistical procedure described above (chapter 2.2.2.3).

3. Results

3.1. Vegetation indices

3.1.1. Multispectral indices

The comparison of mean values related to the VIs and the respective vitality classes revealed varying outcomes depending on the specific VI and the seasonal timing of the UAV surveys. For all indices, severe damage was associated by decreased index values. At the Emmendingen seed orchard, all ten VIs were able to significantly discriminate between the four vitality classes in the summer, with p values < 0.001 for both surveys in June and July (Table 3). At the Schorndorf seed orchard, all indices except the CVI showed significant differentiation in June, only six out of ten indices were significant in July. The VIs generated from the autumn surveys performed worse than those from the summer. Only seven VIs for Emmendingen and five for Schorndorf showed statistically significant differences between the classes. Overall, the multispectral VIs NDVI, GNDVI, Clg, REGI and DVI were able to discriminate between the vitality classes for all surveys in both summer and autumn. The post-hoc tests revealed that the majority of indices presented significant differences between class 1 and 3 and class 1 and 4, whereas typically only a few significant differences between class 1 and 2 and class 3 and 4 could be detected. Due to the extensive size of the post-hoc results, they are not presented here.

For each VI, mean thresholds were calculated across all surveys to distinguish between mild damage (vitality classes 1 and 2) and severe damage (vitality classes 3 and 4). For example, NDVI values above the calculated summer threshold of 0.57 were classified as mildly damaged, whereas NDVI values below this threshold represented severely damaged ash trees. Validation of these mean thresholds applying 10-fold cross-validation revealed varying classification success rates (Table 4). Among the thresholds derived from both summer and autumn surveys, the DVI and GNDVI achieved the highest accuracy and F1 scores, with classification success rates of 71.4 % and 71.5 %, respectively. When considering only the summer surveys, the highest classification success was again observed for DVI and GNDVI, with an OA of 74.9 % and 74.4 %, respectively. Although the REGI ranked third for both summer and autumn data with an accuracy of 70.8 %, the NDVI demonstrated a higher OA of 73.9 % when evaluated solely with summer data. Especially for the summer surveys, the combination of a relatively high OA, a high F1 score, and a moderate MCC suggests that the thresholds perform reasonably well overall. Due to the class imbalance, the overall accuracy (OA) is influenced by the larger class of mildly damaged trees. The high F1 score suggests balanced classification performance across both damage classes. Additionally, the MCC exceeds 0.4, indicating moderate agreement beyond chance, quantifying the effectiveness of the thresholds in distinguishing between mildly and severely damaged trees.

Boxplots illustrating vegetation indices (NDVI, DVI, and GNDVI) from all four summer surveys conducted at the Emmendingen and

Table 3
P-values for the statistical difference between the four vitality classes for the ten selected multispectral VIs at the Emmendingen (E) and Schorndorf (S) seed orchards in 2023; Definition of VIs see Table 2. Bold values: significant at the 5 % level.

	E June 23	E July 23	E Oct 23	S June 23	S July 23	S Oct 23
NDVI	**< 0.001**	**< 0.001**	**< 0.001**	**< 0.001**	**< 0.001**	**0.006**
NDRE	**< 0.001**	**< 0.001**	**0.009**	**< 0.001**	0.057	0.068
GNDVI	**< 0.001**	**< 0.001**	**0.010**	**< 0.001**	**0.001**	**0.019**
Clg	**< 0.001**	**< 0.001**	**0.019**	**< 0.001**	**0.001**	**0.019**
Clre	**< 0.001**	**< 0.001**	**0.009**	**< 0.001**	0.052	0.070
CVI	**< 0.001**	**< 0.001**	0.092	0.181	0.968	0.915
REGI	**< 0.001**	**< 0.001**	**0.015**	**< 0.001**	**< 0.001**	**0.018**
PSRI	**< 0.001**	**< 0.001**	0.148	**< 0.001**	0.757	0.819
DVI	**< 0.001**	**< 0.001**	**< 0.001**	**< 0.001**	**< 0.001**	**0.001**
ARI	**< 0.001**	**< 0.001**	0.068	**< 0.001**	0.220	0.396

Table 4
Established thresholds, overall accuracy (OA), F1 score (F1) and Matthews correlation coefficient (MCC) for the ten selected multispectral VIs, considering combined summer and autumn surveys as well as summer surveys only.

	Summer and autumn surveys				Summer surveys			
	Threshold	OA	F1	MCC	Threshold	OA	F1	MCC
NDVI	0.58	70.2	0.76	0.38	0.57	73.9	0.80	0.44
DVI	0.50	71.4	0.78	0.38	0.52	74.9	0.80	0.46
NDRE	0.48	64.3	0.70	0.29	0.45	68.8	0.75	0.35
Clg	0.36	70.5	0.77	0.37	0.38	72.1	0.79	0.38
Clre	0.46	63.5	0.69	0.28	0.43	68.3	0.74	0.34
GNDVI	0.44	71.5	0.78	0.37	0.46	74.5	0.81	0.43
CVI	0.29	63.4	0.72	0.17	0.31	66.7	0.75	0.26
REGI	0.45	70.8	0.78	0.36	0.47	72.4	0.79	0.38
ARI	0.33	66.3	0.74	0.26	0.37	68.3	0.75	0.32
PSRI	0.50	30.6	0.67	0.21	0.49	63.4	0.71	0.22

Schorndorf seed orchards (Fig. 3) show a clear significant difference in median positions (solid horizontal lines within the boxes), indicating distinct vegetation responses between mildly and severely affected ashes. However, varying degrees of overlap in the interquartile ranges (box height) were evident among indices. The dashed line in Fig. 3 represents the calculated threshold separating mildly and severely damaged trees.

3.1.2. RGB indices

The ten selected RGB indices exhibited varying degrees of suitability for differentiating among the vitality classes. For the RGRI and the ExR indices, severe damage is indicated by higher values, while for all other RGB indices, more severe damage is linked to decreased index values. While some indices demonstrated statistically significant differences among the four vitality classes, only the GLI index proved significance across all surveys conducted from May to October at both study sites (Table 5). The ExG and RGBVI indices also widely displayed statistically significant differences in vitality classes for most surveys, except for the May 2022 survey in Emmendingen. Although the GRVI and GI indices were not significantly different during the autumn 2022 surveys, they achieved statistical significance in October 2023. The autumn surveys for both years indicated a reduced ability of RGB VIs to distinguish between vitality classes. However, in Schorndorf in 2023, most indices achieved statistical significance. As for the multispectral indices, the post-hoc tests (not shown) demonstrated mostly significant differences between class 1 and 3 and class 1 and 4, and only in some cases significant differences be-tween class 1 and 2 and class 3 and 4. Post-hoc test results supported the classification of classes 1 and 2 as mild damage and classes 3 and 4 as severe damage, making this grouping suitable for further threshold analysis.

Thresholds generated for the RGB-derived VIs varied between the combined summer and autumn surveys and the summer-only surveys. Validation through 10-fold cross-validation indicated that the ExG, GLI, and RGRI indices achieved the highest accuracy and F1 scores for the combined summer/autumn surveys, with ExG attaining the highest accuracy at 71.0 %. In contrast, slightly higher accuracies were recorded for the summer-only surveys, where the GRVI, ExG, and RGRI were most effective in distinguishing between mild and severe damage due to ash dieback. The highest OAs were observed during the summer surveys, with the GRVI achieving 73.0 %, followed by the RGRI at 72.5 % and the ExG at 72.2 %. As with the multispectral indices, a relatively high OA was generally associated with a high F1 score and a moderate MCC for the three most successful indices. However, for the RGB indices, the MCC values only exceeded the threshold for moderate agreement of 0.4 for the GRVI in the summer; all other indices presented lower MCC values (Table 6).

Although a clear statistically significant shift in the median is visible (Fig. 4), the determined thresholds (dashed lines) cannot entirely separate the two damage classes due to overlapping interquartile ranges. For GRVI and ExG, more severe damage leads to decreased index values, whereas for RGRI, higher values indicated severe damage.

3.1.3. Combination of indices

The results of the binary logistic regression analysis for three combinations of VIs are presented in Table 7. All three combinations, which include the most appropriate VIs for thresholding, yielded very similar outcomes, with accuracies ranging from 76.7 % to 77.2 %, F1 scores between 0.83 and 0.84, and the MCC between 0.43 and 0.48. The highest classification success was achieved using the combination of two multispectral indices (NDVI and DVI) and one RGB index (ExG), which also exhibited low VIF values. This combination is the only pairing of RGB and multispectral indices with low VIF values; all other combinations exhibited multicollinearity. For instance, the combination of the three RGB indices – GRVI, ExG, and REGI – also showed high VIF values exceeding the threshold of 10 for both GRVI and RGRI, indicating multicollinearity. Conversely, both the multispectral index combination

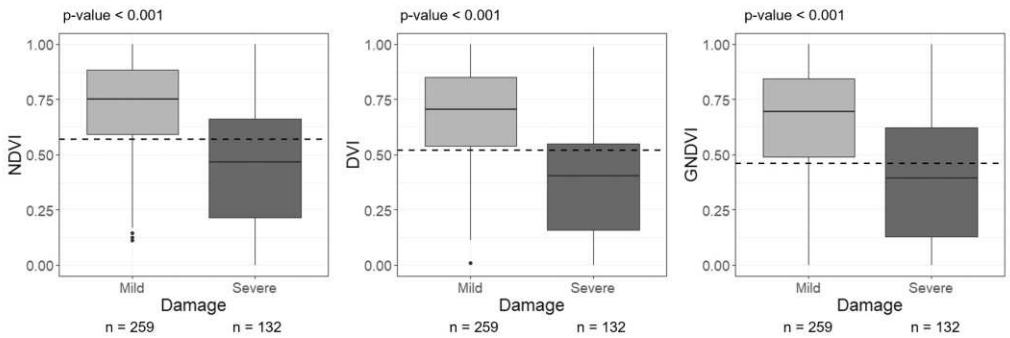

Fig. 3. Boxplots of all four summer surveys for the merged dataset of the Emmendingen and Schorndorf seed orchards, displaying the normalized vegetation indices NDVI, DVI and GNDVI for the trees.

Table 5
P-values for the statistical differences between the four vitality classes for the ten selected RGB VIs at the Emmendingen (E) and Schorndorf (S) seed orchards in 2022 and 2023. Bold values: significant at the 5 % level.

	E May 22	E July 22	E Okt. 22	S June 22	S Okt. 22	E June 23	E July 23	E Okt. 23	S June 23	S July 23	S Okt. 23
GRVI	**< 0.001**	**< 0.001**	0.080	**< 0.001**	0.975	**< 0.001**	**< 0.001**	**< 0.001**	**< 0.001**	**< 0.001**	**0.005**
ExG	0.099	**< 0.001**	**0.001**	**< 0.001**	**0.006**	**< 0.001**	**< 0.001**	**< 0.001**	**< 0.001**	**< 0.001**	**< 0.001**
ExR	0.052	**< 0.001**	0.251	0.444	**< 0.001**	**< 0.001**	**< 0.001**	**0.016**	**0.009**	0.053	0.088
ExGR	**0.004**	**< 0.001**	0.379	0.092	0.060	**< 0.001**	**< 0.001**	**0.002**	**< 0.001**	**0.001**	**0.035**
GLI	**0.034**	**< 0.001**	**0.001**	**< 0.001**	**0.006**	**< 0.001**	**< 0.001**	**< 0.001**	**< 0.001**	**< 0.001**	**< 0.001**
RGBVI	0.130	**0.012**	**< 0.001**	**< 0.001**	**0.001**	**0.010**	**0.037**	**0.003**	**< 0.001**	**< 0.001**	**< 0.001**
GI	**< 0.001**	**< 0.001**	0.080	**< 0.001**	0.978	**< 0.001**	**< 0.001**	**< 0.001**	**< 0.001**	**< 0.001**	**0.003**
RGRI	**< 0.001**	**< 0.001**	0.073	**< 0.001**	0.976	**< 0.001**	**< 0.001**	**< 0.001**	**< 0.001**	**< 0.001**	**0.005**
GBRI	0.568	0.258	**0.003**	**< 0.001**	**< 0.001**	0.751	0.362	**0.04**	**< 0.001**	**< 0.001**	**< 0.001**
TGI	0.199	0.026	**0.002**	**< 0.001**	**< 0.001**	**0.034**	0.017	**< 0.001**	**< 0.001**	**< 0.001**	**< 0.001**

Table 6
Established thresholds, overall accuracy (OA), F1 score (F1) and Matthews correlation coefficient (MCC) for the ten selected RGB VIs for the combined summer and autumn surveys and the summer-only surveys.

	Summer and autumn surveys				Summer surveys			
	Threshold	OA	F1	MCC	Threshold	OA	F1	MCC
GRVI	0.42	67.3	0.74	0.34	0.37	73.0	0.80	0.40
ExG	0.45	71.0	0.78	0.36	0.42	72.2	0.80	0.35
ExR	0.61	60.3	0.68	0.18	0.58	63.0	0.69	0.27
ExGR	0.37	63.6	0.71	0.24	0.38	67.6	0.74	0.34
GLI	0.48	70.2	0.77	0.35	0.45	71.5	0.79	0.35
RGBVI	0.48	68.0	0.76	0.29	0.47	67.5	0.75	0.27
RGRI	0.60	69.3	0.76	0.33	0.60	72.5	0.79	0.39
GBRI	0.48	63.2	0.71	0.21	0.47	60.8	0.69	0.18
TGI	0.47	66.5	0.74	0.27	0.46	65.7	0.74	0.25
GI	0.37	65.9	0.72	0.34	0.32	70.8	0.77	0.38

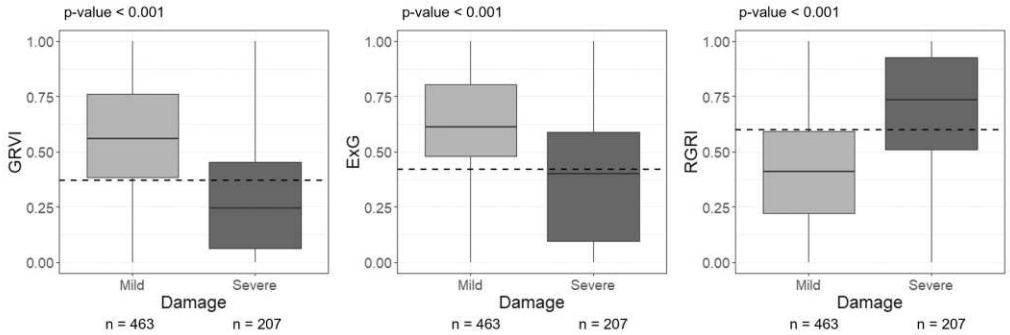

Fig. 4. Boxplots of all seven summer surveys for the merged data of the Emmendingen and Schorndorf seed orchards, displaying the vegetation indices GRVI, ExG and RGRI for the trees surveyed in the summer.

and the combined RGB and multispectral indices displayed low VIF values, suggesting the absence of multicollinearity.

The correlations among the six selected VIs (Fig. 5) partially revealed strong relationships not only within the RGB and multispectral datasets but also across them. These high correlations limited the improvement in damage severity identification, resulting in a 2 % higher OA compared to using individual indices alone.

3.2. *Thermal images*

The analysis of the thermal images in relation to the different vitality classes revealed different distributions of crown temperatures for the four vitality classes. Statistically significant differences were recorded in only two of the ten UAV surveys (Fig. 6). Specifically, in June ($p < 0.001$) and in October ($p = 0.021$) 2023 at the Schorndorf seed orchard, a significant increase in crown temperature was observed in more severely affected ash trees. The post-hoc test for the June survey revealed significant differences between class 1 and class 4 ($p = 0.006$), class 2 and class 4 ($p < 0.001$), and class 3 and class 4 ($p = 0.025$). In the October survey, a statistically significant difference was observed only between class 1 and class 4 ($p = 0.031$). Although a similar trend was visually apparent in some other UAV surveys, it did not reach statistical significance in those cases. An exception was the May 2022 survey in Emmendingen, which exhibited an opposing pattern with a temperature decrease of over 2 °C between the medians of vitality classes 1–4.

4. Discussion

In this study, three different camera systems - RGB, thermal and multispectral - were tested for their suitability to differentiate between varying degrees of damage caused by ash dieback.

Due to the rapid progression of ash dieback, no healthy tree could be included in this study. Consequently, the analysis focused solely on trees exhibiting varying degrees of damage. However, it is important to note

Table 7
Logistic regression equations for three different combinations of indices with their overall accuracy (OA), F1 score (F1), Matthews correlation coefficient (MCC) and the variance inflation factor (VIF).

Data	Logistic Regression Equation	OA	F1	MCC	VIF
MS	y = 0.9294608–0.3666048 NDVI - 1.386887 DVI - 1.005055 GNDVI	76.7 %	0.83	0.46	NDVI: 2.4 DVI: 1.5 GNDVI: 1.9
RGB	y = 0.5276535–0.7400043 GRVI - 0.869358 ExG - 0.6269988 RGRI	76.9 %	0.84	0.43	GRVI: 14.2 ExG: 1.3 RGRI: 13.8
MS and RGB	y = 1.024588–0.613737) NDVI - 1.44662 DVI - 0.8624887 ExG	77.2 %	0.83	0.48	NDVI: 1.8 DVI: 1.5 ExG: 1.3

that only a few severely damaged trees (class 4) existed on both study sites. We propose that classification performance could improve at sites with a higher prevalence of both healthy and severely damaged trees. This is because the contrast in spectral reflectance properties between the healthiest and most damaged trees is likely to provide clearer distinctions for analysis. Therefore, we suggest that further studies should especially focus on trees in class 4 and, if possible, also in class 0.

4.1. RGB and multispectral UAV data

Clear results could be obtained using RGB data for differentiation between mild and severe damage due to ash dieback. As outlined below, numerous studies have demonstrated similar results, emphasising the usability of RGB data in the context of plant diseases especially in agricultural crops. A significant relationship between RGB indices and winter wheat foliage disease severity has been proven using a low-cost UAV equipped with a digital camera (Bhandari et al., 2020). RGB images focusing on citrus trees (*Citrus* spp.) affected by diseases were able to demonstrate lower triangular greenness index (TGI) values for diseased trees (Garza et al., 2020). For the detection of narrow brown leaf spot severity in rice (*Oryza* spp.), the ExGR index was the most suitable for detecting high levels of disease (Cai et al., 2018). Various indices were tested for each case study and the success of each VI to differentiate between the damage severity varied greatly. In this study, the GRVI, ExG and RGRI were found to be capable of differentiating between mild and severe damage with the applied threshold with the highest accuracies. RGB VIs can amplify subtle differences in vegetation health that may not be visually discernible in raw RGB images, making them a valuable tool for in-depth plant health analysis by providing quantifiable and standardized metrics of vegetation condition.

The generated multispectral data in combination with various VIs and associated thresholds were also successfully applied to differentiate between mild and severe damage. Numerous studies utilized multispectral indices to identify disease occurrence or severity in plants. For citrus trees (*Citrus* spp.), infected by Citrus greening disease, four VIs demonstrated significant higher index values in healthy than in diseased trees (Chang et al., 2020). Multispectral indices were also suitable for the differentiation between healthy banana plants (*Musa* spp.) and plants affected by banana Fusarium wilt disease (Ye et al., 2020). The detection of canker infected citrus trees (*Citrus* spp.) was possible utilizing multispectral VIs (Abdulridha et al., 2019). Although in our study all multispectral indices were able to distinguish between mild and

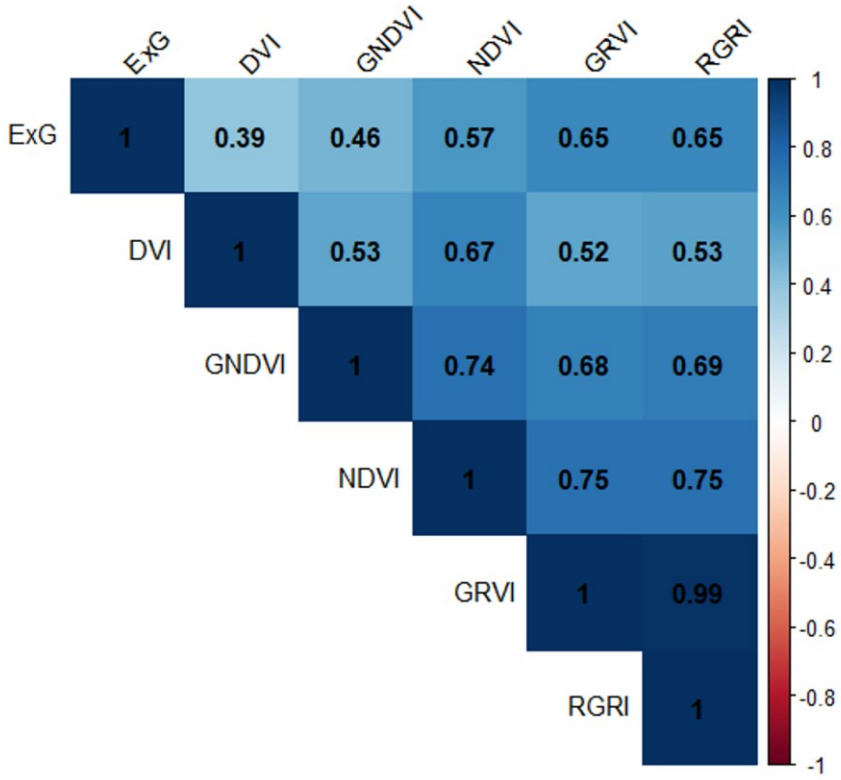

Fig. 5. Correlations between the three selected RGB and multispectral indices: ExG, DVI, GNDVI, NDVI, GRVI and RGRI.

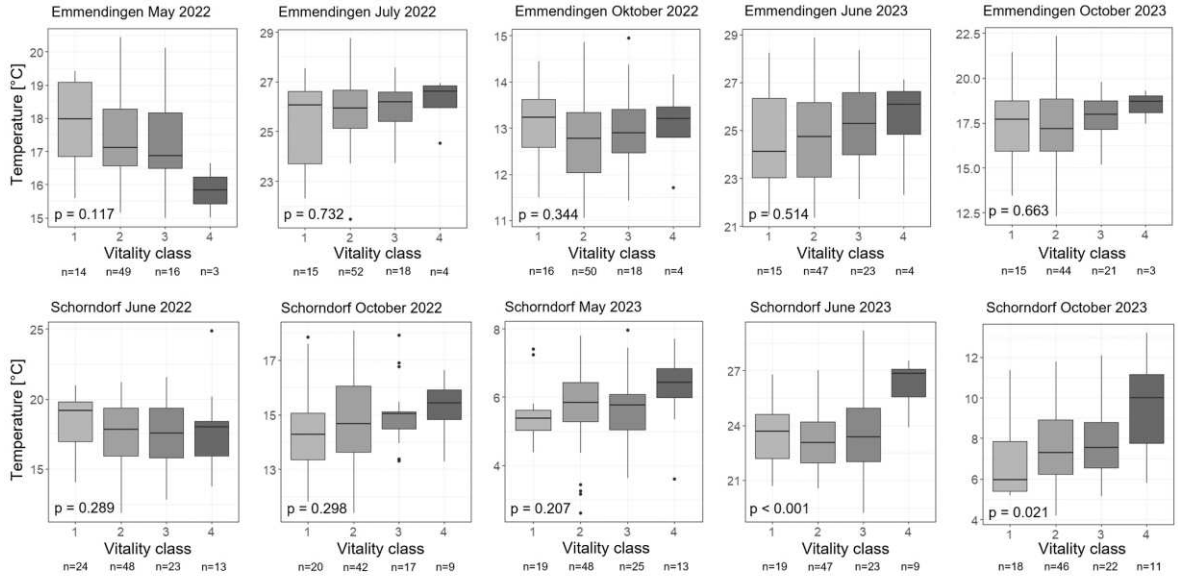

Fig. 6. Boxplots of the crown temperature of the ash trees for the different vitality classes for 2022 and 2023 for both study sites.

severe damage, the highest accuracies were achieved for the GNDVI, NDVI and DVI. While red-edge indices are often highlighted as being effective in identifying diseased plants (Chang et al., 2020, Ye et al., 2020), we found that they did not outperform indices without the red-edge band. Instead, the red, green, and NIR bands were particularly successful in determining the severity of damage caused by ash dieback.

Autumn UAV surveys for both RGB and multispectral data performed worse compared to those conducted in the summer. Overall, the autumn indices showed fewer significant differences between the four vitality classes than the indices calculated from the summer surveys. When factored into the calculated mean threshold, the accuracy of classifying the two damage classes was lower than during the summer months only, indicating reduced effectiveness. Since the autumn surveys were conducted in October, early stages of leaf senescence had likely begun, influencing the spectral reflectance of the leaves and reducing the observable effects of ash dieback. Despite this, VIs from October surveys effectively distinguished between mild and severe damage, confirming that UAV-based assessments are possible throughout the entire vegetation period of the common ash. However, thresholds solely from summer surveys were more reliable, making summer the recommended period for more accurate and stable assessments.

4.2. Thermal UAV data

The use of a thermal UAV camera in our study proved less effective than the RGB and multispectral data in distinguishing crown temperatures of ash trees in relation to disease severity. While an expected increase in crown temperature with more advanced symptoms of ash dieback was observed in seven out of ten conducted surveys, the difference between the damage classes were only seldom statistically significant. In contrast, numerous studies, focusing on agricultural crops, have demonstrated clearer results when applying thermal cameras for plant disease detection. For tomato (*Solanum* spp.) plants infected with *O. neolycopersici*, thermal images provided information in regards to the identification of diseased plants (Raza et al., 2015). Rose plants (*Rosa hybrida* L.), affected by powdery mildew (*Podosphaera pannosa var. rosae*) and gray mold (*Botrytis cinerea*) also presented clear changes in their thermal appearance (Jafari et al., 2017). With an accuracy of over 90 %, disease-induced spots in banana (*Musa* spp.) leaves were able to be identified using a thermal camera (Anasta et al., 2021). A significant leaf surface temperature increase was observed for avocado (*Persea americana* Mill.) plants infected with white root rot (Granum et al., 2015) as well as sunflower (*Helianthus annuus* L.) plants infected with *Orobanche cumana* (Ortiz-Bustos et al., 2017). However, these studies primarily focused on ground-based thermal images of individual leaves or smaller plants, allowing for precise identification of affected areas. In contrast, our study employed UAV-based thermal imaging at a flight height of 80 m above the ground, with an image resolution of 10.48 cm/pixel. This approach may have limited the ability to detect small areas of increased temperature associated with ash dieback and might not be represented proportionately in the final orthophoto. The mean temperature per tree crown calculated in this study could therefore underrepresent leaf areas with increased temperature due to an infection with ash dieback and the associated presumed stress-induced closure of stomata.

For detecting *Xylella fastidiosa* infections in olive (*Olea europaea*) orchards using remote sensing techniques, the integration of thermal imaging with multispectral data significantly enhanced identification accuracy, highlighting the potential of thermal remote sensing data to detect plant diseases (Poblete et al., 2020). Smigaj et al. (2015) proved that UAV-borne thermal image data can detect temperature differences linked to red band needle blight (*Dothistroma septosporum*) infection status at the tree level for pine trees (*Pinus sylvestris* and *Pinus contorta*) in a forest. Studies investigating leaf temperature changes in disease-inoculated plants have documented an initial temperature decrease before visible symptoms emerge, followed by a subsequent increase as the disease progresses. The pre-symptomatic temperature reduction is linked to stomatal opening, while the later rise above healthy tissue levels is associated with chlorosis and cell death (Lindenthal et al., 2005, Baranowski et al., 2015, Jafari et al., 2017). Therefore, contradicting results as found in our study, might hinder a clear interpretation of thermal images. In our approach, the mean crown temperature includes all leaves within a tree crown, meaning that variations in thermal dynamics due to differing infection statuses among the leaves cannot be ruled out and may counterbalance each other. The thermal sensor of the Mavic 2 EA has been proven to record temperatures with a deviation of up to 2 °C compared to ground-based temperature measurements (Leblanc et al., 2021). Additionally, factors such

as wind direction and flight speed can influence the accuracy of thermal imaging (Malbéteau et al., 2021). Although the captured thermal images were calibrated in terms of emissivity, relative humidity and camera-target-distance, inaccuracies related to the actual crown temperatures cannot be entirely excluded. Further studies would benefit from the inclusion of more severely damaged trees as these trees were underrepresented at our study sites. We suggest that this group of trees can be best delineated from other vitality classes, as demonstrated by most surveys in Schorndorf. In Emmendingen, proper conclusions are especially lacking due to the low number of ashes in class 4 with very severe damage ($n < 5$). Since the pattern observed in our study suggests that crown temperature differences exist, further investigations and a continuing monitoring of thermal characteristics in the context of ash dieback could be promising. UAV surveys with a lower flight height could improve the resolution of the images and are therefore recommended for further studies.

4.3. Vegetation index thresholding

The use of fixed threshold, whether to distinguish healthy from diseased plants or to differentiate between varying degrees of damage, provides a clear and practical method for interpreting VIs. Various thresholding techniques in the context of VIs and remote sensing data have already been tested in prior studies (Suh et al., 2020). Albetis et al. (2017) identified optimal thresholds for various VIs to distinguish grapevines (*Vitis vinifera* L.) affected by *Flavescence dorée* disease from healthy, symptom-free individuals. However, the optimal thresholds varied among the different studied cultivars, limiting the reproducibility. Similarly, VI thresholds calculated for *Flavescence dorée* disease and Grapevine Trunk Disease demonstrated the challenge of correctly distinguishing between the two diseases and asymptomatic plants (Albetis et al., 2019).

In our study, a perfect separation of mild and severe damage due to ash dieback using a threshold was difficult to achieve. The highest accuracy of 74.9 % was obtained calculating the DVI threshold. However, the overlap between mild and severe damage classes likely reflects the "fluid" health status of the ash trees, which were categorized into fixed classes. The vitality assessments in the field relied on the observer's judgment, and although all evaluations were performed by the same trained expert, minor discrepancies may have occurred. The distinction between class 2, representing mild damage, and class 3, representing severe damage, is often minimal, e.g., for the least healthy trees in class 2 and the healthiest trees in class 3. Since the use of a threshold is highly praxis-oriented, this study focused on a simple, manageable workflow for forest practitioners as an alternative to more complex classifying methods, an approach also emphasized by Otsu et al. (2019).

The correlation analysis of the three RGB and three multispectral indices indicated high correlations between all indices. As a result, combining multiple indices – whether RGB, multispectral, or a mix of both – did not substantially improve classification accuracy. The most promising combination in determining the severity of ash dieback damage, with an accuracy of 77.2 %, was achieved combining the two multispectral indices NDVI and DVI and the RGB index ExG. However, due to the limited number of datasets, the training datasets used to calculate the mean thresholds were resampled for validation, which may result in slightly higher accuracy scores, as noted by Yadav and Shukla (2016).

Few studies have aimed to classify ash dieback severity using remote sensing data, and achieving fully accurate classifications remains a challenge. Waser et al. (2014) used WorldView-2 satellite data with 19 VIs to classify four levels of ash health in a German forest site, achieving an overall accuracy of 77 %, which is similar to our classification results. An analysis using hyperspectral forest data, providing a broader range of wavelengths, likewise reached a 77 % accuracy in classifying damage severity within a Random Forest model (Chan et al., 2021). Polk et al. (2022) identified ash trees infected with *Hymenoscyphus fraxineus* at a forest site without focusing on severity, achieving 71 % accuracy using hyperspectral data. In another study, Kampen et al. (2019) used UAV-based multispectral data and a Random Forest classifier to identify five levels of ash dieback severity at an ash seed orchard, achieving an accuracy of 61.7 %. The results of these studies highlight the difficulty of correctly separating ash dieback damage classes.

The differentiation of damage severity, however, can be achieved not only with hyper- or multispectral data. As our study revealed, a single RGB index, such as GRVI, can also be used to determine damage severity with an OA of 73 %. While ash seed orchards offer advantages in detecting individual ash trees, previous studies have shown that ash dieback severity analysis can also be achieved in forest sites (Waser et al., 2014, Chan et al., 2021, Polk et al., 2022).

Both RGB and multispectral data effectively assess ash dieback severity using VIs and thresholds, though thermal data was less effective. Multispectral data provided slightly higher classification accuracy, but RGB data also performed well. While both UAV systems are similar in cost and usability, multispectral cameras are generally more expensive and complex to operate.

Ash dieback presents an important threat to common ash trees across Europe, and largescale health assessments of affected trees have been highly time-consuming and labor-intensive. The use of fixed thresholds applied to orthophotos generated from UAV surveys offers new, practical opportunities for assessing the health status of *Fraxinus excelsior* L. This method offers a significant time advantage, particularly for large-scale assessments, while also enabling the monitoring of otherwise inaccessible areas. Beyond health monitoring, this approach also holds potential for large-scale phenotyping and other applications. For conservation purposes, identifying ash trees with only mild damage symptoms is particularly relevant, as some individuals exhibit greater resistance to ash dieback than others (McKinney et al., 2011). Our method allows for the detection of trees with mild damage and facilitates long-term monitoring of their health status, which is crucial for further investigation and conservation efforts. Although this study focuses on ash seed orchards with relatively high tree spacing, the outlined approach is also applicable to forest stands. However, before applying the established VI thresholds, it is essential to identify the individual ash trees, e.g. as demonstrated by Waser et al. (2014) and Chan et al. (2021). Since our determined thresholds are based on the normalized range of VIs, applying them requires following our proposed workflow.

Due to the fluid progression of the state of health, a 100 % accurate classification of the damage in accordance with the field assessment is likely very difficult to achieve, however an estimation of the health status based on VIs is possible. The application of thresholds can enable targeted forestry care efforts to conserve this endangered tree species. Given current recommendation to preserve mildly affected ash trees rather than remove them (FNR, 2024), identifying trees with mild damage is highly relevant. With the ongoing progression of ash dieback, accurately identifying mildly damaged ash trees will become increasingly important for the long-term conservation of *Fraxinus excelsior* L.

5. Conclusion

UAV images are an important tool to investigate large areas of ash trees affected by ash dieback in a short time. Our study determined that UAV images captured during the summer months yield the most consistent results, offering comparable VI thresholds. Both RGB and multispectral data successfully enabled the generation of multiple VIs capable of identifying damage severity due to ash dieback. The thresholds derived in this study represent an important advancement for assessing extensive areas of affected ash trees, with single indices achieving classification accuracies of up to 74.9 % for estimating disease severity. The straightforward workflow, along with the specified thresholds for various indices, offers forest practitioners an important tool for identifying and managing ash dieback damage. However, given that our datasets were spatially, and temporally limited, further research

focused on refining these thresholds and enhancing classification accuracy is recommended.

Funding

This study was conducted within the project FraxVir "Detection, characterisation and analyses of the occurrence of viruses and ash dieback in special stands of *Fraxinus excelsior* – a supplementary study to the FraxForFuture demonstration project" and receives funding via the Waldklimafonds (WKF) funded by the German Federal Ministry of Food and Agriculture (BMEL) and Federal Ministry for the Environment, Nature Conservation, Nuclear Safety and Consumer Protection (BMUV) administrated by the Agency for Renewable Resources (FNR) under grant agreement 2220WK40A4.

CRediT authorship contribution statement

Lisa Buchner: Writing – original draft, Methodology, Investigation, Formal analysis. **Anna-Katharina Eisen:** Writing – review & editing, Methodology. **Susanne Jochner-Oette:** Writing – review & editing, Supervision, Funding acquisition, Conceptualization.

Declaration of Generative AI and AI-assisted technologies in the writing process

During the preparation of this work the authors used ChatGPT in order to improve readability and grammar of a few sentences. After using this tool, the authors reviewed and edited the content as needed and take full responsibility for the content of the published article.

Declaration of Competing Interest

The authors declare that they have no known competing financial interests or personal relationships that could have appeared to influence the work reported in this paper.

Acknowledgements

We thank the Forestry Baden-Wuerttemberg and the Forest Research Institute Baden-Wuerttemberg for providing the seed orchards as study sites. We thank Tobias Heckmann and Manuel Stark for insightful discussions and support. Special thanks to all student assistants and Kathrin and Marlene Buchner for their technical assistance.

Data availability

Data will be made available on request.

References

Abd El-Ghany, N.M., Abd El-Aziz, S.E., Marei, S.S., 2020. A review: application of remote sensing as a promising strategy for insect pests and diseases management. Environ. Sci. Pollut. Res. Int. 27 (27), 33503–33515. https://doi.org/10.1007/s11356-020-09517-2.

Abdulridha, J., Batuman, O., Ampatzidis, Y., 2019. UAV-based remote sensing technique to detect citrus canker disease utilizing hyperspectral imaging and machine learning. Remote Sens. 11 (11), 1373. https://doi.org/10.3390/rs11111373.

Albetis, J., Duthoit, S., Guttler, F., Jacquin, A., Goulard, M., Poilvé, H., Féret, J.-B., Dedieu, G., 2017. Detection of *Flavescence dorée* grapevine disease using Unmanned aerial vehicle (UAV) multispectral imagery. Remote Sens. 9 (4), 308. https://doi.org/10.3390/rs9040308.

Albetis, J., Jacquin, A., Goulard, M., Poilvé, H., Rousseau, J., Clenet, H., Dedieu, G., Duthoit, S., 2019. On the potentiality of UAV multispectral imagery to detect *Flavescence dorée* and grapevine trunk diseases. Remote Sens. 11 (1), 23. https://doi.org/10.3390/rs11010023.

Anasta, N., Setyawan, F.X.A., Fitriawan, H., 2021. Disease detection in banana trees using an image processing-based thermal camera. IOP Conf. Ser. Earth Environ. Sci. 739 (1), 12088. https://doi.org/10.1088/1755-1315/739/1/012088.

Ashourloo, D., Mobasheri, M., Huete, A., 2014. Evaluating the effect of different wheat rust disease symptoms on vegetation indices using hyperspectral measurements. Remote Sens. 6 (6), 5107–5123. https://doi.org/10.3390/rs6065107.

Baral, H.-O., Queloz, V., Hosoya, T., 2014. *Hymenoscyphus fraxineus*, the correct scientific name for the fungus causing ash dieback in Europe. Int. Mycol. Assoc. Fungus 79–80.

Baranowski, P., Jedryczka, M., Mazurek, W., Babula-Skowronska, D., Siedliska, A., Kaczmarek, J., 2015. Hyperspectral and thermal imaging of oilseed rape (*Brassica napus*) response to fungal species of the genus Alternaria. PloS One 10 (3), e0122913. https://doi.org/10.1371/journal.pone.0122913.

Barbedo, J., 2019. A review on the use of unmanned aerial vehicles and imaging sensors for monitoring and assessing plant stresses. Drones 3 (2), 40. https://doi.org/10.3390/drones3020040.

Barbosa, B.D.S., Araújo e Silva Ferraz, G., Mendes dos Santos, L., Santana, L.S., Bedin Marin, D., Rossi, G., Conti, L., 2021. Application of RGB images obtained by UAV in coffee farming. Remote Sens. 13 (12), 2397. https://doi.org/10.3390/rs13122397.

Bendig, J., Yu, K., Aasen, H., Bolten, A., Bennertz, S., Broscheit, J., Gnyp, M.L., Bareth, G., 2015. Combining UAV-based plant height from crop surface models, visible, and near infrared vegetation indices for biomass monitoring in barley. Int. J. Appl. Earth Obs. Geoinf. 39, 79–87. https://doi.org/10.1016/j.jag.2015.02.012.

Bhandari, M., Ibrahim, A.M., Xue, Q., Jung, J., Chang, A., Rudd, J.C., Maeda, M., Rajan, N., Neely, H., Landivar, J., 2020. Assessing winter wheat foliage disease severity using aerial imagery acquired from small Unmanned aerial vehicle (UAV). Comput. Electron. Agric. 176, 105665. https://doi.org/10.1016/j.compag.2020.105665.

Buchner, L., Eisen, A.-K., Jochner-Oette, S., 2024. Effects of ash dieback on leaf physiology and leaf morphology of *Fraxinus excelsior* L. Trees. https://doi.org/10.1007/s00468-024-02546-1.

Buchner, L., Eisen, A.-K., Sikoparija, B., Jochner-Oette, S., 2022. Pollen viability of *Fraxinus excelsior* in storage experiments and investigations on the potential effect of long-range transport. Forests 13 (4), 600. https://doi.org/10.3390/f13040600.

Bundesministerium für Ernährung und Landwirtschaft (BMEL) (2024) Der Wald in Deutschland - Ausgewählte Ergebnisse der vierten Bundeswaldinventur.

Cai, N., Zhou, X., Yang, Y., Wang, J., Zhang, D., Hu, R., 2018. Use of UAV images to assess narrow brown leaf spot severity in rice. Int. J. Precis. Agric. Aviat. 1 (1), 38–42. https://doi.org/10.33440/j.ijpaa.20190202.47.

Candiago, S., Remondino, F., Giglio, M. de, Dubbini, M., Gattelli, M., 2015. Evaluating multispectral images and vegetation indices for precision farming applications from UAV images. Remote Sens. 7 (4), 4026–4047. https://doi.org/10.3390/rs70404026.

Castro, A.I. de, Shi, Y., Maja, J.M., Peña, J.M., 2021. UAVs for vegetation monitoring: overview and recent scientific contributions. Remote Sens. 13 (11), 2139. https://doi.org/10.3390/rs13112139.

Chaerle, L., van Caeneghem, W., Messens, E., Lambers, H., van Montagu, M., van der Straeten, D., 1999. Presymptomatic visualization of plant–virus interactions by thermography. Nat. Biotechnol. 17, 813–816.

Chan, A.H.Y., Barnes, C., Swinfield, T., Coomes, D.A., 2021. Monitoring ash dieback (*Hymenoscyphus fraxineus*) in british forests using hyperspectral remote sensing. Remote Sens Ecol. Conserv 7 (2), 306–320. https://doi.org/10.1002/rse2.190.

Chang, A., Yeom, J., Jung, J., Landivar, J., 2020. Comparison of canopy shape and vegetation indices of citrus trees derived from UAV multispectral images for characterization of citrus greening disease. Remote Sens. 12 (24), 4122. https://doi.org/10.3390/rs12244122.

Chicco, D., Jurman, G., 2020. The advantages of the Matthews correlation coefficient (MCC) over F1 score and accuracy in binary classification evaluation. BMC Genom. 21 (1), 6. https://doi.org/10.1186/s12864-019-6413-7.

Choosumrong, S., Hataitara, R., Sujipuli, K., Weerawatanakorn, M., Preechaharn, A., Premjet, D., Laywisadkul, S., Raghavan, V., Panumonwatee, G., 2023. Bananas diseases and insect infestations monitoring using multi-spectral camera RTK UAV images. Spat. Inf. Res. 31 (4), 371–380. https://doi.org/10.1007/s41324-022-00504-y.

Coker, T.L.R., Rozsypálek, J., Edwards, A., Harwood, T.P., Butfoy, L., Buggs, R.J.A., 2019. Estimating mortality rates of European ash (*Fraxinus excelsior*) under the ash dieback (*Hymenoscyphus fraxineus*) epidemic. Plants People Planet 1 (1), 48–58. https://doi.org/10.1002/ppp3.11.

Dalponte, M., Reyes, F., Kandare, K., Gianelle, D., 2015. Delineation of individual tree crowns from ALS and hyperspectral data: a comparison among four methods. Eur. J. Remote Sens. 48 (1), 365–382. https://doi.org/10.5721/EuJRS20154821.

Dash, J.P., Watt, M.S., Pearse, G.D., Heaphy, M., Dungey, H.S., 2017. Assessing very high resolution UAV imagery for monitoring forest health during a simulated disease outbreak. ISPRS J. Photogramm. Remote Sens. 131, 1–14. https://doi.org/10.1016/j.isprsjprs.2017.07.007.

DJI (2022) DJI Mavic 3M User Manual.

Eisen, A.-K., Buchner, L., Fussi, B., Jochner-Oette, S., 2024. Does ash dieback affect the reproductive ecology of *Fraxinus excelsior* L.? J. For. Res. 35 (1). https://doi.org/10.1007/s11676-023-01670-x.

Enderle, R., Fussi, B., Lenz, H.D., Langer, G., Nagel, R., Metzler, B., 2017a. Ash dieback in Germany: research on disease development, resistance and management options. In: Vasaitis, R., Enderle, R. (Eds.), Dieback of European Ash (*Fraxinus* spp.) - Consequences and Guidelines for Sustainable Management. Swedish University of Agricultural Sciences, Uppsala, Schweden, pp. 89–105.

Enderle, R., Nakou, A., Thomas, K., Metzler, B., 2015. Susceptibility of autochthonous German *Fraxinus excelsior* clones to *Hymenoscyphus pseudoalbidus* is genetically determined. Ann. For. Sci. 72 (2), 183–193. https://doi.org/10.1007/s13595-014-0413-1.

Enderle, R., Sander, F., Metzler, B., 2017b. Temporal development of collar necroses and butt rot in association with ash dieback. iForest 10 (3), 529–536. https://doi.org/10.3832/ifor2407-010.

Enderle, R., Stenlid, J., Vasaitis, R., 2019. An overview of ash (*Fraxinus* spp.) and the ash dieback disease in Europe. CABI Rev. 1–12. https://doi.org/10.1079/PAVSNNR201914025.

Fawcett, T., 2006. An introduction to ROC analysis. Pattern Recognit. Lett. 27 (8), 861–874. https://doi.org/10.1016/j.patrec.2005.10.010.
Fachagentur Nachwachsende Rohstoffe e. V. (FNR) (2024) Zukunft der Esche. Empfehlungen zum forstbetrieblichen Umgang mit dem Eschentriebsterben.
Foody, G.M., 2023. Challenges in the real world use of classification accuracy metrics: from recall and precision to the Matthews correlation coefficient. PloS One 18 (10), e0291908. https://doi.org/10.1371/journal.pone.0291908.
Fuchs, S., Häuser, H., Peters, S., Knauf, L., Rentschler, F., Kahlenberg, G., Kätzel, R., Evers, J., Paar, U., Langer, G.J., 2024. Ash dieback assessments on intensive monitoring plots in Germany: influence of stand, site and time on disease progression. J. Plant Dis. Prot. https://doi.org/10.1007/s41348-024-00889-y.
Garza, B.N., Ancona, V., Enciso, J., Perotto-Baldivieso, H.L., Kunta, M., Simpson, C., 2020. Quantifying citrus tree health using true color UAV images. Remote Sens. 12 (1), 170. https://doi.org/10.3390/rs12010170.
Granum, E., Pérez-Bueno, M.L., Calderón, C.E., Ramos, C., Vicente, A. de, Cazorla, F.M., Barón, M., 2015. Metabolic responses of avocado plants to stress induced by *Rosellinia necatrix* analysed by fluorescence and thermal imaging. Eur. J. Plant Pathol. 142 (3), 625–632. https://doi.org/10.1007/s10658-015-0640-9.
Guo, A., Huang, W., Dong, Y., Ye, H., Ma, H., Liu, B., Wu, W., Ren, Y., Ruan, C., Geng, Y., 2021. Wheat yellow rust detection using UAV-based hyperspectral technology. Remote Sens. 13 (1), 123. https://doi.org/10.3390/rs13010123.
Harrap, M.J.M., Hempel de Ibarra, N., Whitney, H.M., Rands, S.A., 2018. Reporting of thermography parameters in biology: a systematic review of thermal imaging literature. R. Soc. Open Sci. 5 (12), 181281. https://doi.org/10.1098/rsos.181281.
Hashim, I.C., Shariff, A.R.M., Bejo, S.K., Muharam, F.M., Ahmad, K., Hashim, H., 2020. Application of thermal imaging for plant disease detection. IOP Conf. Ser. Earth Environ. Sci. 540 (1), 12052. https://doi.org/10.1088/1755-1315/540/1/012052.
Holzwarth, S., Thonfeld, F., Kacic, P., Abdullahi, S., Asam, S., Coleman, K., Eisfelder, C., Gessner, U., Huth, J., Kraus, T., Shatto, C., Wessel, B., Kuenzer, C., 2023. Earth-observation-based monitoring of forests in Germany—recent progress and research frontiers: a review. Remote Sens. 15 (17), 4234. https://doi.org/10.3390/rs15174234.
Huete, A.R., 2012. Vegetation indices, remote sensing and forest monitoring. Geogr. Compass 6 (9), 513–532. https://doi.org/10.1111/j.1749-8198.2012.00507.x.
Hultberg, T., Sandström, J., Felton, A., Öhman, K., Rönnberg, J., Witzell, J., Cleary, M., 2020. Ash dieback risks an extinction cascade. Biol. Conserv. 244, 108516. https://doi.org/10.1016/j.biocon.2020.108516.
Jafari, M., Minaei, S., Safaie, N., 2017. Detection of pre-symptomatic rose powdery-mildew and gray-mold diseases based on thermal vision. Infrared Phys. Technol. 85, 170–183. https://doi.org/10.1016/j.infrared.2017.04.023.
James, G., Witten, D., Hastie, T., Tibshirani, R., Taylor, J., 2023. An Introduction to Statistical Learning. Springer International Publishing, Cham.
Jie, P., Heng, Z., Yunwei, J., Zhenfeng, L., 2015. Early monitoring of pine wilt disease in *Pinus massioniana* based on hyperspectral data. Plant Dis. Pests 6 (4-5), 1–5.
Kampen, M., Lederbauer, S., Mund, J.-P., Immitzer, M., 2019. UAV-based multispectral data for tree species classification and tree vitality analysis. Dreiländertagung der DGPF, der OOVG und der SGPF in Wien. Österreich (28).
Kattenborn T. (2023) DJI thermal rpeg to tif (v. 0.5). ⟨https://github.com/tejakattenborn/dji_h20t_rpeg_to_tif⟩.
Kleinsmann, J., Verbesselt, J., Kooistra, L., 2023. Monitoring individual tree phenology in a multi-species forest using high resolution UAV images. Remote Sens. 15 (14), 3599. https://doi.org/10.3390/rs15143599.
Kowalski, T., 2006. *Chalara fraxinea* sp. nov. associated with dieback of ash (*Fraxinus excelsior)* in Poland. For. Pathol. 36, 264–270. https://doi.org/10.1111/j.1439-0329.2006.00453.x.
Leblanc, G., Kalacska, M., Arroyo-Mora, J.P., Lucanus, O., Todd, A., 2021. A practical validation of uncooled thermal imagers for small RPAS. Drones 5 (4), 132. https://doi.org/10.3390/drones5040132.
Lee, S., Pradhan, B., 2007. Landslide hazard mapping at Selangor, Malaysia using frequency ratio and logistic regression models. Landslides 4 (1), 33–41. https://doi.org/10.1007/s10346-006-0047-y.
Lenz, H., Straßer, L., Baumann, M., Baier, U., 2012. Boniturschlüssel zur Einstufung der Vitalität von Alteschen. AFZ-DerWald 18–19.
Lindenthal, M., Steiner, U., Dehne, H.-W., Oerke, E.-C., 2005. Effect of downy mildew development on transpiration of cucumber leaves visualized by digital infrared thermography. Am. Phytopathol. Soc. 95 (3), 233–240. https://doi.org/10.1094/PHYTO-95-0233.
Lussem, U., Bolten, A., Gnyp, M.L., Jasper, J., Bareth, G., 2018. Evaluation of RGB-based vegetation indices from UAV imagery to estimate forage yield in grassland. Int. Arch. Photogramm. Remote Sens. Spat. Inf. Sci. XLII-3, 1215–1219. https://doi.org/10.5194/isprs-archives-XLII-3-1215-2018.
Mahlein, A.-K., Rumpf, T., Welke, P., Dehne, H.-W., Plümer, L., Steiner, U., Oerke, E.-C., 2013. Development of spectral indices for detecting and identifying plant diseases. Remote Sens. Environ. 128, 21–30. https://doi.org/10.1016/j.rse.2012.09.019.
Malbéteau, Y., Johansen, K., Aragon, B., Al-Mashhawari, S.K., McCabe, M.F., 2021. Overcoming the challenges of thermal infrared orthomosaics using a swath-based approach to correct for dynamic temperature and wind effects. Remote Sens. 13 (16), 3255. https://doi.org/10.3390/rs13163255.
McKinney, L.V., Nielsen, L.R., Hansen, J.K., Kjær, E.D., 2011. Presence of natural genetic resistance in *Fraxinus excelsior* (Oleraceae) to *Chalara fraxinea* (Ascomycota): an emerging infectious disease. Heredity 106 (5), 788–797. https://doi.org/10.1038/hdy.2010.119.
Metzler, B., Herbstritt, S., 2014. Sicherheitsrisiko durch Stammfußnekrosen an Eschen, insbesondere auf Nassstandorten. FVA Waldschutz-INFO.
Miraki, M., Sohrabi, H., Fatehi, P., Kneubuehler, M., 2021. Individual tree crown delineation from high-resolution UAV images in broadleaf forest. Ecol. Inf. 61, 101207. https://doi.org/10.1016/j.ecoinf.2020.101207.
Mitchell, R.J., Broome, A., Beaton, J.K., Bellamy, P.E., Ellis, C.J., Hester, A.J., Hodgetts, N.G., Iason, G.R., Littlewood, N.A., Newey, S., Pozsgai, G., Ramsay, S., Riach, D., Stockan, J.A., Taylor, A.F.S., Woodward, S., 2017. Challenges in assessing the ecological impacts of tree diseases and mitigation measures: the case of *Hymenoscyphus fraxineus* and *Fraxinus excelsior*. Balt. For. 23 (1), 116–140.
Mohan, M., Silva, C., Klauberg, C., Jat, P., Catts, G., Cardil, A., Hudak, A., Dia, M., 2017. Individual tree detection from unmanned aerial vehicle (UAV) derived canopy height model in an open canopy mixed conifer forest. Forests 8 (9), 340. https://doi.org/10.3390/f8090340.
Murfitt, J., He, Y., Yang, J., Mui, A., Mille, K. de, 2016. Ash decline assessment in emerald ash borer infested natural forests using high spatial resolution images. Remote Sens. 8 (3), 256. https://doi.org/10.3390/rs8030256.
Neupane, K., Baysal-Gurel, F., 2021. Automatic identification and monitoring of plant diseases using unmanned aerial vehicles: a review. Remote Sens. 13 (19), 3841. https://doi.org/10.3390/rs13193841.
Ortiz-Bustos, C.M., Pérez-Bueno, M.L., Barón, M., Molinero-Ruiz, L., 2017. Use of blue-green fluorescence and thermal imaging in the early detection of sunflower infection by the root parasitic weed *Orobanche cumana* Wallr. Front. Plant Sci. 8, 833. https://doi.org/10.3389/fpls.2017.00833.
Otsu, K., Pla, M., Duane, A., Cardil, A., Brotons, L., 2019. Estimating the threshold of detection on tree crown defoliation using vegetation indices from UAS multispectral Imagery. Drones 3 (4), 80. https://doi.org/10.3390/drones3040080.
Panagiotidis, D., Abdollahnejad, A., Surový, P., Chiteculo, V., 2017. Determining tree height and crown diameter from high-resolution UAV imagery. Int. J. Remote Sens. 38 (8-10), 2392–2410. https://doi.org/10.1080/01431161.2016.1264028.
Park, J., Muller-Landau, H., Lichstein, J., Rifai, S., Dandois, J., Bohlman, S., 2019. Quantifying leaf pheNology of Individual Trees and Species in A Tropical Forest Using Unmanned Aerial Vehicle (UAV) images. Remote Sens. 11 (13), 1534. https://doi.org/10.3390/rs11131534.
Pautasso, M., Aas, G., Queloz, V., Holdenrieder, O., 2013. European ash (*Fraxinus excelsior*) dieback – a conservation biology challenge. Biol. Conserv. 158, 37–49. https://doi.org/10.1016/j.biocon.2012.08.026.
Peters, S., Langer, G., Kätzel, R. (Eds.), 2021. Eschentriebsterben. Kriterien zur Schadensbonitur an Eschen, 1. Auflage. Fachagentur Nachwachsende Rohstoffe (FNR), Gülzow-Prüzen.
Poblete, T., Camino, C., Beck, P., Hornero, A., Kattenborn, T., Saponari, M., Boscia, D., Navas-Cortes, J.A., Zarco-Tejada, P.J., 2020. Detection of *Xylella fastidiosa* infection symptoms with airborne multispectral and thermal imagery: assessing bandset reduction performance from hyperspectral analysis. ISPRS J. Photogramm. Remote Sens. 162, 27–40. https://doi.org/10.1016/j.isprsjprs.2020.02.010.
Polk, S.L., Chan, A.H.Y., Cui, K., Plemmons, R.J., Coomes, D.A., Murphy, J.M., 2022. Unsupervised detection of ash dieback disease (Hymenoscyphus fraxineus) using diffusion-based hyperspectral image clustering. IGARSS 2022 - 2022 IEEE Int. Geosci. Remote Sens. Symp. 2287–2290. https://doi.org/10.1109/IGARSS46834.2022.9883429.
Pontius, J., Martin, M., Plourde, L., Hallett, R., 2008. Ash decline assessment in emerald ash borer-infested regions: a test of tree-level, hyperspectral technologies. Remote Sens. Environ. 112 (5), 2665–2676. https://doi.org/10.1016/j.rse.2007.12.011.
Qiu, L., Jing, L., Hu, B., Li, H., Tang, Y., 2020. A new individual tree crown delineation method for high resolution multispectral imagery. Remote Sens. 12 (3), 585. https://doi.org/10.3390/rs12030585.
Raza, S.-A., Prince, G., Clarkson, J.P., Rajpoot, N.M., 2015. Automatic detection of diseased tomato plants using thermal and stereo visible light images. PloS One 10 (4), e0123262. https://doi.org/10.1371/journal.pone.0123262.
Sanseechan, P., Saengprachathanarug, K., Posom, J., Wongpichet, S., Chea, C., Wongphati, M., 2019. Use of vegetation indices in monitoring sugarcane white leaf disease symptoms in sugarcane field using multispectral UAV aerial imagery. IOP Conf. Ser. Earth Environ. Sci. 301 (1), 12025. https://doi.org/10.1088/1755-1315/301/1/012025.
Skovsgaard, J.P., Wilhelm, G.J., Thomsen, I.M., Metzler, B., Kirisits, T., Havrdová, L., Enderle, R., Dobrowolska, D., Cleary, M., Clark, J., 2017. Silvicultural strategies for *Fraxinus excelsior* in response to dieback caused by *Hymenoscyphus fraxineus*. For. Int. J. For. Res. 90 (4), 455–472. https://doi.org/10.1093/forestry/cpx012.
Smigaj, M., Gaulton, R., Barr, S.L., Suárez, J.C., 2015. UAV-borne thermal imaging for forest health monitoring: detection of disease-induced canopy temperature increase. Int. Arch. Photogramm. Remote Sens. Spat. Inf. Sci. XL-3/W3, 349–354. https://doi.org/10.5194/isprsarchives-XL-3-W3-349-2015.
Starý, K., Jelínek, Z., Kumhálová, J., Chyba, J., Balážová, K., 2020. Comparing RGB-based vegetation indices from UAV imageries to estimate hops canopy area. 10.15159/AR.20.169.
Steddom, K., Bredehoeft, M.W., Khan, M., Rush, C.M., 2005. Comparison of visual and multispectral radiometric disease evaluations. Plant Dis. 153–158. https://doi.org/10.1094/PD-89-0153.
Suh, H.K., Hofstee, J.W., van Henten, E.J., 2020. Investigation on combinations of colour indices and threshold techniques in vegetation segmentation for volunteer potato control in sugar beet. Comput. Electron. Agric. 179, 105819. https://doi.org/10.1016/j.compag.2020.105819.
Timmermann, V., Børja, I., Hietala, A.M., Kirisits, T., Solheim, H., 2011. Ash dieback: pathogen spread and diurnal patterns of ascospore dispersal, with special emphasis on Norway. OEPP/EPPO Bull. 41, 14–20. https://doi.org/10.1111/j.1365-2338.2010.02429.x.
Torresan, C., Berton, A., Carotenuto, F., Di Gennaro, S.F., Gioli, B., Matese, A., Miglietta, F., Vagnoli, C., Zaldei, A., Wallace, L., 2017. Forestry applications of UAVs

in Europe: a review. Int. J. Remote Sens. 38 (8-10), 2427–2447. https://doi.org/10.1080/01431161.2016.1252477.

Torres-Sánchez, J., Peña, J.M., Castro, A.I. de, López-Granados, F., 2014. Multi-temporal mapping of the vegetation fraction in early-season wheat fields using images from UAV. Comput. Electron. Agric. 103, 104–113. https://doi.org/10.1016/j.compag.2014.02.009.

Vilela, E.F., Da Silva, C.A., Botti, J.M.C., Martins, E.F., Santana, C.C., Marin, D.B., Freitas, A.Rd.J., Jaramillo-Giraldo, C., Lopes, I.Pd.C., Corrêdo, Ld.P., Queiroz, D.M. de, Rossi, G., Bambi, G., Conti, L., Venzon, M., 2024. Detection of coffee leaf miner using RGB aerial imagery and machine learning. AgriEngineering 6 (3), 3174–3186. https://doi.org/10.3390/agriengineering6030181.

Waser, L., Küchler, M., Jütte, K., Stampfer, T., 2014. Evaluating the potential of worldview-2 data to classify tree species and different levels of ash mortality. Remote Sens. 6 (5), 4515–4545. https://doi.org/10.3390/rs6054515.

Wu, D., Yu, L., Yu, R., Zhou, Q., Li, J., Zhang, X., Ren, L., Luo, Y., 2023. Detection of the monitoring window for pine wilt disease using multi-temporal UAV-based multispectral imagery and machine learning algorithms. Remote Sens. 15 (2), 444. https://doi.org/10.3390/rs15020444.

Xue, J., Su, B., 2017. Significant remote sensing vegetation indices: a review of developments and applications. J. Sens. 2017, 1–17. https://doi.org/10.1155/2017/1353691.

Yadav, S., Shukla, S., 2016. Analysis of k-Fold cross-validation over hold-out validation on colossal datasets for quality classification. 2016 IEEE 6th Int. Conf. Adv. Comput. (IACC) 78–83. https://doi.org/10.1109/IACC.2016.25.

Ye, H., Huang, W., Huang, S., Cui, B., Dong, Y., Guo, A., Ren, Y., Jin, Y., 2020. Recognition of banana Fusarium wilt based on UAV remote sensing. Remote Sens. 12 (6), 938. https://doi.org/10.3390/rs12060938.

Zhang, J., Virk, S., Porter, W., Kenworthy, K., Sullivan, D., Schwartz, B., 2019. Applications of unmanned aerial vehicle based imagery in turfgrass field trials. Front. Plant Sci. 10, 279. https://doi.org/10.3389/fpls.2019.00279.

4.3 How precise is precise enough? Tree crown segmentation using high resolution close-up multispectral UAV images and its effect on NDVI accuracy in *Fraxinus excelsior* L. trees

Journal of Forestry Research (2025) 36:137
https://doi.org/10.1007/s11676-025-01929-5

ORIGINAL PAPER

How precise is precise enough? Tree crown segmentation using high resolution close-up multispectral UAV images and its effect on NDVI accuracy in *Fraxinus excelsior* L. trees

Lisa Buchner[1] · Anna-Katharina Eisen[1] · Susanne Jochner-Oette[1]

Received: 13 May 2025 / Accepted: 24 June 2025

Abstract Detailed individual tree crown segmentation is highly relevant for the detection and monitoring of *Fraxinus excelsior* L. trees affected by ash dieback, a major threat to common ash populations across Europe. In this study, both fine and coarse crown segmentation methods were applied to close-range multispectral UAV imagery. The fine tree crown segmentation method utilized a novel unsupervised machine learning approach based on a blended NIR–NDVI image, whereas the coarse segmentation relied on the segment anything model (SAM). Both methods successfully delineated tree crown outlines, however, only the fine segmentation accurately captured internal canopy gaps. Despite these structural differences, mean NDVI values calculated per tree crown revealed no significant differences between the two approaches, indicating that coarse segmentation is sufficient for mean vegetation index assessments. Nevertheless, the fine segmentation revealed increased heterogeneity in NDVI values in more severely damaged trees, underscoring its value for detailed structural and health analyses. Furthermore, the fine segmentation workflow proved transferable to both individual UAV images and orthophotos from broader UAV surveys. For applications focused on structural integrity and spatial variation in canopy health, the fine segmentation approach is recommended.

Keywords Leaf mass segmentation · Machine learning · Segment anything model · Ash dieback

Introduction

Remote sensing technologies provide powerful tools for surveying large-scale tree populations, enabling efficient, long-term monitoring of tree health and disease progression across broad landscapes. Unmanned aerial vehicles (UAVs) equipped with different sensor types have been proven to be suitable for the identification and monitoring of plant diseases in the context of various species (Torresan et al. 2017; Barbedo 2019). Disease-induced damage symptoms can often be detected through changes in reflectance within the visible and near-infrared (NIR) spectrum. Multispectral sensors mounted on UAVs are particularly well-suited for detecting diseased plants, offering high spatial resolution and the ability to capture subtle physiological changes across large areas (Zhang et al. 2019; Neupane and Baysal-Gurel 2021). Vegetation indices, derived from mathematical combinations of reflectance values across multiple wavelengths, are widely used to analyse spectral reflectance patterns. These indices provide valuable insights into plant physiological traits and are therefore important tools

Project funding: This study was conducted within the project FraxVir "Detection, characterisation and analyses of the occurrence of viruses and ash dieback in special stands of Fraxinus excelsior—a supplementary study to the FraxForFuture demonstration project" and receives funding via the Waldklimafonds (WKF) funded by the German Federal Ministry of Food and Agriculture (BMEL) and Federal Ministry for the Environment, Nature Conservation, Nuclear Safety and Consumer Protection (BMUV) administrated by the Agency for Renewable Resources (FNR) under grant agreement 2220WK40A4.

The online version is available at https://link.springer.com/.

Corresponding editor: Lei Yu

✉ Lisa Buchner
lbuchner@ku.de

[1] Physical Geography/Landscape Ecology and Sustainable Ecosystem Development, Catholic University of Eichstätt-Ingolstadt, 85072 Eichstätt, Germany

Published online: 09 October 2025

for detecting disease symptoms and monitoring vegetation health (Huete 2012). The Normalized Difference Vegetation Index (NDVI), which is based on the differential reflectance of red and near-infrared wavelengths by plant canopies, is one of the most commonly and effective vegetation indices for detecting plant stress, as it enables early detection of physiological responses to stressors (Neupane and Baysal-Gurel 2021).

An increasingly important application of remote sensing technologies is the detection and monitoring of ash dieback, a disease that poses a major threat to European forest ecosystems. Since the introduction of the invasive fungal pathogen *Hymenoscyphus fraxineus* (Baral et al. 2014) in Europe and the first disease reports in Poland in the 1990s, ash dieback has severely affected populations of European common ash (*Fraxinus excelsior* L.). The fungal pathogen produces airborne ascospores that primarily infect leaves (Timmermann et al. 2011), initially causing necrotic lesions on leaflets and rachises. From there, the infection spreads into twigs and shoots, leading to branch dieback, wilting, and necrotic bark lesions, especially in young tissues. Eventually, the infection progresses into larger branches and stems, resulting in crown dieback characterised by extensive leaf loss (Gross et al. 2014; Timmermann et al. 2017; Fuchs et al. 2024). In advanced stages, necroses may also develop at the stem base, further weakening the tree (Langer 2017). This disease trajectory, from initial leaf infection to full crown dieback, can vary in speed depending on environmental conditions, tree age, and genetic resistance, but often results in high mortality within a few years after the onset of visible symptoms (Timmermann et al. 2017; Klesse et al. 2021). The European common ash is ecologically vital, supporting numerous dependent species (Mitchell et al. 2017; Hultberg et al. 2020) and is expected to experience severe population declines across Europe in the coming decades due to ash dieback (Coker et al. 2019). Therefore, efforts to identify, monitor and characterise affected ash trees are crucial for the long-term conservation of this ecologically important species.

The application of remote sensing technologies for assessing ash tree health remains limited. Some research has focused on monitoring damage caused by the emerald ash borer (*Agrilus planipennis*), a major insect pest threating ash populations, analysing hyperspectral (Pontius et al. 2008) and satellite data (Murfitt et al. 2016). Hyperspectral data have also been successfully used to identify ash trees damaged by ash dieback (Chan et al. 2021; Polk et al. 2022). The more frequently available multispectral data and the thereof calculated vegetation indices have been used to identify and segment ash tree crowns in a mixed forest and subsequently to classify the damage caused by ash dieback (Waser et al. 2014). Kampen et al. (2019) likewise analysed multispectral UAV data and successfully segmented ash tree crowns and characterised ash dieback severity. A different approach was taken by Flynn et al. (2024), who analysed 3D RGB point cloud data from UAV surveys of individual ash trees regarding the different internal crown greenness patterns of trees with differing degrees of damage. Furthermore, Buchner et al. (2025) examined vegetation index values across different damage classes using both RGB and multispectral data, identifying clear value ranges distinguishing mildly from severely affected trees. However, while Buchner et al. (2025) manually delineated ash tree crowns to only analyse leaf mass, no study to date has focused on automatically segmenting ash tree crowns from their surroundings to exclusively study the leaf mass in relation to ash dieback. As the crown of severely affected ash trees decreases drastically and typically presents multiple crown gaps, the exclusion of ground pixels is crucial for the accuracy of further analysis.

Multiple approaches for tree crown segmentation have been successfully developed utilising a wide range of different data, including airborne laser scanning (Dalponte et al. 2015; Argamosa et al. 2016; Douss and Farah 2022), hyperspectral data (Dalponte et al. 2015), satellite data (Lassalle et al. 2022), as well as RGB (Mohan et al. 2017; Huang et al. 2018; Tahar et al. 2021) and multispectral data (Qiu et al. 2020; Ulku et al. 2022). These diverse datasets support a broad spectrum of tree crown delineation techniques, ranging from traditional methods such as valley following, region growing or marker-controlled watershed segmentation to more recent machine and deep learning models (Ke and Quackenbush 2011; Kestur et al. 2018; Freudenberg et al. 2022; Zheng et al. 2025). While tree crown segmentation has been widely explored, the focus in many studies often lies in detecting and counting individual trees rather than on analysing the structural or physiological condition of the crown itself (Ke and Quackenbush 2011; Zheng et al. 2025). Nevertheless, segmentation precision is essential in downstream tasks such as disease detection, where accurate delineation of crown boundaries and internal features become critical.

This study, therefore, investigated two approaches for segmenting tree crowns, producing both fine and coarse tree crown masks, to assess whether the choice of segmentation method significantly affects the calculation of mean NDVI. In addition, we examined how varying levels of crown damage influence the spatial homogeneity of NDVI values within individual tree crowns.

Materials and methods

Study sites

This study was conducted in 2023 at two ash seed orchards in the federal state of Baden-Wuerttemberg, located in

southern Germany (Fig. 1). Both sites have already been included in previous studies on ash dieback (Enderle et al. 2015, Buchner et al. 2022, Eisen et al. 2022, 2023, 2024; Buchner et al. 2024, 2025).

The first site, the Emmendingen orchard (48° 7′ N, 7° 52′ E, 210 m a.s.l.) is situated about 15 km north of Freiburg. Covering 2.7 ha, this plantation was established in 1995 with an initial layout of 228 ash trees planted in a 10 m × 10 m grid. While no thinning operations were conducted, many trees had to be removed due to the impact of ash dieback. The site also contains a variety of other tree and shrub species growing close to the ash trees.

The second site, the Schorndorf orchard (48°46′ N, 9°25′ E, 420 m a.s.l.), lies east of Stuttgart, the capital of Baden-Wuerttemberg. It was established in 1992 with an original planting density of 7 m × 7 m, spanning approximately 2.27 ha. Initially, 416 ash trees were planted, but over time, more than half of them have been removed as a result of both thinning measures and the effects of ash dieback. Additional tree species, such as fruit trees, are also present on the orchard.

For the close-up UAV images, 30 ash trees were selected at each study site. These trees were evenly distributed throughout the orchards, exhibiting varying degrees of ash dieback symptoms, from mild to very severe symptoms.

Vitality assessment

Each selected tree was individually assessed for its vitality status in the field at the end of July 2023. Using a vitality scoring system (Peters et al. 2021) trees were classified based on their visible damage symptoms. Due to the widespread presence of ash dieback in Germany (Fuchs et al. 2024), no completely healthy trees were found at either of the two ash seed orchards. Consequently, the healthy tree category (class 0) was omitted. Trees with mild damage symptoms were assigned to classes 1 and 2, while those with severe damage symptoms were classified as classes 3 and 4. Dead trees (class 5) were not relevant to our study. Each damage class was defined by multiple criteria, including leaf loss, the percentage of dead shoots and branches, the presence of epicormic shoots and stem rot necrosis, with increasing symptom severity from class 1 to class 4.

Image acquisition

Close-up UAV images

For both study sites, individual close-up images of the 30 selected ash tree crowns were recorded using the UAV system DJI Mavic 3 Multispectral (Mavic 3 M) during June, July and October 2023. The Mavic 3 M is equipped with a 20 MP RGB camera and four 5 MP multispectral sensors, allowing for simultaneous capture of both RGB and multispectral images. The multispectral sensors cover four wavelength bands: NIR (860 nm ± 26 nm), red edge (730 nm ± 16 nm), red (650 nm ± 16 nm), and green (560 nm ± 16 nm). Additionally, an integrated sun sensor measures solar radiation to enable light compensation during post-processing (DJI 2022).The images were captured at an altitude of approximately 8 m above the tree crowns,

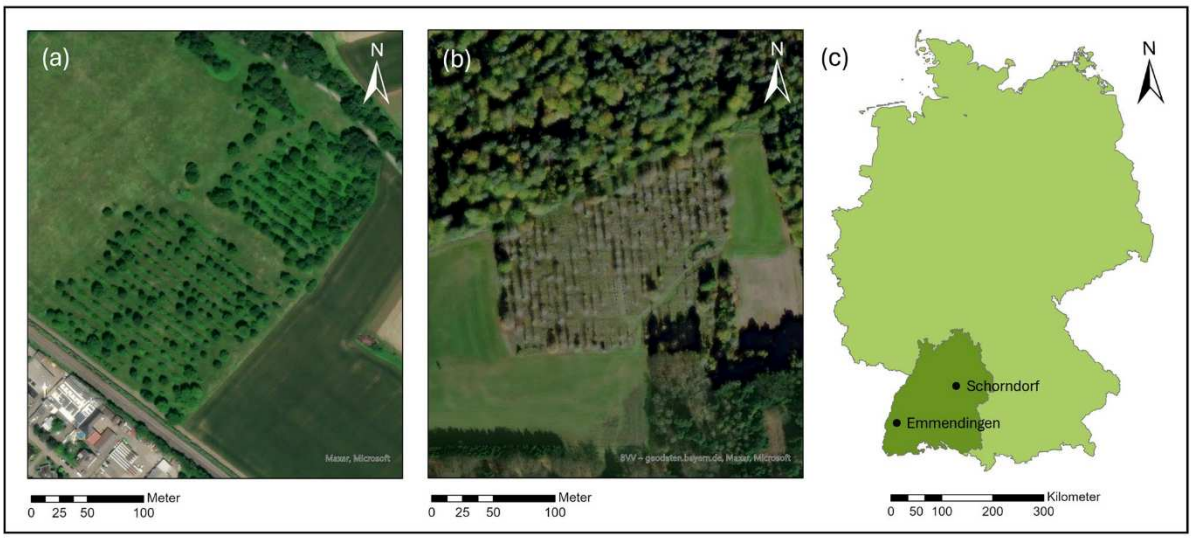

Fig. 1 Study sites Emmendingen (**a**) and Schorndorf (**b**) in the federal state of Baden-Wuerttemberg (dark green) in Germany (**c**, light green), *Source*: Esri Base Map, BKG 2025dl-de/by-2-0

providing an exceptionally high spatial resolution that ensures detailed image quality.

UAV survey

Additionally, a UAV survey was conducted at the Schorndorf orchard in July 2023 at a flight altitude of 80 m to further test the newly developed tree crown segmentation method. The Mavic 3 M followed a pre-planned flight plan with 85% front and side overlap and a flight speed of 4 m/s. This ensured a ground sampling distance of 2.77 cm/pixel for the captured multispectral images. The survey was divided into two flight missions, due to the size of the plantation and UAV specific battery capacity. However, the missions were conducted back-to-back to minimize variations in the environmental conditions.

The images were georeferenced using the integrated RTK data and processed into an orthophoto by aligning the images and generating a point cloud using the software Agisoft Metashape Professional (version 1.8.1).

Post-processing of the close-up UAV images

Due to the slight spatial offset between the four built-in multispectral sensors in the UAV system, the individual close-up images captured by each sensor were not perfectly aligned, resulting in minor misregistration between spectral bands. As a result, precise image alignment was required prior to further processing. Using a custom-built Python (version 3.13.0) script, the NIR, red edge, and red band images were co-registered to the green sensor image for each capture, which served as the reference. The applied homography-based image registration algorithm implemented in OpenCV aligned the images by calculating a 3×3 transformation matrix that mapped matching points from the non-reference images to the green reference image. Throughout the co-registration process, the original metadata of the images was retained.

Tree crown segmentation

Two different methods of individual tree crown segmentation were applied, creating a coarse and a fine mask for each tree crown. While the coarse mask was designed to capture the general outline of the tree crown, the fine mask aimed to incorporate the detailed crown structure, including internal gaps and irregularities.

To extract the coarse tree crown masks from UAV-based imagery, we applied the pre-trained Segment Anything Model (SAM) (Kirillov et al. 2024), a general-purpose segmentation framework developed for prompt-driven object segmentation, using a custom-built Python (version 3.11.0) script. SAM features a modular architecture consisting of an image encoder, a prompt encoder, and a mask decoder. The image encoder converts the input image into a latent representation capturing spatial and semantic features. User-provided prompts are processed by the prompt encoder and guide the segmentation process. Finally, the mask decoder integrates both embeddings to produce one or more segmentation masks (Kirillov et al. 2024; Speckenwirth et al. 2024). In this study, grayscale NIR images were converted to 3-channel grayscale RGB images to match the input format expected by the model. A single foreground point was manually placed near the centre of each image to indicate the approximate location of the tree crown. Based on this input, multiple candidate masks were generated by SAM. Each mask was visually assessed, and the most accurate one representing the crown shape was selected and exported as a binary mask for further analysis.

The fine tree crown masks were generated using a custom-built R (version 4.1.1) script, executed in R Studio (version 2021.09.0). The script integrated spectral, textural, and edge-based features into a multistep segmentation workflow comprising image preprocessing, feature extraction, unsupervised clustering, and morphological refinement (Fig. 2). First, the NIR and red bands were normalized to a range of 0–1, and the NDVI was computed as follows:

$$NDVI = \frac{NIR - Red}{NIR + Red} \quad (1)$$

To enhance vegetation signals, a hybrid image was constructed using a weighted combination of NDVI and NIR, assigning a weight of 0.4 to NDVI and 0.6 to NIR:

$$Hybrid\ image = 0.4 * NDVI + 0.6 * NIR \quad (2)$$

The hybrid image was subsequently normalized and enhanced using histogram equalization based on the empirical cumulative distribution function (ECDF) to improve local contrast. To characterize spatial structure, texture metrics (contrast, entropy, mean, and variance) were calculated from the equalized hybrid image using a grey level co-occurrence matrix (GLCM) with a 5×5 moving window. In addition, edge features were extracted using the Sobel operator by computing gradient magnitudes in both horizontal and vertical directions to enhance boundary detection. All derived features were compiled into a multilayer raster stack, providing a comprehensive representation of spectral, textural, and structural scene characteristics. Pixel-level values were extracted into a data frame and subjected to k-means clustering with $k = 2$, using Euclidean distance and random initialization. The cluster most representative of vegetation was identified by selecting the one with the highest mean texture value, and a corresponding binary mask was generated. To improve segmentation accuracy, morphological post-processing was applied. Small gaps within the

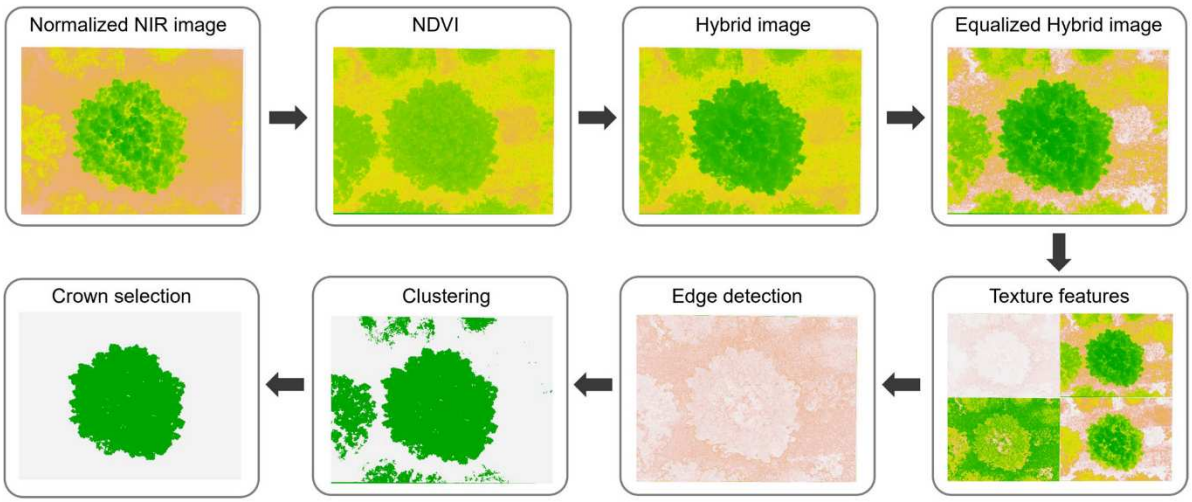

Fig. 2 Workflow for segmenting a fine tree crown mask

crown mask were filled using a 3 × 3 maximum filter, and boundaries were smoothed using a 3 × 3 mean filter. Pixels with smoothed values greater than 0.5 were retained in the final binary mask. To select only the tree crown, a minimum size threshold of 900 pixels was applied. The resulting mask constitutes a spatially constrained and structurally refined representation of the tree crown.

Each segmented fine and coarse tree crown mask was visually validated with the RGB image of the tree crown. Additionally, two sections from two different tree crowns were chosen and manually segmented. Due to the required level of segmentation detail, not all trees were segmented manually; only a representative subset of twelve trees in total, three typical trees per vitality class, was selected for validation. In ArcGIS Pro (version 2.8.3), the manual segmentation was executed, and a tree crown polygon was generated for all three mask types: manual, fine and coarse. The total area was calculated for all masks. To quantify the overlap between the segmentations, we employed the *Intersect* tool to create an intersection polygon (Area_overlap), for both the comparison of the manual and automated fine and coarse segments. This allowed to compute the Intersection over Union (IoU), a widely used metric for segmentation accuracy (Mishra et al. 2021; Sahin et al. 2023; Speckenwirth et al. 2024). The IoU is defined as the ratio of the overlapping area between the manual segmentation (A) and the automated segmentation masks (B) to the total area encompassed by both, as defined by Eq. 3.

$$\mathrm{IoU} = \frac{A \cap B}{A \cup B} \tag{3}$$

In addition to IoU, we examined false positives and false negatives to identify over- and under-segmentation. The *Erase* tool in ArcGIS Pro was used to extract false positives, representing areas detected by the automated segmentations but absent in the manual delineation. False negatives, on the other hand, represent regions that were included in the manual segmentation but missed by the automated methods. To further evaluate segmentation performance, Precision and Recall were computed, as shown in Eqs. 4 and 5:

$$Precision = \frac{Area_{overlap}}{Area_{overlap} + Area_{falsepositive}} \tag{4}$$

$$Recall = \frac{Area_{overlap}}{Area_{overlap} + Area_{falsenegative}} \tag{5}$$

Based on these, we derived the F1-score as described by Eq. 6, which highlights the correctly identified true positives and true negatives:

$$F1score = 2 \times \frac{Precision * Recall}{Precision + Recall} \tag{6}$$

As an additional test, the novel fine tree crown segmentation workflow was applied to the orthophoto of the Schorndorf orchard. Following the generation of a binary tree crown mask, the output was spatially aligned with the georeferenced tree positions recorded using the Stonex S9III (STONEX® Srl, Paderno Dugnano, Italy). This alignment enabled the integration of the segmentation results with precise ground-truth coordinates.

Statistical analysis

For both fine and coarse segmented tree crown masks, a mean NDVI value was calculated. To assess differences in the mean values and standard deviation (SD) of NDVI values between the fine and coarse mask types across vitality classes, pairwise statistical comparisons were conducted using the Wilcoxon rank-sum test.

To assess differences between the coarse and the fine tree crown segmentations, the proportion of crown area differences between the two mask types was quantified. Since tree crowns vary in size, direct comparisons of absolute differences would be misleading. Therefore, the difference area was expressed as a proportion of the total coarse mask area, ensuring an unbiased comparison across trees of different sizes. The resulting proportionate difference values were analysed in relation to tree health classifications to identify potential differences in segmentation refinements across different vitality conditions.

Additionally, only the NDVI values of the fine mask were further analysed to assess the homogeneity of index values per tree crown in relation to vitality class. Both the SD and coefficient of variation (CV) were calculated per tree crown and tested for statistical differences between the four vitality classes. A Kruskal–Wallis test was performed to determine whether significant variation existed between vitality classes. Post-hoc pairwise comparisons were conducted using the Wilcoxon rank-sum test with Bonferroni correction.

Results

Segmentation results and evaluation

Both methods applied for the automatic segmentation of ash tree crowns successfully identified and delineated the crown shape, as illustrated in Fig. 3, which shows four exemplary ash trees representative of the four vitality classes analysed

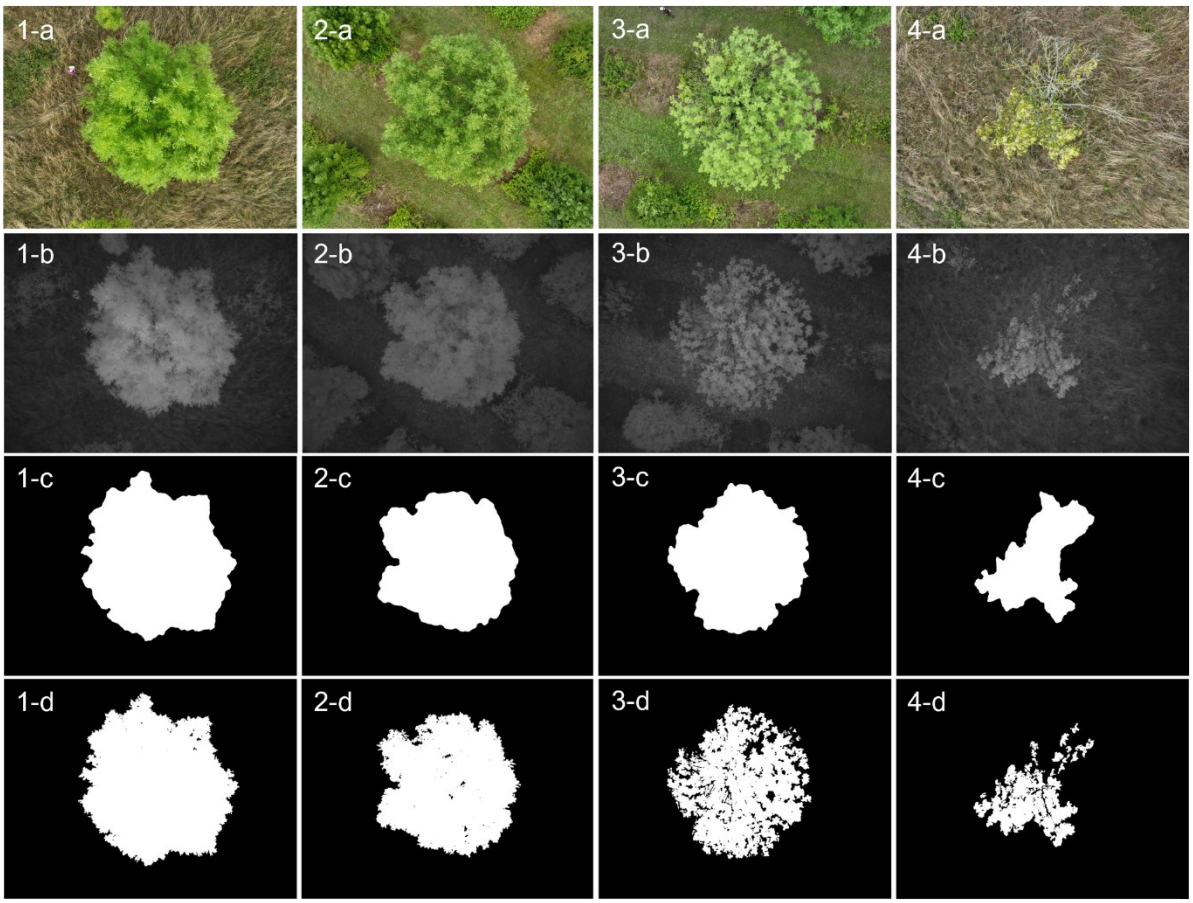

Fig. 3 RGB image (**a**), NIR image (**b**), coarse mask (**c**) and fine mask (**d**) of four exemplary ash tree crowns for the four vitality classes 1 to 4

in this study. The coarse mask worked well for trees with only mildly damage (Fig. 3: 1-c and 2-c). However, for trees with more severe damage, crown gaps were not sufficiently considered (Fig. 3: 3-c and 4-c). Particularly for trees with very severe damage (vitality class 4) large areas of ground pixels were included in the coarse crown mask. In comparison, the fine mask was able to segment the leaf mass in more detail, especially for the more severely damaged trees (Fig. 3: 3-d and 4-d). While segmentation results from the fine and coarse masks were visually similar for trees in vitality classes 1 and 2, the fine mask provided a more precise representation of the crown for trees in classes 3 and 4.

All 360 segmented tree crown masks were validated visually in comparison with the RGB images. Six individual trees, three of the coarse and three of the fine masks did not accurately segment the tree crown. Consequently, both mask types for these six trees were subsequently excluded from further analysis.

To systematically evaluate the segmentation performance across varying crown conditions, the fine and coarse segmentation masks were compared to manually delineated reference crowns across four vitality classes (Table 1). Both masks achieved high IoU values (mean IoU of 0.94 for the fine and 0.93 for the coarse mask). The manually segmented mask accurately represented internal gaps, while the coarse mask did not present any crown gaps. As a result, even over-segmented crowns, such as those from the coarse mask, could still achieve a high IoU due to increased overlap with the manual reference crown. Nevertheless, differences between the fine and coarse mask emerged in the precision and F1-score, particularly under more structurally heterogeneous conditions for trees with severe damage due to ash dieback. Both mask types were able to capture the outline of the crown (Fig. 4c, d), however while the fine mask was able to represent internal crown gaps in high detail, the coarse mask only captured the outline of the crown (Fig. 4g, h). The fine mask exhibited consistently higher accuracy across most metrics. Notably, in vitality class 4, representing crowns with severe damage and increased structural irregularity, the fine mask substantially outperformed the coarse mask in terms of precision (0.86 vs. 0.78) and F1-score (0.91 vs. 0.85), indicating an increased ability to avoid over-segmentation in complex canopy structures. While both mask types achieved similarly high recall values across all vitality classes (≥ 0.97), reflecting a general robustness in detecting crown presence, the fine mask demonstrated greater consistency and balance across all evaluated metrics. The overall higher precision (0.94 vs. 0.91) and F1-score (0.96 vs. 0.94) of the fine mask further underscore its enhanced delineation quality. These results suggest that increased spatial detail in

Table 1 Mean investigated metrics to evaluate the success of segmentation of the fine and coarse mask in comparison the manual segmentation (ground truth) for the four vitality classes, each class represented by three individual trees

Class	Ground truth—fine mask				Ground truth—coarse mask			
	IoU	Precision	Recall	F1	IoU	Precision	Recall	F1
Class 1	0.97	0.98	0.99	0.98	0.96	0.99	0.98	0.98
Class 2	0.95	0.96	0.99	0.98	0.93	0.96	0.98	0.97
Class 3	0.92	0.97	0.95	0.96	0.89	0.92	0.97	0.95
Class 4	0.93	0.86	0.98	0.91	0.94	0.78	0.97	0.85
Overall mean	0.94	0.94	0.98	0.96	0.93	0.91	0.97	0.94

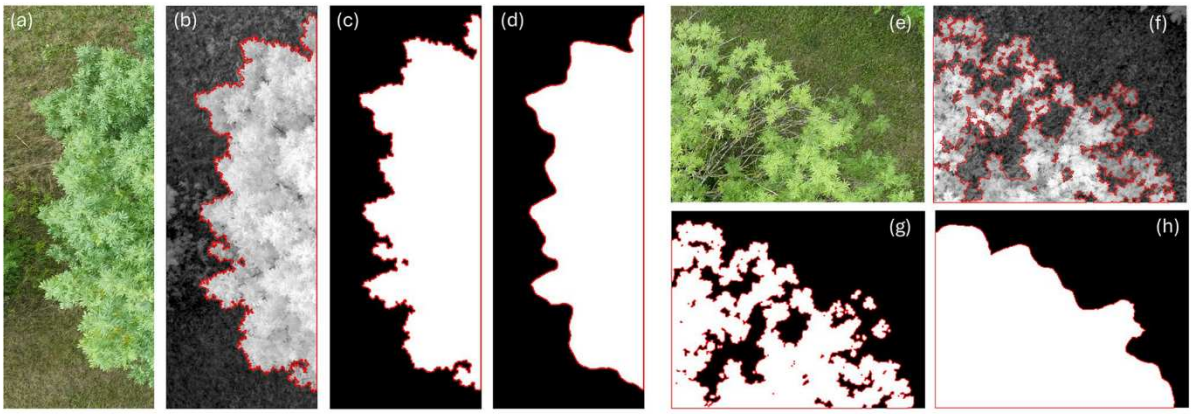

Fig. 4 RGB image (**a**, **e**), detailed manual segmentation of a part of a tree crown (**b**, **f**), fine segmentation (**c**, **g**) and coarse segmentation (**d**, **h**) of the edge area of an ash tree crown (**a**–**d**) and a crown with severe gaps (**e**–**h**)

crown segmentation enhances accuracy, particularly under conditions of elevated canopy heterogeneity.

Differences per mask type

Based on the 174 individual images of analysed ash trees derived from the different flight missions in June, July and October from both ash orchards, slightly higher NDVI values were recorded for the fine mask in comparison to the coarse mask. However, these differences were not statistically significant in any of the four vitality classes (Fig. 5). Independent from the mask type, a decrease in NDVI values was observed with an increasing damage due to ash dieback. Additionally, the mean NDVI calculated for the difference area (the region included in the coarse mask but excluded in the fine mask) was significantly lower than that of the fine mask in all vitality classes ($p < 0.001$), indicating that the excluded areas, mainly ground pixels beneath the crown and large exposed branches, have substantially lower NDVI values.

In contrast to the mean NDVI results, the SD values differed between the fine and coarse mask, with a significant difference observed between mask types in both vitality classes 2 and 3 (Fig. 5). The SD of the NDVI values increased with vitality class, demonstrating greater variability in NDVI values for severely damaged ash tree crowns.

The proportionate difference area between the coarse and fine mask, demonstrated an increase with more severely damaged ash trees (Fig. 6). The Kruskal–Wallis test proved statistical significance ($p = 0.022$). While the area between the two mask types differed only slightly for class 1, the difference was much more pronounced in classes 3 and 4, indicating differing fine and coarse segmentations. The post-hoc test revealed a statistically significant difference only for class 1 and 3 ($p = 0.033$). However, these results indicate an increasing deviation of the segmented areas of the two mask types with increasing damage severity, likely attributable to the increase of crown gaps with more severe damage.

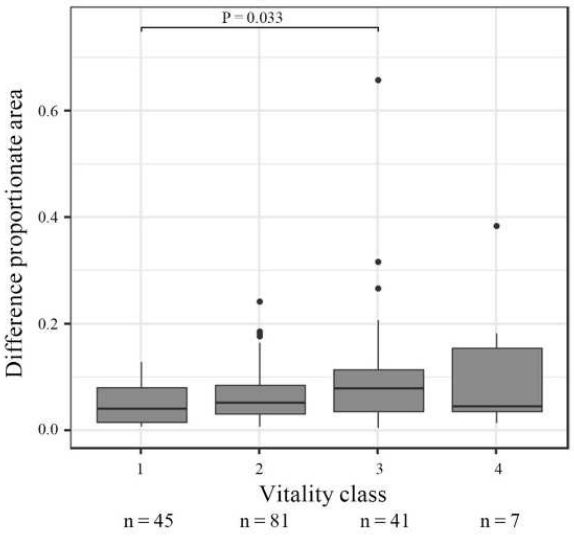

Fig. 6 Difference proportionate area between coarse and fine masks for the four vitality classes for the analysed 174 images from ash trees at the two seed orchards

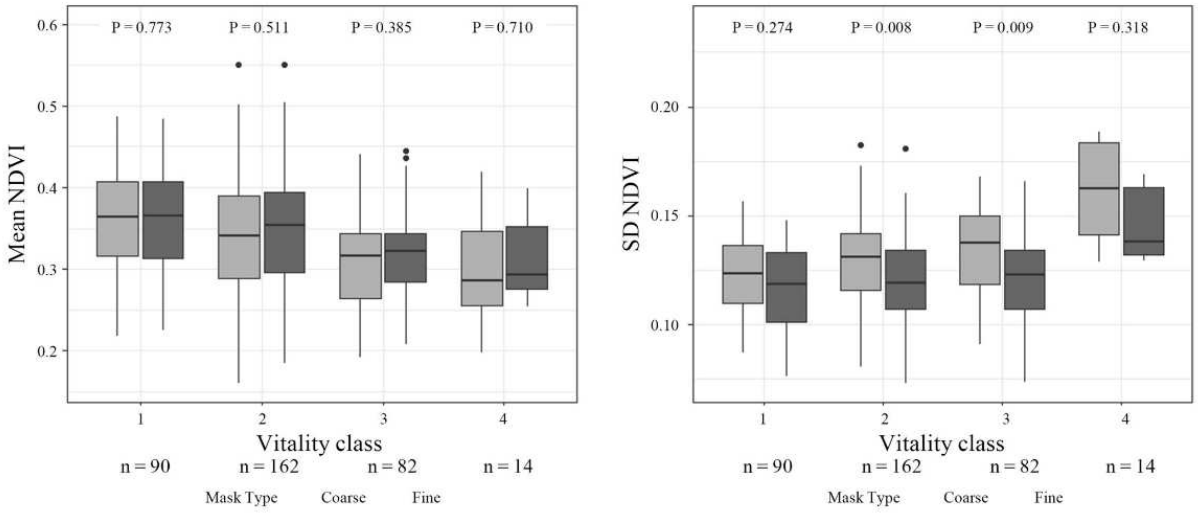

Fig. 5 Boxplots of the mean and SD NDVI values calculated from the two mask types, analysed among the 174 images for both coarse and fine masks, for the four vitality classes at the two seed orchards

Homogeneity of NDVI values

To assess spatial variability of NDVI in relation to canopy condition, the SD and CV of NDVI values were calculated for individual trees applying the fine crown segmentation method and compared across vitality classes (Fig. 7). Boxplot analysis revealed a significant increase in both NDVI SD (Kruskal–Wallis, p-value = 0.024) and NDVI CV (Kruskal–Wallis, p-value = 0.012) with declining tree vitality. Notably, trees in class 4 exhibited significantly higher NDVI SD than those in class 1 to 3, indicating greater heterogeneity in canopy reflectance.

Moreover, the CV showed a consistent upward trend from class 1 to class 4, with a statistically significant difference between class 1 and 4. This suggests that, in addition to the observed decrease in NDVI values with increasing disease severity (Fig. 5), the relative variability of NDVI within individual tree crowns becomes more pronounced. While SD reflects the absolute spread of NDVI values, the CV normalizes this spread by accounting for mean differences between trees, thus emphasizing the disproportionate increase in heterogeneity among more severely damaged individuals. Therefore, healthier trees have both higher and more consistent NDVI values, whereas trees suffering from advanced ash dieback show lower NDVI and increased spatial irregularity across their crowns.

Tree crown segmentation in orthophoto

The application of the newly developed workflow for a detailed tree crown segmentation was also successfully applied to an orthophoto generated from a UAV-survey. Despite the lower image resolution due to the flight height of 80 m, individual tree crowns were successfully delineated from their surroundings (Fig. 8). Not only the shape of the tree crowns was replicated but also gaps in the tree crowns (Fig. 8, purple frame), both in large trees and in smaller ash trees with severe damage (Fig. 8, orange frame). However, in cases where trees were in contact to surrounding trees, segmentation often merged them into a single object (Fig. 8, blue frame), highlighting a limitation of the method. These results emphasize the importance of spatial separation between individual trees for the segmentation technique to function reliably.

Discussion

Fine and coarse tree crown masks

A novel workflow for the detailed segmentation of ash tree crowns was developed in this study and successfully applied to multispectral close-up UAV imagery and an orthophoto of trees affected by ash dieback.

The ash trees investigated in this study were located on two ash tree orchards, with generous spacing between individual trees. While this setup provides clear crown outlines, the surrounding vegetation, primarily tall grass and small bushes, adds background complexity. Despite these conditions, both tree crown segmentation methods were able to successfully segment the crowns from their surroundings. Accurate segmentation of green plant material is readily

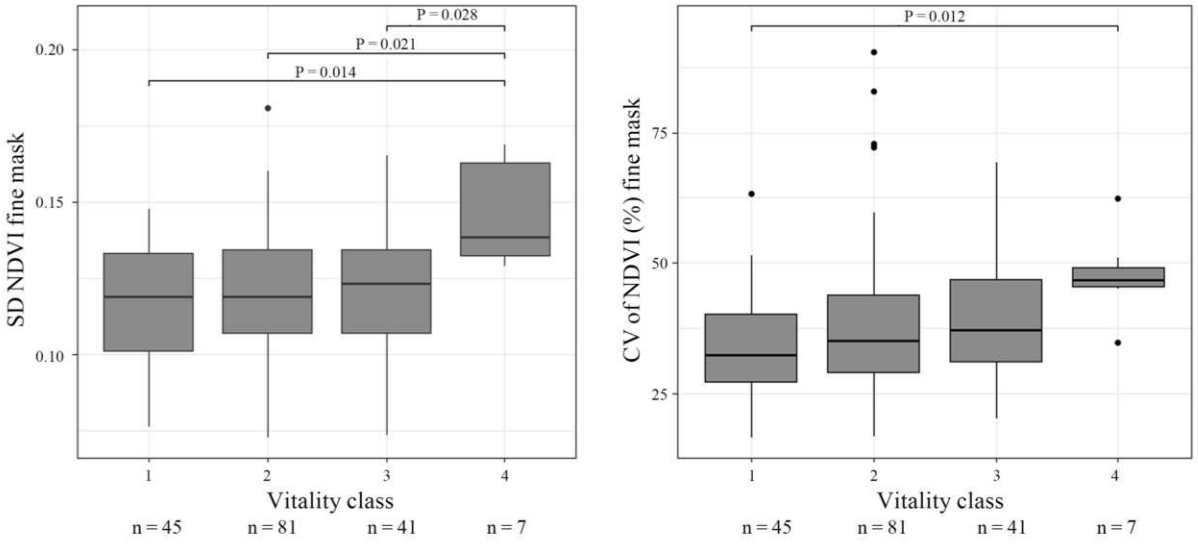

Fig. 7 SD of the NDVI values of the fine mask per vitality class and CV of NDVI of the fine mask per vitality class with significant post-hoc results displayed as bars at the top for the analysed 174 images

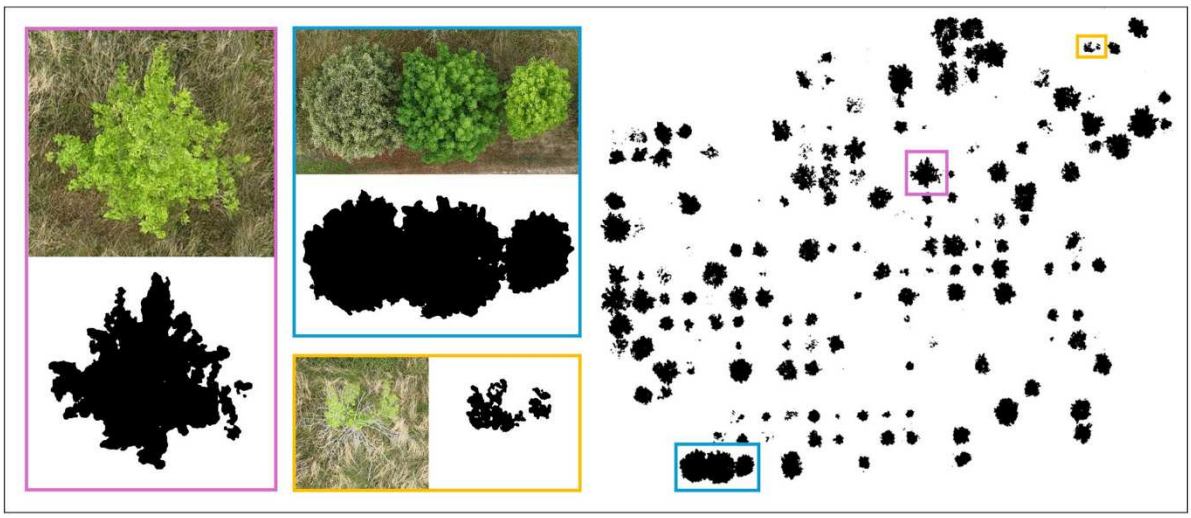

Fig. 8 Segmented tree crowns from an orthophoto with highlighted examples: the crown of a single ash tree (purple frame), detailed images of merged trees (blue frame) and a small, severely damaged ash (orange frame)

achievable when close-up images feature a uniform background. This has been demonstrated among others by Khan et al. (2022), who applied semantic segmentation techniques, and by Wacker et al. (2024), who employed multispectral imaging in combination with chlorophyll fluorescence to enable segmentation. However, as noted by Mishra et al. (2021), segmentation becomes considerably more challenging when the background contains vegetation with similar spectral properties. For instance, while deep-learning models were able to differentiate between crop and weed, difficulties in separating the plant material from the surrounding soil and similar vegetation were reported (Sahin et al. 2023). However, the results of this study demonstrate that successful crown delineation is achievable even in semi-structured environments with vegetation with similar spectral properties.

Many studies on tree crown segmentation rely on remote sensing data acquired from UAVs or satellites (Heenkenda et al. 2015; Zhang et al. 2020; Lassalle et al. 2022). While these datasets often offer relatively high spatial resolution, they frequently lack the detail necessary to capture fine-scale crown structures, such as small canopy gaps, resulting in coarser crown outlines that may not accurately reflect true crown morphology. Only a few studies reported tree crown segmentation results with a level of detail comparable to that achieved in the present study. For instance, LiDAR point clouds have been used to accurately calculate crown volume and segment citrus trees with high morphological accuracy (Liu et al. 2021). Similarly, morphological image analysis applied to multispectral UAV data has enabled detailed crown segmentation in olive orchards (Sarabia et al. 2020), and similar methods were also successfully tested on other orchard species, including lemon and orange trees (Ponce et al. 2022). Additionally, adaptive thresholding combined with watershed segmentation enabled precise delineation of peach tree crowns (Mu et al. 2018). Beyond morphological techniques, deep learning models have shown considerable potential for high-precision crown segmentation. For example, frameworks combining object detection models such as YOLOv4 with LiDAR-derived heightmaps have effectively segmented tree crowns (Sun et al. 2022). UAV-borne LiDAR datasets have been applied across diverse forest types (Chen et al. 2021), and multiple semantic segmentation architectures have been evaluated on multispectral aerial and satellite imagery, further demonstrating the versatility of deep learning approaches for crown segmentation (Ulku et al. 2022).

A key strength of the novel approach developed in our study lies in its ability to segment tree crown areas without the need for annotated training data, making it particularly valuable for large study sites. The combination of spectral and textural indicators—such as NDVI, NIR reflectance, and GLCM-derived metrics—enhances robustness of the method against within-crown variability and background interference. By incorporating edge information and applying unsupervised k-means clustering, the workflow effectively captures the structural heterogeneity commonly observed in high-resolution UAV imagery. The application of k-means clustering in this context has proven to be a viable tool for vegetation or tree crown segmentation, as supported by previous studies. For example, Moussaid et al. (2021) applied k-means clustering to multispectral satellite images of

orchards to segment overlapping tree crowns, successfully distinguishing vegetation from soil and shadows. Similarly, Cinat et al. (2019) compared k-means with other unsupervised methods for segmenting vineyard canopies using UAV-acquired RGB and NIR-Red-Green imagery, demonstrating the applicability of the method in agricultural contexts.

Texture features have been shown to significantly enhance the segmentation and classification of tree crowns. Both Wu et al. (2004) and Erdem and Bayrak (2023) demonstrated that incorporating texture information, ranging from simple image gradients to advanced radiomic descriptors, can improve accuracy in identifying crown boundaries and distinguishing species.

In our novel tree crown segmentation approach, the NIR image and derived NDVI serve as the basis input for all further segmentation steps. The suitability of NDVI and NIR imagery for tree crown segmentation has been consistently demonstrated across multiple studies. Kang et al. (2017) showed that UAV-acquired NIR imagery provided strong spectral contrast between eucalyptus crowns and their surroundings, enabling accurate segmentation. Furthermore, Safonova et al. (2021) highlighted, that models trained on NDVI and GNDVI (Green Normalized Difference Vegetation Index) outperformed those using RGB alone for segmenting olive tree crowns. These studies confirm that NDVI and NIR imagery can enhance crown visibility. Despite these advantages, using the NIR image for segmentation alone can introduce variability due to different illumination conditions, especially in shadowed areas within the crown diminishing visual consistency. Conversely, NDVI by itself often lacks sufficient contrast to clearly distinguish the tree crown from spectrally similar surrounding vegetation. As demonstrated in our study, generating a hybrid image by merging NIR and NDVI data enhances crown delineation. This fusion highlights crown structure while simultaneously reducing the visual impact of shadowed regions and thereby offering a more consistent and robust basis for segmentation.

The UAV close-up images were captured at two study sites from June to October, covering different stages of the vegetation period of the common ash. No differences in segmenting the images were noted for the three analysed months, indicating that the developed segmentation algorithm can be applied to images captured during the entire vegetation period of the common ash. However, as Lu et al. (2022) pointed out, natural illumination can cause shaded and non-shaded areas within individual crowns. These effects were minimized by generating the hybrid NIR-NDVI image in our study. Additionally, a more evenly distribution of shadowed areas can be achieved by performing UAV surveys under overcast conditions, which avoids the harsh contrasts caused by direct sunlight.

Although the SAM model did not capture crown gaps and lacked detail along the crown edges, it was still able to generate tree crown masks that accurately represented the overall crown outline. However, in our study, the SAM model was applied exclusively to individual images of tree crowns, with the crown consistently positioned at the centre of each image. The SAM model was also able to detect and segment tree crowns to analyse changes in riparian woodland (Dawson et al. 2025). Similarly Balasundaram et al. (2024) reported successful background separation of plants using SAM. However, in a comparative evaluation, SAM underperformed relative to three other deep learning models (Speckenwirth et al. 2024). In our study, the SAM model was configured to generate three segmentation masks per ash tree crown. Each mask was manually reviewed, and the most accurate one was selected. However, relying solely on the model's confidence scores would have occasionally led to the selection of an incorrect mask.

Validation of a representative subset of the data revealed a high IoU for both the fine and coarse segmentation masks. However, a closer examination of precision and F1-score metrics indicated that the fine mask more accurately captured the true shape of the tree crowns. These findings suggest that, although both segmentation approaches performed reasonably well in delineating the general crown area, the fine mask provided a more accurate representation of the actual crown structure. This advantage was particularly evident in severely damaged trees, where accurate depiction of remaining leaf mass is critical. Therefore, fine-scale segmentation is strongly recommended in contexts where detailed crown morphology and subtle structural variation are of analytical importance. This distinction proves as particularly important when assessing the health condition of ash trees, where crown size and internal structure serve as key indicators of disease severity. In severely damaged crowns, structural complexity increases due to the emergence of epicormic shoots (Enderle et al. 2015). These dense clusters can partially close crown gaps and create a more heterogeneous crown surface. As a result, the coarse segmentation approach tends to miss fine structural details and underestimates the distribution of living biomass, especially where small, scattered shoots predominate.

Both the development of the fine-scale tree crown segmentation workflow and the application of the SAM model were conducted on very high-resolution images of individual ash trees. To assess the workflow's transferability to coarser spatial scales, its performance was further evaluated on lower resolution orthophotos. Despite the reduced resolution, the segmentation approach, designed to isolate leaf mass, proved effective when applied to an entire ash tree orchard. These results demonstrated the method's scalability and robustness, highlighting its potential for broader application in landscape-level crown analysis. While crown gaps were accurately identified and the reduced leaf mass in severely damaged trees was well captured, cases where tree

canopies overlapped often resulted in a single segmented crown encompassing multiple adjacent trees. This challenge was also observed by Mu et al. (2018) and Sarabia et al. (2020). However, additional processing steps like morphological erosion (Marques et al. 2019) or seed markers from regional maxima and a watershed algorithm (Ponce et al. 2022) can further improve the tree crown masks and separate connecting masks.

NDVI analysis

One of the main objectives of this study was to assess whether delineating only the coarse crown outline is sufficient for calculating mean vegetation index values in severely damaged ash tree crowns. In particular, we examined whether the increasing presence of crown gaps significantly affects these values. While no significant differences in mean vegetation index values were observed between the fine and coarse crown segmentations, the analysis of the difference area, i.e., the part included in the coarse but excluded from the fine mask, revealed substantially lower NDVI values across all vitality classes. This suggests that although the inclusion of ground pixels does not markedly alter the overall mean index when comparing full crown masks, it does introduce a component with clearly lower vegetation activity, particularly reflecting gaps and exposed background beneath sparse crowns.

The observed decline in mean NDVI values with increasing damage due to ash dieback is in accordance with the findings of Buchner et al. (2025), who also reported lower NDVI values in severely damaged ash trees compared to those with only mild symptoms. This decrease in NDVI is explained by the loss of chlorophyll-rich foliage in damaged crowns, leading to reduced reflectance in the NIR spectrum relative to the red spectrum.

The comparison between coarse and fine crown masks revealed notable differences in NDVI variability across vitality classes. While SD of NDVI increased with declining tree vitality, significant differences between mask types were observed particularly in moderately damaged trees (classes 2 and 3). In these cases, coarse masks yielded higher variability, likely due to the inclusion of non-foliar elements such as exposed branches and crown gaps. In contrast, the fine masks, which focused on leaf mass, provided a more consistent and presumably a more biologically relevant measure of canopy composition. The area difference between the fine and coarse masks also increased with damage severity, reflecting the greater inclusion of non-leaf pixels in coarse masks as crown gaps expanded.

The analysis of NDVI variability within in detail segmented ash tree crowns, revealed a consistent increase in heterogeneity in index values with rising damage severity, indicating that NDVI values vary within the crown, especially in trees with severe damage. Similarly, Flynn et al. (2024) documented a spatial pattern in greenness (green chromatic coordinate) decline toward the crown extremities, whereas healthy ash trees, not affected by ash dieback, showed increased greenness at the edges. These results suggest that infection increases within-crown heterogeneity. Accordingly, while mean NDVI values can reliably represent overall crown condition in trees with mild symptoms, they may not fully capture the internal variability of crowns in more severely damaged individuals.

The proposed workflow, designed to account for significant crown gaps in ash trees affected by dieback, proved effective in evaluating the influence of external pixel inclusion on mean vegetation index values and in capturing differences in crown homogeneity across damage classes. Its main limitation lies in the requirement for isolated ash trees without overlapping foliage from surrounding vegetation. However, the workflow offers considerable flexibility, such as adjustable hybrid blending and clustering parameters, making it readily adaptable to other vegetation types and research objectives.

Conclusion

Detailed segmentation of the leaf mass in ash trees affected by ash dieback is feasible and can be applied not only to individual close-range multispectral UAV images but also to orthophotos generated from broader UAV surveys. This novel workflow effectively captures both fine crown edges and internal crown gaps. However, as demonstrated by the comparison between fine and coarse crown segmentation, there was no significant difference in mean vegetation index values per crown, indicating that coarse tree crown segmentation is sufficient for such calculations. Nonetheless, the fine segmentation revealed increasing heterogeneity in NDVI values with greater symptom severity. Therefore, for in-depth crown analysis, particularly when assessing structural integrity or spatial variation in canopy health, the fine segmentation method is recommended. Our approach supports remote, scalable, and reproducible monitoring of forest health, applicable beyond ash dieback and relevant to tree species under similar stressors.

Acknowledgements We thank the Forestry Baden-Wuerttemberg and the Forest Research Institute Baden-Wuerttemberg for providing the seed orchards as study sites. We thank Tobias Heckmann for insightful discussions. Special thanks to all student assistants for their technical assistance.

Funding Open Access funding enabled and organized by Projekt DEAL.

Declarations

Conflict of interest The authors have no relevant financial or non-financial interests to disclose.

References

Agostinelli M, Nguyen D, Witzell J, Cleary M (2021) Mycobiome of *Fraxinus excelsior* with different phenotypic susceptibility to ash dieback. Front Glob Change 4:580514. https://doi.org/10.3389/ffgc.2021.580514

Argamosa RJL, Paringit EC, Quinton KR, Tandoc FAM, Faelga RAG, Ibañez CAG, Posilero MAV, Zaragosa GP (2016) Fully automated gis-based individual tree crown delineation based on curvature values from a lidar derived canopy height model in a coniferous plantation. Int Arch Photogramm Remote Sens Spatial Inf Sci XLI-B8:563–569. https://doi.org/10.5194/isprsarchives-xli-b8-563-2016

Balasundaram A, Sharma A, Kumaravelan S, Shaik A, Kavitha MS (2024) An improved normalized difference vegetation index (NDVI) estimation using grounded *Dino* and segment anything model for plant health classification. IEEE Access 12:75907–75919. https://doi.org/10.1109/ACCESS.2024.3403520

Baral HO, Queloz V, Hosoya T (2014) *Hymenoscyphus fraxineus*, the correct scientific name for the fungus causing ash dieback in Europe. IMA Fungus 5(1):79–80. https://doi.org/10.5598/imafungus.2014.05.01.09

Barbedo JGA (2019) A review on the use of unmanned aerial vehicles and imaging sensors for monitoring and assessing plant stresses. Drones 3(2):40. https://doi.org/10.3390/drones3020040

Buchner L, Eisen AK, Šikoparija B, Jochner-Oette S (2022) Pollen viability of *Fraxinus excelsior* in storage experiments and investigations on the potential effect of long-range transport. Forests 13(4):600. https://doi.org/10.3390/f13040600

Buchner L, Eisen AK, Jochner-Oette S (2024) Effects of ash dieback on leaf physiology and leaf morphology of *Fraxinus excelsior* L. Trees 38(5):1205–1221. https://doi.org/10.1007/s00468-024-02546-1

Buchner L, Eisen AK, Jochner-Oette S (2025) Identification of damage severity in *Fraxinus excelsior* L. trees caused by ash dieback using multisensory and multitemporal UAV imagery. For Ecol Manage 585:122660. https://doi.org/10.1016/j.foreco.2025.122660

Chan AHY, Barnes C, Swinfield T, Coomes DA (2021) Monitoring ash dieback (*Hymenoscyphus fraxineus*) in British forests using hyperspectral remote sensing. Remote Sens Ecol Conserv 7(2):306–320. https://doi.org/10.1002/rse2.190

Chen XX, Jiang K, Zhu YS, Wang XJ, Yun T (2021) Individual tree crown segmentation directly from UAV-borne LiDAR data using the PointNet of deep learning. Forests 12(2):131. https://doi.org/10.3390/f12020131

Cinat P, Di Gennaro SF, Berton A, Matese A (2019) Comparison of unsupervised algorithms for vineyard canopy segmentation from UAV multispectral images. Remote Sens 11(9):1023. https://doi.org/10.3390/rs11091023

Coker TLR, Rozsypálek J, Edwards A, Harwood TP, Butfoy L, Buggs RJA (2019) Estimating mortality rates of European ash (*Fraxinus excelsior*) under the ash dieback (*Hymenoscyphus fraxineus*) epidemic. Plants People Planet 1(1):48–58. https://doi.org/10.1002/ppp3.11

Dalponte M, Reyes F, Kandare K, Gianelle D (2015) Delineation of individual tree crowns from ALS and hyperspectral data: a comparison among four methods. Eur J Remote Sens 48(1):365–382. https://doi.org/10.5721/EuJRS20154821

Dawson M, Dawson H, Gurnell A, Lewin J, Macklin MG (2025) Ai-assisted interpretation of changes in riparian woodland from archival aerial imagery using Meta's segment anything model. Earth Surf Process Landf 50(1):e6053. https://doi.org/10.1002/esp.6053

DJI (2022) DJI Mavic 3M user manual

Douss R, Farah IR (2022) Extraction of individual trees based on canopy height model to monitor the state of the forest. Trees for People 8:100257. https://doi.org/10.1016/j.tfp.2022.100257

Eisen AK, Fussi B, Šikoparija B, Jochner-Oette S (2022) Aerobiological pollen deposition and transport of *Fraxinus excelsior* L. at a small spatial scale. Forests 13(3):424. https://doi.org/10.3390/f13030424

Eisen AK, Semizer-Cuming D, Jochner-Oette S, Fussi B (2023) Pollination success of *Fraxinus excelsior* L. in the context of ash dieback. Ann for Sci 80(1):22. https://doi.org/10.1186/s13595-023-01189-5

Eisen AK, Buchner L, Fussi B, Jochner-Oette S (2024) Does ash dieback affect the reproductive ecology of *Fraxinus excelsior* L.? J for Res 35(1):16. https://doi.org/10.1007/s11676-023-01670-x

Enderle R, Nakou A, Thomas K, Metzler B (2015) Susceptibility of autochthonous German *Fraxinus excelsior* clones to *Hymenoscyphus pseudoalbidus* is genetically determined. Ann for Sci 72(2):183–193. https://doi.org/10.1007/s13595-014-0413-1

Erdem F, Bayrak OC (2023) Evaluating the effects of texture features on *Pinus sylvestris* classification using high-resolution aerial imagery. Ecol Inform 78:102389. https://doi.org/10.1016/j.ecoinf.2023.102389

Flynn WRM, Grieve SWD, Henshaw AJ, Owen HJF, Buggs RJA, Metheringham CL, Plumb WJ, Stocks JJ, Lines ER (2024) UAV-derived greenness and within-crown spatial patterning can detect ash dieback in individual trees. Ecol Solut Evid 5(2):e12343. https://doi.org/10.1002/2688-8319.12343

Freudenberg M, Magdon P, Nölke N (2022) Individual tree crown delineation in high-resolution remote sensing images based on U-net. Neural Comput Appl 34(24):22197–22207

Fuchs S, Häuser H, Peters S, Knauf L, Rentschler F, Kahlenberg G, Kätzel R, Evers J, Paar U, Langer GJ (2024) Ash dieback assessments on intensive monitoring plots in Germany: influence of stand, site and time on disease progression. J Plant Dis Prot 131(5):1355–1372. https://doi.org/10.1007/s41348-024-00889-y

Gross A, Holdenrieder O, Pautasso M, Queloz V, Sieber TN (2014) *Hymenoscyphus* pseudoalbidus, the causal agent of European ash dieback. Mol Plant Pathol 15(1):5–21. https://doi.org/10.1111/mpp.12073

Heenkenda MK, Joyce KE, Maier SW (2015) Mangrove tree crown delineation from high-resolution imagery. Photogramm Eng Remote Sens 81(6):471–479. https://doi.org/10.14358/PERS.81.6.471

Huang HY, Li X, Chen CC (2018) Individual tree crown detection and delineation from very-high-resolution UAV images based on bias

field and marker-controlled watershed segmentation algorithms. IEEE J Sel Top Appl Earth Obs Remote Sens 11(7):2253–2262. https://doi.org/10.1109/JSTARS.2018.2830410

Huete AR (2012) Vegetation indices, remote sensing and forest monitoring. Geogr Compass 6(9):513–532. https://doi.org/10.1111/j.1749-8198.2012.00507.x

Hultberg T, Sandström J, Felton A, Öhman K, Rönnberg J, Witzell J, Cleary M (2020) Ash dieback risks an extinction cascade. Biol Conserv 244:108516. https://doi.org/10.1016/j.biocon.2020.108516

Kampen M, Lederbauer S, Mund J-P, Immitzer M (2019) UAV-based multispectral data for tree species classification and tree vitality analysis. Dreiländertagung der DGPF, der OVG und der SGPF in Wien, Österreich – Publikationen der DGPF (28), pp 623–639

Kang J, Wang L, Chen F, Niu Z (2017) Identifying tree crown areas in undulating *Eucalyptus* plantations using JSEG multi-scale segmentation and unmanned aerial vehicle near-infrared imagery. Int J Remote Sens 38(8–10):2296–2312

Ke YH, Quackenbush LJ (2011) A review of methods for automatic individual tree-crown detection and delineation from passive remote sensing. Int J Remote Sens 32(17):4725–4747. https://doi.org/10.1080/01431161.2010.494184

Kestur R, Angural A, Bashir B, Omkar SN, Anand G, Meenavathi MB (2018) Tree crown detection, delineation and counting in UAV remote sensed images: a neural network based spectral–spatial method. J Indian Soc Remote Sens 46(6):991–1004. https://doi.org/10.1007/s12524-018-0756-4

Khan K, Khan RU, Albattah W, Qamar AM (2022) End-to-end semantic leaf segmentation framework for plants disease classification. Complexity 2022:1168700. https://doi.org/10.1155/2022/1168700

Kirillov A, Mintun E, Ravi N, Mao HZ, Rolland C, Gustafson L, Xiao TT, Whitehead S, Berg AC, Lo WY, Dollár P, Girshick R (2024) Segment anything. In: 2023 IEEE/CVF international conference on computer vision (ICCV). IEEE, Paris, pp 3992–4003

Klesse S, Abegg M, Hopf SE, Gossner MM, Rigling A, Queloz V (2021) Spread and severity of ash dieback in Switzerland–tree characteristics and landscape features explain varying mortality probability. Front for Glob Change 4:645920. https://doi.org/10.3389/ffgc.2021.645920

Langer G (2017) Collar rots in forests of Northwest Germany affected by ash dieback. Balt for 23(1):4–19

Lassalle G, Ferreira MP, La Rosa LEC, de Souza Filho CR (2022) Deep learning-based individual tree crown delineation in mangrove forests using very-high-resolution satellite imagery. ISPRS J Photogramm Remote Sens 189:220–235. https://doi.org/10.1016/j.isprsjprs.2022.05.002

Liu XY, Wang YX, Kang F, Yue Y, Zheng YJ (2021) Canopy parameter estimation of *Citrus grandis* var. longanyou based on LiDAR 3D point clouds. Remote Sens 13(9):1859. https://doi.org/10.3390/rs13091859

Lu ZA, Qi LJ, Zhang H, Wan JJ, Zhou JR (2022) Image segmentation of UAV fruit tree canopy in a natural illumination environment. Agriculture (Basel) 12(7):1039. https://doi.org/10.3390/agriculture12071039

Marques P, Pádua L, Adão T, Hruška J, Peres E, Sousa A, Sousa JJ (2019) UAV-based automatic detection and monitoring of chestnut trees. Remote Sens 11(7):855. https://doi.org/10.3390/rs11070855

Mishra P, Sadeh R, Bino E, Polder G, Boer MP, Rutledge DN, Herrmann I (2021) Complementary chemometrics and deep learning for semantic segmentation of tall and wide visible and near-infrared spectral images of plants. Comput Electron Agric 186:106226. https://doi.org/10.1016/j.compag.2021.106226

Mitchell RJ, Broome A, Beaton JK, Bellamy PE, Ellis CJ, Hester AJ, Hodgetts NG, Iason GR, Littlewood NA, Newey S, Pozsgai G, Ramsay S, Riach D, Stockan JA, Taylor AF, Woodward S (2017) Challenges in assessing the ecological impacts of tree diseases and mitigation measures: the case of *Hymenoscyphus fraxineus* and *Fraxinus excelsior*. Baltic for 23(1):116–140

Mohan M, Silva CA, Klauberg C, Jat P, Catts G, Cardil A, Hudak AT, Dia M (2017) Individual tree detection from unmanned aerial vehicle (UAV) derived canopy height model in an open canopy mixed conifer forest. Forests 8(9):340. https://doi.org/10.3390/f8090340

Moussaid A, El Fkihi S, Zennayi Y (2021) Tree crowns segmentation and classification in overlapping orchards based on satellite images and unsupervised learning algorithms. J Imaging 7(11):241. https://doi.org/10.3390/jimaging7110241

Mu Y, Fujii Y, Takata D, Zheng BY, Noshita K, Honda K, Ninomiya S, Guo W (2018) Characterization of peach tree crown by using high-resolution images from an unmanned aerial vehicle. Hortic Res 5:74. https://doi.org/10.1038/s41438-018-0097-z

Murfitt J, He YH, Yang J, Mui A, De Mille K (2016) Ash decline assessment in emerald ash borer infested natural forests using high spatial resolution images. Remote Sens 8(3):256. https://doi.org/10.3390/rs8030256

Neupane K, Baysal-Gurel F (2021) Automatic identification and monitoring of plant diseases using unmanned aerial vehicles: a review. Remote Sens 13(19):3841. https://doi.org/10.3390/rs13193841

Polk SL, Chan AHY, Cui KN, Plemmons RJ, Coomes DA, Murphy JM (2022) Unsupervised detection of ASH dieback disease (*Hymenoscyphus fraxineus*) using diffusion-based hyperspectral image clustering. In: IGARSS 2022—2022 IEEE international geoscience and remote sensing symposium. Kuala Lumpur, Malaysia. IEEE, pp 2287–2290

Ponce JM, Aquino A, Tejada D, Al-Hadithi BM, Andújar JM (2022) A methodology for the automated delineation of crop tree crowns from UAV-based aerial imagery by means of morphological image analysis. Agronomy 12(1):43. https://doi.org/10.3390/agronomy12010043

Pontius J, Martin M, Plourde L, Hallett R (2008) Ash decline assessment in emerald ash borer-infested regions: a test of tree-level, hyperspectral technologies. Remote Sens Environ 112(5):2665–2676. https://doi.org/10.1016/j.rse.2007.12.011

Qiu L, Jing LH, Hu BX, Li H, Tang YW (2020) A new individual tree crown delineation method for high resolution multispectral imagery. Remote Sens 12(3):585. https://doi.org/10.3390/rs12030585

Safonova A, Guirado E, Maglinets Y, Alcaraz-Segura D, Tabik S (2021) Olive tree biovolume from UAV multi-resolution image segmentation with mask R-CNN. Sensors 21(5):1617. https://doi.org/10.3390/s21051617

Sahin HM, Miftahushudur T, Grieve B, Yin HJ (2023) Segmentation of weeds and crops using multispectral imaging and CRF-enhanced U-net. Comput Electron Agric 211:107956. https://doi.org/10.1016/j.compag.2023.107956

Sarabia R, Aquino A, Ponce JM, López G, Andújar JM (2020) Automated identification of crop tree crowns from UAV multispectral imagery by means of morphological image analysis. Remote Sens 12(5):748. https://doi.org/10.3390/rs12050748

Speckenwirth S, Brandmeier M, Paczkowski S (2024) Treeseg—a toolbox for fully automated tree crown segmentation based on high-resolution multispectral UAV data. Remote Sens 16(19):3660. https://doi.org/10.3390/rs16193660

Peters S, Langer G, Kätzel R (eds) (2021) Eschentriebsterben. Kriterien zur Schadensbonitur an Eschen, 1. Auflage. Fachagentur Nachwachsende Rohstoffe (FNR), Gülzow-Prüzen

Sun CX, Huang CW, Zhang HQ, Chen BQ, An F, Wang LW, Yun T (2022) Individual tree crown segmentation and crown width extraction from a heightmap derived from aerial laser scanning data using a deep learning framework. Front Plant Sci 13:914974. https://doi.org/10.3389/fpls.2022.914974

Tahar KN, Asmadin MA, Sulaiman SAH, Khalid N, Idris AN, Razali MH (2021) Individual tree crown detection using UAV orthomosaic. Eng Technol Appl Sci Res 11(2):7047–7053. https://doi.org/10.48084/etasr.4093

Timmermann V, Børja I, Hietala AM, Kirisits T, Solheim H (2011) Ash dieback: pathogen spread and diurnal patterns of ascospore dispersal, with special emphasis on Norway. EPPO Bull 41(1):14–20. https://doi.org/10.1111/j.1365-2338.2010.02429.x

Timmermann V, Nagy N, Hietala A, Børja I, Solheim H (2017) Progression of ash dieback in Norway related to tree age, disease history and regional aspects. Balt for 23:150–158

Torresan C, Berton A, Carotenuto F, Di Gennaro SF, Gioli B, Matese A, Miglietta F, Vagnoli C, Zaldei A, Wallace L (2017) Forestry applications of UAVs in Europe: a review. Int J Remote Sens 38(8–10):2427–2447. https://doi.org/10.1080/01431161.2016.1252477

Ulku I, Akagündüz E, Ghamisi P (2022) Deep semantic segmentation of trees using multispectral images. IEEE J Sel Top Appl Earth Obs Remote Sens 15:7589–7604. https://doi.org/10.1109/JSTARS.2022.3203145

Wacker K, Kim C, van Iersel MW, Sidore B, Pham T, Haidekker M, Seymour L, Ferrarezi RS (2024) Development of an automated low-cost multispectral imaging system to quantify canopy size and pigmentation. Sensors 24(17):5515. https://doi.org/10.3390/s24175515

Waser L, Küchler M, Jütte K, Stampfer T (2014) Evaluating the potential of worldview-2 data to classify tree species and different levels of ash mortality. Remote Sens 6(5):4515–4545. https://doi.org/10.3390/rs6054515

Wu L, Zhang Y, Gao Y, Zhang YI (2004) Tree crown detection and delineation in high resolution RS image. IEEE Int Geosci Remote Sens Sympos 2004:3841–3844. https://doi.org/10.1109/IGARSS.2004.1369961

Zhang JC, Huang YB, Pu RL, Gonzalez-Moreno P, Yuan L, Wu KH, Huang WJ (2019) Monitoring plant diseases and pests through remote sensing technology: a review. Comput Electron Agric 165:104943. https://doi.org/10.1016/j.compag.2019.104943

Zhang N, Wang YT, Zhang XL (2020) Extraction of tree crowns damaged by *Dendrolimus tabulaeformis* Tsai et Liu *via* spectral-spatial classification using UAV-based hyperspectral images. Plant Methods 16:135. https://doi.org/10.1186/s13007-020-00678-2

Zheng JP, Yuan S, Li WJ, Fu HH, Yu L, Huang JX (2025) A review of individual tree crown detection and delineation from optical remote sensing images: current progress and future

5 Discussion

5.1 Linking visual symptoms with leaf-level physiological and morphological traits

Ash dieback manifests as a complex interaction between pathogen infection and host response, resulting in both visible symptoms and less apparent physiological changes (Semizer-Cuming et al. 2019, Eisen et al. 2024, Przybylski et al. 2025). While crown dieback and leaf loss are well-known and easily recognizable signs of infection, these visible symptoms provide only limited insight into the underlying functional changes of affected trees.

A closer examination of leaf-level traits can reveal how ash dieback connects to key physiological processes, such as photosynthetic performance and morphological changes, that may reflect the tree's ability to cope with or resist the pathogen. However, while Publication 1 found that SLA decreases with increasing ash dieback severity, it remains unclear whether this trait is a cause or consequence of infection. In other words, it is yet to be determined whether trees with inherently lower SLA are more susceptible to ash dieback, or if SLA is reduced as a physiological response to the disease. Toome et al. (2010) reported a link between low SLA and reduced susceptibility of willows (*Salix* spp.) to leaf rust, while McIntire (2023) also associated variation in SLA with disease symptom severity. In contrast, Call and St Clair (2017) observed reduced SLA in infected aspen (*Populus tremuloides* Michx.) but emphasized that it remains unclear whether this trait is a cause or a consequence of infection. To resolve this, longitudinal studies tracking individual trees affected by ash dieback over time, prior to and following infection, would be essential. Such an approach could identify whether trees exhibiting lower SLA before visible symptoms emerge are more likely to experience severe decline. Additionally, including unaffected control populations from regions where ash dieback progression is not yet as advanced, could help distinguish baseline SLA variation from disease-induced changes. Only through these approaches can SLA be validated as a reliable early indicator of tree resilience or vulnerability to *Hymenoscyphus fraxineus*. Importantly, Publication 1 could not include completely healthy trees due to the widespread presence of ash dieback in Germany (Fuchs et al. 2024), no healthy trees were found on any of the study sites. Therefore, comparisons were limited to mildly versus severely damaged trees.

Publication 1 assessed five traits related to leaf physiology and morphology to determine the impact of ash dieback severity on a leaf-level scale. Among them, only specific traits showed significant differences between mildly and severely affected ash trees. Ash dieback severity was assessed by visually rating the disease symptoms (Peters et al. 2021), and these severity levels were then analysed in relation to the measured leaf traits.

Chlorophyll fluorescence:

Although chlorophyll fluorescence is widely used to detect plant stress (Mandal et al. 2009, Rosyara et al. 2010, Martínez-Ferri et al. 2016), its interpretation in the context of ash dieback proved challenging. While some sites and years showed lower F_v/F_m values in severely affected trees, this pattern was not consistent. Environmental stressors, particularly drought during sampling at the site Grabenstätt, likely confounded results. While low F_v/F_m can be indicators of stress, the cause of stress cannot be determined. The fungal pathogen *Hymenoscyphus fraxineus* follows a hemibiotrophic infection pattern (Mansfield et al. 2019), alternating between utilizing living host tissue (biotrophic phase) and dead host tissue (necrotrophic phase) (Perfect and Green 2001). Consequently, leaf-level stress responses may remain undetectable during the biotrophic phase, as damage to chloroplasts within the leaves is likely to occur primarily during the necrotrophic stage (Ajigboye et al. 2016).

Chlorophyll content:

Chlorophyll content measurements exhibited site-dependent trends. While the two seed plantations presented lower SPAD values in severely affected trees, the opposite was observed at the Grabenstätt site. Consistent with the observed decrease in chlorophyll content in severely damaged ash trees at the two plantation sites, numerous studies have reported reduced chlorophyll content levels in plants affected by various diseases (Zhao et al. 2011, Yahya et al. 2020, Arafat et al. 2021). The inconsistency of higher and lower SPAD values with severe damage may reflect local additional environmental influences.

Specific Leaf Area:

SLA was consistently lower in severely damaged ash trees across all study sites and in both study years, although the differences were not always statistically significant. This trend aligns with findings from studies on other diseased species (España-Guechá et al. 2020, McIntire 2023). However, SLA can vary within tree crowns depending on sunlight availability, with studies reporting higher SLA in shaded leaves and those located at the lower canopy levels in *Fraxinus excelsior* L. (Petriţan et al. 2009, Legner et al. 2014). Although this study controlled for light conditions during sampling, some within-crown variability in SLA remains possible. A negative relationship between SLA and chlorophyll content was observed, with higher chlorophyll levels corresponding to lower SLA. This pattern, also reported in other diseased plant species (Nageswara Rao et al. 2001, Nigam and Aruna 2008, Marenco et al. 2009), suggests that increased chlorophyll concentration may serve as a compensatory mechanism to offset the reduced surface area available for light absorption (Basu et al. 2019).

Leaf thickness:

Severely affected trees also tended to have thicker leaves, although this difference was statistically significant in only two of the investigations and was correlated with a reduced SLA. Thicker leaves are reported in other stressed plants as part of a defensive response (Alonso-Villaverde et al. 2011, Ahn et al. 2020), potentially due to increased cell wall development or a higher water content (McIntire 2023). However, for some species, no clear relationship between leaf thickness and infection has been observed (Jarosz et al. 1982), suggesting species-specific physiological responses. Moreover, assessing leaf hydration could provide valuable context, as it may help account for environmental influences on leaf structure (White and Montes-R 2005).

Fluctuating Asymmetry:

FA did not show significant differences between trees with varying levels of ash dieback damage. Significant differences were limited to one principal component at a single site. These findings are consistent with previous research reporting mixed results regarding the effectiveness of FA in detecting subtle stress symptoms (Ambo-Rappe et al. 2008, García-Jain et al. 2022, Gavrikov et al. 2023). These limitations, along with concerns about high measurement error and limited reproducibility (Kozlov 2015, Kozlov et al. 2017, Dodonov et al. 2024), reduce the reliability of FA as a stress indicator.

In summary, neither chlorophyll fluorescence nor FA showed significant correlations with ash dieback severity, while chlorophyll content and leaf thickness demonstrated only weak or inconsistent associations. Among all assessed traits, only SLA consistently and significantly responded to increasing disease severity, underscoring a strong relationship between ash dieback pressure and morphological changes in the leaves of *Fraxinus excelsior* L.

5.2 Assessing ash dieback severity using multisensory remote sensing

While Publication 1 investigated how visual symptoms of ash dieback relate to physiological and morphological changes at the leaf level, Publication 2 approaches the same visual severity framework from a remote sensing perspective. It complements the findings of Publication 1 by exploring whether these visually assessed severity levels can be reliably detected through UAV-derived vegetation indices and sensor data. This shared reliance on visual field ratings as a reference point links the two studies conceptually, while highlighting different methodological pathways: ground-based trait measurements versus airborne spectral analysis for assessing disease impact.

Vegetation indices derived from remote sensing imagery can highlight variations in spectral properties, often emphasizing biochemical parameters such as chlorophyll content (Cui and Zhou 2017). They are commonly used to distinguish between healthy and diseased plants at the canopy level (Yu et al. 2014). Hunt et al. (2013) demonstrated a strong and consistent correlation between a specific vegetation index and field-measured chlorophyll content, thereby highlighting the close connection between canopy physiology and remotely sensed spectral data.

Publication 2 focused on assessing the potential of UAV-based remote sensing to detect and classify ash dieback severity in *Fraxinus excelsior* L. Using RGB, multispectral, and thermal sensors across different stages of the vegetation period of the common ash, the study evaluated how well vegetation indices and newly determined thresholds could reflect visually assessed damage levels.

The results demonstrated that thresholds derived from multispectral vegetation indices, particularly DVI (Difference Vegetation Index), NDVI (Normalized Difference Vegetation Index), and GNDVI (Green Normalized Difference Vegetation Index), were most effective in distinguishing between mildly and severely affected ash trees. RGB-based indices performed slightly less well overall, although GRVI (Green-Red Vegetation Index), ExG (Excess Green Index), and RGRI (Red-Green Ratio Index) achieved the highest classification accuracies within this group. The combination of two multispectral and one RGB index led to an even higher accuracy of 77.2 %. In the context of ash dieback, multispectral vegetation indices have been shown to effectively detect varying degrees of disease severity (Waser et al. 2014, Kampen et al. 2019). More broadly, multispectral remote sensing and the derived vegetation indices have been widely recognized as valuable tools for assessing disease impact across a range of different species (Abdulridha et al. 2019, Chang et al. 2020, Ye et al. 2020). Similarly, RGB imagery, a more readily available data source, has also been reported as highly effective in detecting plant disease impacts (Cai et al. 2018, Bhandari et al. 2020, Garza et al. 2020), as it has been proven in Publication 2.

The study introduced a novel threshold-based classification approach, identifying vegetation index value ranges capable of distinguishing between mild and severe ash dieback damage. Classification accuracies of individual vegetation index thresholds reached up to 74.9 %, allowing for a realistic estimation of disease progression at the level of individual trees. However, achieving a perfect binary separation between damage classes remains challenging due to the inherently continuous and dynamic nature of tree health status. In this study, both RGB and multispectral data types successfully distinguished between varying levels of ash dieback

severity by applying threshold-based classifications to separate vegetation index values associated with mild and severe damage. UAV surveys conducted during the summer months yielded more stable and reliable vegetation index thresholds compared to those including autumn data. Although the application of vegetation index thresholds is feasible throughout the entire growing season of the common ash, surveys performed in summer are recommended to ensure the highest accuracy and consistency of results.

In contrast to multispectral and RGB data, thermal data, despite its proven utility in other plant disease contexts (Raza et al. 2015, Smigaj et al. 2015, Jafari et al. 2017, Poblete et al. 2020) did not significantly exhibit the anticipated pattern of increasing crown temperature with greater ash dieback severity. While increased canopy temperatures were observed in some UAV surveys, the effect was statistically significant in only two instances. One possible explanation lies in the spatial resolution of the thermal imagery; UAV flights were conducted at an altitude of 80 meters, resulting in an image resolution of approximately 10.48 pixels/cm, which may not be sufficient to capture subtle leaf-level temperature variations. Moreover, previous studies have shown a biphasic thermal response to disease, with an initial decrease in temperature during early infection stages followed by an increase as symptoms worsen (Lindenthal et al. 2005, Baranowski et al. 2015, Jafari et al. 2017). Since this study relied on mean canopy-level temperatures, the coexistence of leaves at varying infection stages may have masked finer-scale thermal signals. Additionally, uncertainties related to thermal sensor calibration (Leblanc et al. 2021), as well as external factors such as wind speed, wind direction, and UAV flight velocity (Malbéteau et al. 2021), may further affect the reliability and consistency of thermal measurements. These findings suggest that environmental variability, coupled with disease-specific thermal dynamics, can complicate the interpretation of thermal data for ash dieback monitoring. As such, while thermal imaging holds promise, its utility for detecting ash dieback severity under field conditions may be limited without higher resolution or targeted analyses at finer spatial scales.

Together, these findings on different remote sensing sensors underscore the strong potential of UAV-based monitoring for assessing ash dieback severity. The spectral variability captured through multispectral and RGB remote sensing closely mirrors the progression of disease symptoms identified in field-based visual assessments, demonstrating a reliable correspondence between airborne data and ground observations. Publication 1 revealed that, among the examined leaf traits investigated through field measurements, only SLA consistently showed a significant relationship with ash dieback severity. This limited number of significant leaf-level indicators

underscores that UAV-based remote sensing approaches should be prioritized for assessing overall damage severity, as they provide a scalable and efficient means of monitoring larger ash populations. However, UAV data cannot capture the fine-scale physiological and morphological changes in the same detail as field-based measurements, which remain essential for understanding specific tree responses at the leaf level. Future research should focus on directly comparing ground-based measurements, such as SLA and chlorophyll content, with specific vegetation indices derived from UAV data to link fine-scale leaf traits with large-scale UAV-based remote sensing observations.

UAV-derived methods represent a promising and scalable solution for forest health monitoring, offering practical applications for both research and conservation management, while detailed field measurements, as demonstrated in Publication 1, complement this approach by revealing subtle physiological and morphological alterations due to ash dieback.

5.3 The role of tree crown segmentation precision

While spectral indicators provide valuable insights into ash dieback severity, their accuracy depends heavily on the quality of individual tree crown segmentation. The precision with which individual crowns are delineated directly influences the reliability of vegetation index values, particularly in trees affected by advanced dieback, which often exhibit irregular canopy structures and extensive crown gaps. This leads to Publication 3, which focuses on the critical role of crown segmentation precision in ensuring robust disease assessment using UAV-based remote sensing in the context of ash dieback.

While both segmentation approaches, fine and coarse segmentation, evaluated in publication 3, achieved similarly high Intersection-over-Union (IoU) values, trees classified in vitality classes 3 and 4, characterized by extensive crown gaps, exhibited higher precision scores under the fine segmentation method. This suggests that finer delineation provides a more accurate representation of highly damaged crowns. However, when comparing mean vegetation index values calculated per tree crown across both segmentation methods, no significant differences were observed. This indicates that, for the purpose of calculating mean index values, a coarser segmentation approach remains adequate despite variations in crown structure.

Various methods for automated tree crown segmentation exist, but very few reach the segmentation detail necessary to capture crown gaps and irregular crown edges (Sarabia et al. 2020, Ponce et al. 2022). Many segmentation approaches often prioritize detecting the general outline

of tree crowns rather than capturing their detailed internal structure (Ke and Quackenbush 2011, Zheng et al. 2025). However, the findings from Publication 3 highlight the limitations of such coarse delineation, as NDVI homogeneity decreased noticeably with increasing ash dieback severity, indicating greater within-crown spectral variability in more severely affected trees. This aligns with findings by Flynn et al. (2024) who observed a decline in crown greenness towards the edges in trees exhibiting advanced ash dieback symptoms. These patterns emphasize the importance of refined crown segmentation that accounts for internal canopy structure when assessing disease severity through UAV-derived vegetation indices.

Therefore, although Publication 3 indicates that coarse segmentation is generally sufficient for calculating mean vegetation index values, the observed variability in NDVI homogeneity across vitality classes suggests that the inclusion of non-foliage elements, such as ground pixels and exposed branches, can still compromise accuracy. Epicormic shoots, which are often more prevalent in severely damaged trees, tend to be sparse and are more likely to be overlooked in coarse segmentation approaches. Since these shoots may carry possibly more vital leaves, it is crucial to ensure that all leaf areas, including those of epicormic origin, are accurately captured. For the threshold-based classification workflow introduced in Publication 2 to be truly robust, segmentation must delineate the actual leaf mass with precision, as background artifacts may obscure subtle but critical changes in spectral reflectance.

The NDVI analysis of excluded ground pixels in Publication 3 further confirmed that NDVI values from non-foliage areas were significantly lower than those derived from leaf mass. The impact of such background inclusion is context-dependent, influenced by ground cover type, such as exposed soil, understory vegetation, gras, or leaf litter, which introduces spectral noise that can vary seasonally. These confounding elements can distort mean NDVI values and weaken the correspondence with true canopy health. This underscores the importance of accurate crown delineation that excludes non-leaf components. Ultimately, UAV-based ash dieback severity classification methods, such as vegetation index thresholding, are only meaningful when they accurately reflect underlying physiological stress at the leaf level.

5.4 Challenges and limitations

While the methods applied in this dissertation offer valuable insights into ash dieback monitoring, several methodological and practical challenges must be acknowledged.

Visual assessment methods, such as the vitality assessment score, developed by Peters et al. (2021) based on Lenz et al. (2012), are widely used in forest health monitoring due to their low cost and operational simplicity. However, some limitations remain. Observer bias and inconsistency are recurring challenges, with assessments often depending heavily on expert interpretation. Lausch et al. (2017) noted that subjective field observations may vary across observers, making standardization difficult and limiting comparability. To ensure consistency across the three studies, all vitality assessments were conducted by a single trained observer. This approach minimizes inter-observer variability, which is a common limitation in visual assessments. However, it is important to recognize that the health status of ash trees is not static but rather dynamic and subject to gradual change. As such, the classification of trees into one of the six vitality classes inherently involves subjective judgement, particularly for individuals that exhibit characteristics near the threshold between two classes. This highlights the challenge of assigning discrete categories to a continuous spectrum of decline, even under standardized observation protocols.

Additionally, all ash trees across the four study sites exhibited visible symptoms of ash dieback, and no entirely healthy individuals were identified. Consequently, all three publications are limited to analyzing differences among damage classes 1 to 4, representing a gradient from mild to very severe disease symptoms. None of the studies include a true baseline comparison with unaffected trees. This limitation reflects the broader reality of ash populations in Germany, where the disease is now so widespread that finding healthy individuals has become increasingly rare. In a comprehensive nationwide study comprising over 1,300 ash trees distributed across Germany, only four were recorded as healthy (Fuchs et al. 2024), underscoring the scarcity of unaffected ash trees in current field conditions.

This widespread disease presence not only limits the availability of unaffected trees for comparative analyses but also requires careful selection of leaf samples to minimize confounding effects from visible damage or secondary stressors. Therefore, for all investigations on leaf physiology and morphology, only leaves without obvious damage were selected. Leaves showing signs of insect damage, pronounced rippling, or other unclear causes of damage were excluded during sampling. Although all sampled trees exhibited symptoms of ash dieback, only visually intact leaves were used for trait measurements. This selection approach therefore leads to a potential underestimation of disease-related stress responses at the leaf level. By focusing exclusively on visually undamaged leaf tissue, visibly affected or necrotic leaves were omitted, even if these symptoms were possibly related to ash dieback. While this was necessary to

maintain consistency in trait measurement and avoid confounding variables, it also limits the ability to capture the full spectrum of leaf-level responses to ash dieback.

This constraint on sampling scope is echoed at the canopy level, where the effectiveness of remote sensing-based classification similarly depends on capturing the full gradient of disease severity within the study population. The novel vegetation index thresholds developed in Publication 2 are based on the premise that the full spectrum of ash dieback severity, from mild (class 1) to very severe (class 4), is represented within the investigated site. For this threshold-based classification workflow to be reliably applied to other locations, those sites must similarly include trees spanning the complete range of vitality classes. If the site lacks individuals at either end of the damage spectrum, particularly those in class 1 or class 4, the validity and accuracy of the derived thresholds may be compromised. Consequently, the transferability of this approach hinges on the local presence of a comparable distribution of disease severity. Additionally, given the limited dataset size, the same data had to be reused for both training and validation purposes. This overlap can lead to optimistic accuracy estimation, as noted by Yadav and Shukla (2016).

One of the primary objectives of Publication 2 was to design a user-friendly workflow that could be implemented by forest practitioners working with real-world ash populations, without requiring extensive analytical expertise. The derived vegetation index thresholds, applied after only a few processing steps, offer a practical basis for estimating ash dieback severity. However, questions remain regarding the actual practicality of the workflow. While the use of pre-defined thresholds is straightforward, the preceding steps, including UAV surveying, orthomosaic generation, crown segmentation, vegetation index calculation, and subsequent post-processing steps, demand a certain level of technical proficiency. In practice, a foundational understanding of the required software tools is likely essential, even if the workflow can be followed after a brief introduction and explanation. To achieve a more comprehensive and robust threshold-based damage estimation, the segmentation workflow presented in Publication 3 should ideally be integrated into the approach outlined in Publication 2. However, the unsupervised machine learning algorithm employed for detailed crown delineation is considerably more complex than the straightforward application of thresholds. As such, it would likely demand a higher level of technical expertise and may not be as easily accessible to practitioners without more extensive training.

The two plantation sites, investigated with UAVs, offered several advantages, notably a spacious planting grid that mostly prevented crown overlap between ash trees. However, the novel

tree crown segmentation method developed in Publication 3 is currently not capable of individually segmenting overlapping tree crowns. Additionally, while ash tree identification on the seed plantations was straightforward due to the spacious planting grid, this task becomes considerably more complex in mixed forest stands. In such environments, an initial step would be required to accurately identify and differentiate ash trees from co-occurring species before applying segmentation or damage assessment workflows. Multiple studies have successfully developed methods to detect ash trees within mixed forest stands, highlighting the feasibility of species-specific identification in complex canopy environments. For instance, Waser et al. (2014) reported an overall accuracy of 83 % in identifying ash trees using WorldView-2 data, while Sapkota and Liang (2020) achieved a comparable accuracy of 82 %. Notably, Chan et al. (2021) demonstrated even higher classification performance, with accuracies ≥90% using UAV-based hyperspectral imagery. In complex urban environments, ash trees were identified with an accuracy of 81 % (Pontius et al. 2017). These results underscore the potential for reliably identifying ash trees in diverse forest contexts.

However, overlapping tree crowns remain a challenge in dense or unmanaged stands. To address this, additional analytical steps are required to segment individual crowns. Studies by Marques et al. (2019) and Ponce et al. (2022) have demonstrated that various advanced segmentation techniques can effectively separate overlapping crowns, thereby enhancing the accuracy of crown-level analyses in mixed-species settings.

5.5 Implications for the conservation of the common ash

Monitoring ash dieback effectively requires a multiscale approach that captures both subtle leaf-level responses and broader canopy-level symptoms. Publication 1 explored physiological and morphological changes at the leaf scale, while Publications 2 and 3 expanded this focus to the crown level, using UAV-derived spectral and structural data to assess disease severity. Together, these studies illustrate how early indicators of infection may appear at the leaf level, whereas advanced decline becomes detectable through canopy structure and reflectance patterns, underscoring the importance of integrating biological and spatial scales in disease monitoring. This work exemplifies the value of an interdisciplinary lens. By combining ground truth data (e.g. vitality assessments, SLA, chlorophyll measurements), advanced UAV-based remote sensing, and data-driven classification techniques (e.g. vegetation index thresholding, crown segmentation algorithms), it bridges the fields of plant physiology, remote sensing, and machine learning. This interdisciplinary toolkit is essential for addressing complex forest disease dynamics, where

early detection, scalability, and precision are critical for effective monitoring and conservation efforts.

Gašparović et al. (2023) emphasize the transformative role of UAVs in forest health monitoring, highlighting their capacity to extend assessments beyond traditional plot-based observations, particularly in the context of ash dieback. Similarly, Ecke et al. (2022) underscore the need for integrating UAV-based forest health monitoring into scalable, multi-temporal frameworks, highlighting the importance of early stress detection and multi-sensor strategies, to enhance long-term surveillance and adaptive management.

One of the most significant advantages of UAVs lies in their non-invasive capability to efficiently survey large, often inaccessible areas, making them particularly valuable for monitoring forest diseases such as ash dieback. Given the widespread presence of *Fraxinus excelsior* L. across both forested and urban landscapes in Europe, scalable tools for assessing disease progression across large populations are critically needed. Accurate assessments of disease severity provide vital insights into both the current health status of individual trees and the broader epidemiological progression of the disease, information that is essential for informed forest management and conservation planning.

Current recommendations, such as those by the FNR (2024) advise against the immediate removal of infected ash trees, particularly those that only show mild to moderate symptoms. Instead, they advocate for a cautious, adaptive approach focused on preserving less-affected individuals, thereby maintaining ecosystem stability and potentially supporting natural regeneration. Similarly, Skovsgaard et al. (2017) emphasize the importance of selective intervention, recommending the removal of high-risk trees, such as those near roads or infrastructure, while Enderle et al. (2019) also advise to conserve individuals that display signs of tolerance or resilience. This approach not only reduces safety risks but also facilitates natural selection by allowing potentially resistant genotypes to persist.

UAV-based remote sensing offers a promising pathway to support these management strategies. By enabling repeated, high-resolution observations over time, UAVs can aid in the long-term identification of disease-tolerant individuals. These ash trees could then serve as candidates for conservation or breeding programs aimed at enhancing resistance within ash populations, as highlighted by Adamčíková et al. (2023) and Seidel et al. (2025). Thus, integrating UAV monitoring into disease management frameworks provides both practical and strategic benefits for the conservation of *Fraxinus excelsior* L.

To further enhance monitoring and response capabilities, future research should explore longitudinal studies that track individual trees over multiple years to better understand disease progression and trait variability. Expanding the application of threshold-based workflows to new regions with differing ash population structures will be critical to evaluate their robustness and transferability. Additionally, improving crown-level detection in mixed forest stands, especially those with overlapping canopies, remains a key technical challenge. Finally, developing user-friendly analytical tools is essential to lower the entry barrier for forest practitioners and facilitate broader adoption of UAV-based monitoring strategies.

The results presented here serve as a blueprint for robust, multiscale monitoring of ash dieback and can be adapted for broader forest health applications, including different species and various plant diseases. As UAV and sensor technologies evolve, their convergence with plant pathology and data science will be central to conserving *Fraxinus excelsior* L. and managing emergent forest threats.

6 Conclusion

Ash dieback remains one of the most severe biotic threats to *Fraxinus excelsior* L. across Europe, with a progressive disease trajectory and widespread ecological implications. Monitoring the extent and severity of this disease is crucial for developing informed conservation strategies aimed at preserving this ecologically important native species. While the visible symptoms of ash dieback, such as crown thinning, shoot dieback, and premature leaf loss, are well recognized, the findings from this dissertation reveal that the physiological and morphological impacts extend beyond what can be assessed visually.

Publication 1 demonstrated that ash dieback correlates with changes in leaf-level traits. Notably, chlorophyll content showed a trend of decline in severely damaged trees at plantation sites, and leaf thickness increased in parallel with disease severity. Among all examined traits, SLA was the only one to consistently and significantly decrease with higher damage severity. This underscores the potential of SLA as a sensitive morphological indicator of disease impact, though it remains unclear whether this change is a response to the infection or a predisposing factor for susceptibility.

At the crown scale, Publications 2 and 3 established that remote sensing data, specifically RGB and multispectral UAV imagery, can detect and classify ash dieback severity. Vegetation indices

such as the GRVI for RGB imagery and the DVI for multispectral data proved especially effective. When used in combination, RGB and multispectral indices achieved classification accuracies of up to 77 %, validating UAV-based monitoring as a practical tool for surveying large ash populations.

Tree crown segmentation precision, explored in Publication 3, revealed that coarse segmentation was sufficient for calculating mean vegetation index values. However, as NDVI homogeneity declined with increased crown damage, detailed segmentation, specifically excluding crown gaps and non-foliage elements, is of high relevance.

This dissertation contributes a multiscale, interdisciplinary framework for ash dieback monitoring that integrates plant physiology, remote sensing, and machine learning. It offers a framework for practical implementation, particularly for forest managers and conservation practitioners. By translating UAV-derived data into actionable thresholds and classification routines, it bridges the gap between academic insight and operational forest health monitoring.

Furthermore, the methodologies and findings presented here can contribute to adaptive conservation strategies, especially by identifying trees with potential tolerance to the disease and enabling targeted preservation efforts with long-term monitoring. In the context of increasing forest disease pressures, such scalable approaches are essential for timely interventions and long-term ecological resilience.

7 Publication list

Reviewed publications:

1. **Buchner, L**; Eisen, A-K; Jochner-Oette, S (2025): How precise is precise enough? Tree crown segmentation using high resolution close-up multispectral UAV images and its effect on NDVI accuracy in *Fraxinus excelsior* L. trees. Journal of Forestry Research, 36. DOI: 10.1007/s11676-025-01929-5

2. **Buchner, L**; Eisen, A-K; Jochner-Oette, S (2025): Identification of damage severity in *Fraxinus excelsior* L. trees caused by ash dieback using multisensory and multitemporal UAV imagery. Forest Ecology and Management, 585. DOI: 10.1016/j.foreco.2025.122660

3. **Buchner, L**; Eisen, A-K; Jochner-Oette, S (2024): Effects of ash dieback on leaf physiology and leaf morphology of *Fraxinus excelsior* L. Trees, 38. DOI: 10.1007/s00468-024-02546-1

4. Eisen, A.-K; **Buchner, L**; Fussi, B; Jochner-Oette, S (2024): Does ash dieback affect the reproductive ecology of *Fraxinus excelsior* L.? Journal of Forestry Research, 35: 16. DOI: 10.1007/s11676-023-01670-x

5. **Buchner, L**; Eisen, A.-K; Šikoparija, B; Jochner-Oette, S (2022): Pollen Viability of *Fraxinus excelsior* in Storage Experiments and Investigations on the Potential Effect of Long-Range Transport. Forests, 13:600. DOI: 10.3390/f13040600

Publications in preparation:

6. Kahlenberg, G; **Buchner, L**; Eisen, A-K; Jochner-Oette, S: Does the health condition of the common ash tree affect its pollen viability? In preparation for Forests.

7. Fussi, B; Šeho, M; Kavaliauskas, D; Rempel, S; **Buchner, L**; Jochner-Oette, S: Klimafitness der Bäume: Phänologie und genetische Vielfalt. In preparation for AFZ – Der Wald.

Conference contributions

Oral presentations

Buchner, L; Kahlenberg, G; Eisen, A-K; Jochner-Oette, S (2024): Effects of ash dieback on pollen viability of *Fraxinus excelsior* L. and investigations on the potential effect of long-range transport on pollen viability. World Aerobiology, 1th – 5th July 2024 in Vilnius, Lithuania.

Buchner, L; Eisen, A-K; Köbölkuti, Z; Böhm, J W; von Bargen, S; Rehanek, M; Kube, M; Büttner, C; Fussi, B; Jochner-Oette, S (2023): Detektion des Einflusses von abiotischen Stressfaktoren, Krankheiten und Schädlingsbefall an Eschen mit multisensorischen und multitemporalen Daten – eine Studie im Projekt FraxVir. FowiTa. Forstwissenschaftliche Tagung, 11th – 13th September 2023 in Dresden, Germany.

Rehanek, M; Fernández Colino, H L; Al Kubrusli, R; Eisen, A-K; **Buchner, L**; Köbölkuti, Z; Böhm, J W; Fussi, B; Kube, M; Jochner-Oette, S; von Bargen, S; Büttner, C (2023): Erfassung und Beurteilung der Virusvielfalt in Eschen - eine Studie im FraxVir Projekt. FowiTa. Forstwissenschaftliche Tagung, 11th – 13th September 2023 in Dresden, Germany.

Buchner, L; Eisen, A-K; Köbölkuti, Z; Böhm, J W; Köpke, K; Al Kubrusli, R; Landgraf, M; von Bargen, S; Fussi, B; Kube, M; Büttner, C; Jochner-Oette, S (2022): Detection of the influence of abiotic and biotic stressors on common ash using multisensorial and multitemporal data. IUFRO. 6th – 9th September in Lisbon, Portugal.

Böhm, J W; Eisen, A-K; **Buchner, L**; Köbölkuti, Z; Landgraf, M; Köpke, K; Al Kubrusli, R; von Bargen, S; Fussi, B; Jochner-Oette, S; Büttner, C; Kube, M (2022): Molecular monitoring of *Hymenoscyphus fraxineus*. IUFRO. 6th – 9th September in Lisbon, Portugal.

Poster presentations

Buchner, L; von Bargen, S; Rehanek, M; Böhm, J W; Köbölkuti, Z; Büttner, C; Kube, M; Fussi, B; Eisen, A-K; Jochner-Oette, S (2023): Detektion des Einflusses von abiotischen Stressfaktoren, Krankheiten und Schädlingsbefall an Eschen mit multisensorischen und multitemporalen Daten. Deutsche Pflanzenschutztagung. 26th – 29th September in Göttingen, Germany.

Rehanek, M; Al Kubrusli, R; Frey, L; Eisen, A-K; **Buchner, L**; Köpke, K; Köbölkuti, Z; Böhm, J W; Fussi, B; Kube, M; Jochner-Oette, S; von Bargen, S; Büttner, C (2023): Untersuchungen zum Virusstatus von Mutterbaumbeständen der Gemeinen Esche im Rahmen des FraxVir Projektes. FowiTa. Forstwissenschaftliche Tagung, 11th – 13th September 2023 in Dresden, Germany.

8 References

Abdulridha J, Batuman O, Ampatzidis Y (2019) UAV-Based Remote Sensing Technique to Detect Citrus Canker Disease Utilizing Hyperspectral Imaging and Machine Learning. Remote Sensing 11(11):1373. doi: 10.3390/rs11111373

Adamčíková K, Pažitný J, Pastirčáková K (2023) Individual resistance of *Fraxinus angustifolia* and *F. excelsior* clones to *Hymenoscyphus fraxineus*. Journal of Plant Protection Research. doi: 10.24425/122937

Ahn E, Odvody G, Prom LK, Magill C (2020) Leaf angle distribution in Johnsongrass, leaf thickness in sorghum and Johnsongrass, and association with response to *Colletotrichum sublineola*. Scientific reports 10:22320. doi: 10.1038/s41598-020-79473-x

Ajigboye OO, Bousquet L, Murchie EH, Ray RV (2016) Chlorophyll fluorescence parameters allow the rapid detection and differentiation of plant responses in three different wheat pathosystems. Functional plant biology 43(4):356–369. doi: 10.1071/FP15280

Albetis J, Duthoit S, Guttler F, Jacquin A, Goulard M, Poilvé H, Féret J-B, Dedieu G (2017) Detection of *Flavescence dorée* Grapevine Disease Using Unmanned Aerial Vehicle (UAV) Multispectral Imagery. Remote Sensing 9(4):308. doi: 10.3390/rs9040308

Alonso-Villaverde V, Gago P, Rodríguez-García MI, Martínez MC (2011) Leaf thickness and structure of *Vitis Vinifera* L. CV. Albariño clones and its possible relation with susceptibility to downy mildew (*Plasmopara Vitivola*) infection. J. Int. Sci. Vigne Vin.(45):161–169. doi: 10.20870/oeno-one.2011.45.3.1492

Ambo-Rappe R, Lajus DL, Schreider MJ (2008) Increased heavy metal and nutrient contamination does not increase fluctuating asymmetry in the seagrass *Halophila ovalis*. Ecological Indicators 8(1):100–103. doi: 10.1016/j.ecolind.2006.12.004

Arafat KH, Hassan M, Hussein EA (2021) Detection, Disease Severity and Chlorophyll Prediction of Date Palm Leaf Spot Fungal Diseases. New Valley Journal of Agricultural Science(2):98–110. doi: 10.21608/nvjas.2022.110022.1027

Argamosa RJL, Paringit EC, Quinton KR, Tandoc FAM, Faelga RAG, Ibañez CAG, Posilero MAV, Zaragosa GP (2016) Fully automated GIS-based individual tree crown delineation based on curvature values from a LiDAR derived canopy height model in a coniferous plantation. Int. Arch. Photogramm. Remote Sens. Spatial Inf. Sci. XLI-B8:563–569. doi: 10.5194/isprsarchives-XLI-B8-563-2016

Baral H-O, Queloz V, Hosoya T (2014) *Hymenoscyphus fraxineus,* the correct scientific name for the fungus causing ash dieback in Europe. International Mycological Association Fungus:79–80. doi: 10.5598/imafungus.2014.05.01.09

Baranowski P, Jedryczka M, Mazurek W, Babula-Skowronska D, Siedliska A, Kaczmarek J (2015) Hyperspectral and thermal imaging of oilseed rape (*Brassica napus*) response to fungal species of the genus Alternaria. PloS one 10(3):e0122913. doi: 10.1371/journal.pone.0122913

Barbedo J (2019) A Review on the Use of Unmanned Aerial Vehicles and Imaging Sensors for Monitoring and Assessing Plant Stresses. Drones 3(2):40. doi: 10.3390/drones3020040

Barón M, Flexas J, Delucia EH (2012) Photosynthetic responses to biotic stress. In: Flexas J, Loreto F, Medrano H (eds) Terrestrial photosynthesis in a changing environment: a molecular, physiological and ecological approach. Cambridge University Press, Cambridge, UK, pp 331–350

Basu PS, Pratap A, Gupta S, Sharma K, Tomar R, Singh NP (2019) Physiological Traits for Shortening Crop Duration and Improving Productivity of Greengram (*Vigna radiata* L. Wilczek) Under High Temperature. Frontiers in plant science 10. doi: 10.3389/fpls.2019.01508

Bates E, Popović M, Marsh C, Clark R, Kovac M, Bahadir Kocer B (2025) Leaf Level Ash Dieback Disease Detection and Online Severity Estimation With UAVs. IEEE Access 13:55499–55511. doi: 10.1109/ACCESS.2025.3541980

Bhandari M, Ibrahim AM, Xue Q, Jung J, Chang A, Rudd JC, Maeda M, Rajan N, Neely H, Landivar J (2020) Assessing winter wheat foliage disease severity using aerial imagery acquired from small Unmanned Aerial Vehicle (UAV). Computers and Electronics in Agriculture 176:105665. doi: 10.1016/j.compag.2020.105665

Buchner L, Eisen A-K, Šikoparija B, Jochner-Oette S (2022) Pollen Viability of *Fraxinus excelsior* in Storage Experiments and Investigations on the Potential Effect of Long-Range Transport. Forests 13(4):600. doi: 10.3390/f13040600

Bundesministerium für Ernährung und Landwirtschaft (BMEL) (2024) Der Wald in Deutschland - Ausgewählte Ergebnisse der vierten Bundeswaldinventur

Cai N, Zhou X, Yang Y, Wang J, Zhang D, Hu R (2018) Use of UAV images to assess narrow brown leaf spot severity in rice. International Journal of Precision Agricultural Aviation 1(1):38–42. doi: 10.33440/j.ijpaa.20190202.47

Call AC, St Clair SB (2017) Outbreak of *Drepanopeziza* fungus in aspen forests and variation in stand susceptibility: leaf functional traits, compensatory growth and phenology. Tree physiology 37(9):1198–1207. doi: 10.1093/treephys/tpx088

Chaerle L, van Caeneghem W, Messens E, Lambers H, van Montagu M, van der Straeten D (1999) Presymptomatic visualization of plant–virus interactions by thermography. Nature Biotechnology(17):813–816

Chan AHY, Barnes C, Swinfield T, Coomes DA (2021) Monitoring ash dieback (*Hymenoscyphus fraxineus*) in British forests using hyperspectral remote sensing. Remote Sens Ecol Conserv 7(2):306–320. doi: 10.1002/rse2.190

Chang A, Yeom J, Jung J, Landivar J (2020) Comparison of Canopy Shape and Vegetation Indices of Citrus Trees Derived from UAV Multispectral Images for Characterization of Citrus Greening Disease. Remote Sensing 12(24):4122. doi: 10.3390/rs12244122

Coker TLR, Rozsypálek J, Edwards A, Harwood TP, Butfoy L, Buggs RJA (2019) Estimating mortality rates of European ash (*Fraxinus excelsior*) under the ash dieback (*Hymenoscyphus fraxineus*) epidemic. Plants People Planet 1(1):48–58. doi: 10.1002/ppp3.11

Cui S, Zhou K (2017) A comparison of the predictive potential of various vegetation indices for leaf chlorophyll content. Earth Sci Inform 10(2):169–181. doi: 10.1007/s12145-016-0281-3

Dalponte M, Reyes F, Kandare K, Gianelle D (2015) Delineation of Individual Tree Crowns from ALS and Hyperspectral data: a comparison among four methods. European Journal of Remote Sensing 48(1):365–382. doi: 10.5721/EuJRS20154821

Dash JP, Watt MS, Pearse GD, Heaphy M, Dungey HS (2017) Assessing very high resolution UAV imagery for monitoring forest health during a simulated disease outbreak. ISPRS Journal of Photogrammetry and Remote Sensing 131:1–14. doi: 10.1016/j.isprsjprs.2017.07.007

Dobrowolska D, Hein S, Oosterbaan A, Wagner S, Clark J, Skovsgaard JP (2011) A review of European ash (*Fraxinus excelsior* L.): implications for silviculture. Forestry 84(2):133–148. doi: 10.1093/forestry/cpr001

Dodonov P, Braga AL, Arruda LH, Alves-Ferreira G, Silva-Matos DM (2024) Is leaf fluctuating asymmetry related to plant and leaf size in *Miconia albicans*, a common Melastomataceae species? Brazilian journal of biology 84:e260884. doi: 10.1590/1519-6984.260884

Ecke S, Dempewolf J, Frey J, Schwaller A, Endres E, Klemmt H-J, Tiede D, Seifert T (2022) UAV-Based Forest Health Monitoring: A Systematic Review. Remote Sensing 14(13):3205. doi: 10.3390/rs14133205

Eisen A-K, Buchner L, Fussi B, Jochner-Oette S (2024) Does ash dieback affect the reproductive ecology of *Fraxinus excelsior* L.? J. For. Res. 35(1). doi: 10.1007/s11676-023-01670-x

Eisen A-K, Fussi B, Šikoparija B, Jochner-Oette S (2022) Aerobiological Pollen Deposition and Transport of *Fraxinus excelsior* L. at a Small Spatial Scale. Forests 13(3):424. doi: 10.3390/f13030424

Eisen A-K, Semizer-Cuming D, Jochner-Oette S, Fussi B (2023) Pollination success of *Fraxinus excelsior* L. in the context of ash dieback. Annals of Forest Science 80(1). doi: 10.1186/s13595-023-01189-5

Enderle R, Bußkamp J, Metzler B (2017a) Growth Performance of Dense Natural Regeneration of *Fraxinus excelsior* under Attack of the Ash Dieback Agent *Hymenoscyphus fraxineus*. Baltic Forestry(23(1)):218–228

Enderle R, Nakou A, Thomas K, Metzler B (2015) Susceptibility of autochthonous German *Fraxinus excelsior* clones to *Hymenoscyphus pseudoalbidus* is genetically determined. Annals of Forest Science 72(2):183–193. doi: 10.1007/s13595-014-0413-1

Enderle R, Sander F, Metzler B (2017b) Temporal development of collar necroses and butt rot in association with ash dieback. iForest 10(3):529–536. doi: 10.3832/ifor2407-010

Enderle R, Stenlid J, Vasaitis R (2019) An overview of ash (*Fraxinus* spp.) and the ash dieback disease in Europe. CABI Reviews:1–12. doi: 10.1079/PAVSNNR201914025

España-Guechá MS, Cayón-Salinas DG, Darghan-Contreras AE, Ochoa-Cadavid I (2020) Leaf area, chlorophyll content, and root dry mass in oil palms (*Elaeis guineensis* Jacq.) affected by the plumero disorder. Agron. Colomb. 38(3):335–341. doi: 10.15446/agron.colomb.v38n3.85309

Fachagentur Nachwachsende Rohstoffe e. V. (FNR) (2024) Zukunft der Esche. Empfehlungen zum forstbetrieblichen Umgang mit dem Eschentriebsterben

Flynn WRM, Grieve SWD, Henshaw AJ, Owen HJF, Buggs RJA, Metheringham CL, Plumb WJ, Stocks JJ, Lines ER (2024) UAV-derived greenness and within-crown spatial patterning can detect ash dieback in individual trees. Ecol Sol and Evidence 5(2). doi: 10.1002/2688-8319.12343

Freudenberg M, Magdon P, Nölke N (2022) Individual tree crown delineation in high-resolution remote sensing images based on U-Net. Neural Comput & Applic 34(24):22197–22207. doi: 10.1007/s00521-022-07640-4

Fuchs S, Häuser H, Peters S, Knauf L, Rentschler F, Kahlenberg G, Kätzel R, Evers J, Paar U, Langer GJ (2024) Ash dieback assessments on intensive monitoring plots in Germany: influence of stand, site and time on disease progression. J Plant Dis Prot 131(5):1355–1372. doi: 10.1007/s41348-024-00889-y

García-Jain SE, Maldonado-López Y, Oyama K, Fagundes M, Faria ML de, Espírito-Santo MM, Cuevas-Reyes P (2022) Effects of forest fragmentation on plant quality, leaf morphology and herbivory of *Quercus deserticola*: is fluctuating asymmetry a good indicator of environmental stress? Trees 36(2):553–567. doi: 10.1007/s00468-021-02228-2

Garza BN, Ancona V, Enciso J, Perotto-Baldivieso HL, Kunta M, Simpson C (2020) Quantifying Citrus Tree Health Using True Color UAV Images. Remote Sensing 12(1):170. doi: 10.3390/rs12010170

Gašparović M, Pilaš I, Klobučar D, Gašparović I (2023) Monitoring Ash Dieback in Europe—An Unrevealed Perspective for Remote Sensing? Remote Sensing 15(5):1178. doi: 10.3390/rs15051178

Gavrikov DE, Zverev V, Rachenko MA, Pristavka AA, Kozlov MV (2023) Experimental Evidence Questions the Relationship between Stress and Fluctuating Asymmetry in Plants. Symmetry 15(2). doi: 10.3390/sym15020339

Goberville E, Hautekèete N-C, Kirby RR, Piquot Y, Luczak C, Beaugrand G (2016) Climate change and the ash dieback crisis. Scientific reports 6:35303. doi: 10.1038/srep35303

Graham JH (2021) Fluctuating Asymmetry and Developmental Instability, a Guide to Best Practice. Symmetry 13(1). doi: 10.3390/sym13010009

Graham JH, Shimizu K, Emlen JM, Freeman DC, Merkel J (2003) Growth models and the expected distribution of fluctuating asymmetry. Biological Journal of the Linnean Society(80):57–65. doi: 10.1046/j.1095-8312.2003.00220.x

Gross A, Holdenrieder O, Pautasso M, Queloz V, Sieber TN (2014) *Hymenoscyphus pseudoalbidus*, the causal agent of European ash dieback. Molecular plant pathology 15(1):5–21. doi: 10.1111/mpp.12073

Hashim IC, Shariff ARM, Bejo SK, Muharam FM, Ahmad K, Hashim H (2020) Application of thermal imaging for plant disease detection. IOP Conf. Ser.: Earth Environ. Sci. 540(1):12052. doi: 10.1088/1755-1315/540/1/012052

Hochwender C, Fritz R (1999) Fluctuating asymmetry in *Salix* hybrid system: The importance of genetic versus environmental causes. Evolution(53):408–416. doi: 10.1111/j.1558-5646.1999.tb03776.x

Huete AR (2012) Vegetation Indices, Remote Sensing and Forest Monitoring. Geography Compass 6(9):513–532. doi: 10.1111/j.1749-8198.2012.00507.x

Hultberg T, Sandström J, Felton A, Öhman K, Rönnberg J, Witzell J, Cleary M (2020) Ash dieback risks an extinction cascade. Biological Conservation 244:108516. doi: 10.1016/j.biocon.2020.108516

Hunt ER, Doraiswamy PC, McMurtrey JE, Daughtry CS, Perry EM, Akhmedov B (2013) A visible band index for remote sensing leaf chlorophyll content at the canopy scale. International Journal of Applied Earth Observation and Geoinformation 21:103–112. doi: 10.1016/j.jag.2012.07.020

Jafari M, Minaei S, Safaie N (2017) Detection of pre-symptomatic rose powdery-mildew and gray-mold diseases based on thermal vision. Infrared Physics & Technology 85:170–183. doi: 10.1016/j.infrared.2017.04.023

Jarosz AM, Sheets M, Levy M (1982) Cuticle thickness in Phlox and resistance to powdery mildew: an unreliable line of defense. American Journal of Botany(69):824–828. doi: 10.2307/2442974

Kamińska A, Lisiewicz M, Kraszewski B, Tkaczyk M, Stereńczak K, Wysocka-Fijorek E (2025) Assessing Ash (*Fraxinus excelsior* L.) Dieback Dynamics in the Białowieża Forest, Poland, Using Bi-Temporal High-Resolution Remote Sensing Data. Forests 16(3):506. doi: 10.3390/f16030506

Kampen M, Lederbauer S, Mund J-P, Immitzer M (2019) UAV-Based Multispectral Data for Tree Species Classification and Tree Vitality Analysis. Dreiländertagung der DGPF, der OVG und der SGPF in Wien, Österreich – Publikationen der DGPF(28):623–639

Katabuchi M (2015) *LeafArea*: an R package for rapid digital image analysis of leaf area. Ecological Research 30(6):1073–1077. doi: 10.1007/s11284-015-1307-x

Ke Y, Quackenbush LJ (2011) A review of methods for automatic individual tree-crown detection and delineation from passive remote sensing. International Journal of Remote Sensing 32(17):4725–4747. doi: 10.1080/01431161.2010.494184

Kestur R, Angural A, Bashir B, Omkar SN, Anand G, Meenavathi MB (2018) Tree Crown Detection, Delineation and Counting in UAV Remote Sensed Images: A Neural Network Based Spectral–Spatial Method. J Indian Soc Remote Sens 46(6):991–1004. doi: 10.1007/s12524-018-0756-4

Khaled AY, Aziz SA, Bejo SK, Nawi NM, Seman IA, Izzuddin MA (2018) Dielectric Constant and Chlorophyll Content Measurements for Basal Stem Tor (BSR) Disease Detection. The 2018 International Conference on Signals and Systems:69–72. doi: 10.1109/ICSIGSYS.2018.8373570

Kirisits T, Matlakova M, Mottinger-Kroupa S, Halmschlager E, Lakatos F (2010) *Chalara fraxinea* associated with dieback of narrow-leafed ash (*Fraxinus angustifolia*). Plant Pathology 59(2):411. doi: 10.1111/j.1365-3059.2009.02162.x

Kjær ED, McKinney LV, Nielsen LR, Hansen LN, Hansen JK (2012) Adaptive potential of ash (*Fraxinus excelsior*) populations against the novel emerging pathogen *Hymenoscyphus pseudoalbidus*. Evolutionary applications 5(3):219–228. doi: 10.1111/j.1752-4571.2011.00222.x

Klesse S, Abegg M, Hopf SE, Gossner MM, Rigling A, Queloz V (2021) Spread and Severity of Ash Dieback in Switzerland – Tree Characteristics and Landscape Features Explain Varying Mortality Probability. Front. For. Glob. Change 4. doi: 10.3389/ffgc.2021.645920

Klisarić NB, Miljković D, Avramov S, Zivković U, Tarasjev A (2014) Fluctuating asymmetry in *Robinia pseudoacacia* leaves—possible in situ biomarker? Environmental science and pollution research international 21:12928–12940. doi: 10.1007/s11356-014-3211-2

Konica Minolta Optics, Inc. (2009) Chlorophyll Meter SPAD-502Plus

Kowalski T (2006) *Chalara fraxinea* sp. nov. associated with dieback of ash (*Fraxinus excelsior)* in Poland. Forest Pathology(36):264–270. doi: 10.1111/j.1439-0329.2006.00453.x

Kozlov MV (2015) How reproducible are the measurements of leaf fluctuating asymmetry? PeerJ 3:e1027. doi: 10.7717/peerj.1027

Kozlov MV, Cornelissen T, Gavrikov DE, Kunavin MA, Lama AD, Milligan JR, Zverev V, Zvereva EL (2017) Reproducibility of fluctuating asymmetry measurements in plants: Sources of variation and implications for study design. Ecological Indicators 73:733–740. doi: 10.1016/j.ecolind.2016.10.033

Kumari A, Kumar M (2015) Physiology of diseased plants and plant response against pathogen attack. In: Sinha A, Srivastava S, Kumar R (eds) Microbial Biodiversity: A Boon for Agriculture Sustainability. Biotech books, New Delhi, pp 525–536

Lamalakshmi Devi E, Kumar S, Basanta Singh T, Sharma SK, Beemrote A, Devi CP, Chongtham SK, Singh CH, Yumlembam RA, Haribhushan A, Prakash N, Wani SH (2017) Adaptation Strategies and Defence Mechanisms of Plants During Environmental Stress. In: Ghorbanpour M, Varma A (eds) Medicinal Plants and Environmental Challenges. Springer International Publishing, Cham, pp 359–413

Langer G (2017) Collar Rots in Forests of Northwest Germany Affected by Ash Dieback. Baltic Forestry(23(1)):4–19

Langer GJ, Fuchs S, Osewold J, Peters S, Schrewe F, Ridley M, Kätzel R, Bubner B, Grüner J (2022) FraxForFuture—research on European ash dieback in Germany. J Plant Dis Prot 129(6):1285–1295. doi: 10.1007/s41348-022-00670-z

Lassalle G, Ferreira MP, La Rosa LEC, Souza Filho CR de (2022) Deep learning-based individual tree crown delineation in mangrove forests using very-high-resolution satellite imagery. ISPRS Journal of Photogrammetry and Remote Sensing 189:220–235. doi: 10.1016/j.isprsjprs.2022.05.002

Lausch A, Erasmi S, King D, Magdon P, Heurich M (2017) Understanding Forest Health with Remote Sensing-Part II—A Review of Approaches and Data Models. Remote Sensing 9(2):129. doi: 10.3390/rs9020129

Leblanc G, Kalacska M, Arroyo-Mora JP, Lucanus O, Todd A (2021) A Practical Validation of Uncooled Thermal Imagers for Small RPAS. Drones 5(4):132. doi: 10.3390/drones5040132

Legner N, Fleck S, Leuschner C (2014) Within-canopy variation in photosynthetic capacity, SLA and foliar N in temperate broad-leaved trees with contrasting shade tolerance. Trees 28(1):263–280. doi: 10.1007/s00468-013-0947-0

Lenz H, Straßer L, Baumann M, Baier U (2012) Boniturschlüssel zur Einstufung der Vitalität von Alteschen. AFZ-DerWald:18–19

Lindenthal M, Steiner U, Dehne H-W, Oerke E-C (2005) Effect of Downy Mildew Development on Transpiration of Cucumber Leaves Visualized by Digital Infrared Thermography. The American Phytopathological Society(95(3)):233–240. doi: 10.1094/PHYTO-95-0233

Lobo A, McKinney LV, Hansen JK, Kjær ED, Nielsen LR (2015) Genetic variation in dieback resistance in *Fraxinus excelsior* confirmed by progeny inoculation assay. Forest Pathology 45(5):379–387. doi: 10.1111/efp.12179

Malbéteau Y, Johansen K, Aragon B, Al-Mashhawari SK, McCabe MF (2021) Overcoming the Challenges of Thermal Infrared Orthomosaics Using a Swath-Based Approach to Correct for Dynamic Temperature and Wind Effects. Remote Sensing 13(16):3255. doi: 10.3390/rs13163255

Mandal K, Saravanan R, Maiti S, Kothari IL (2009) Effect of downy mildew disease on photosynthesis and chlorophyll fluorescence in *Plantago ovata* Forsk. Journal of Plant Diseases and Protection(116):164–168. doi: 10.1007/BF03356305

Mansfield J, Brown I, Papp-Rupar M (2019) Life at the edge – the cytology and physiology of the biotroph to necrotroph transition in *Hymenoscyphus fraxineus* during lesion formation in ash. Plant Pathology 68(5):908–920. doi: 10.1111/ppa.13014

Marenco RA, Antezana-Vera SA, Nascimento H (2009) Relationship between specific leaf area, leaf thickness, leaf water content and *SPAD-502* readings in six Amazonian tree sprecies. Photosynthetica(47):184–190. doi: 10.1007/s11099-009-0031-6

Marques P, Pádua L, Adão T, Hruška J, Peres E, Sousa A, Sousa JJ (2019) UAV-Based Automatic Detection and Monitoring of Chestnut Trees. Remote Sensing 11(7):855. doi: 10.3390/rs11070855

Martínez-Ferri E, Zumaquero A, Ariza MT, Barceló A, Pliego C (2016) Nondestructive Detection of White Root Rot Disease in Avocado Rootstocks by Leaf Chlorophyll Fluorescence. Plant disease 100(1):49–58. doi: 10.1094/PDIS-01-15-0062-RE

Maxwell K, Johnson GN (2000) Chlorophyll flourescence - a practical guide. Journal of experimental botany(51):659–668. doi: 10.1093/jexbot/51.345.659

McIntire CD (2023) Physiological impacts of beech leaf disease across a gradient of symptom severity among understory American beech. Front. For. Glob. Change 6. doi: 10.3389/ffgc.2023.1146742

McKinney LV, Nielsen LR, Collinge DB, Thomsen IM, Hansen JK, Kjær ED (2014) The ash dieback crisis: genetic variation in resistance can prove a long-term solution. Plant Pathology 63(3):485–499. doi: 10.1111/ppa.12196

McKinney LV, Nielsen LR, Hansen JK, Kjær ED (2011) Presence of natural genetic resistance in *Fraxinus excelsior* (Oleraceae) to *Chalara fraxinea* (Ascomycota): an emerging infectious disease. Heredity 106(5):788–797. doi: 10.1038/hdy.2010.119

Metzler B, Herbstritt S (2014) Sicherheitsrisiko durch Stammfußnekrosen an Eschen, insbesondere auf Nassstandorten. FVA Waldschutz-INFO

Mevy JP, Guibal F, Lecareux C, Miglietta F (2020) The decline of *Fraxinus angustifolia* Vahl in a Mediterranean salt meadow: Chlorophyll fluorescence measurements in long-term field experiment. Estuarine, Coastal and Shelf Science 247:107068. doi: 10.1016/j.ecss.2020.107068

Miraki M, Sohrabi H, Fatehi P, Kneubuehler M (2021) Individual tree crown delineation from high-resolution UAV images in broadleaf forest. Ecological Informatics 61:101207. doi: 10.1016/j.ecoinf.2020.101207

Mitchell RJ, Broome A, Beaton JK, Bellamy PE, Ellis CJ, Hester AJ, Hodgetts NG, Iason GR, Littlewood NA, Newey S, Pozsgai G, Ramsay S, Riach D, Stockan JA, Taylor AFS,

Woodward S (2017) Challenges in Assessing the Ecological Impacts of Tree Diseases and Mitigation Measures: the Case of *Hymenoscyphus fraxineus* and *Fraxinus excelsior*. Baltic Forestry(23(1)):116–140

Mohan M, Silva C, Klauberg C, Jat P, Catts G, Cardil A, Hudak A, Dia M (2017) Individual Tree Detection from Unmanned Aerial Vehicle (UAV) Derived Canopy Height Model in an Open Canopy Mixed Conifer Forest. Forests 8(9):340. doi: 10.3390/f8090340

Murchie EH, Lawson T (2013) Chlorophyll fluorescence analysis: a guide to good practice and understanding some new applications. Journal of experimental botany 64(13):3983–3998. doi: 10.1093/jxb/ert208

Nageswara Rao RC, Talwar HS, Wright GC (2001) Rapid Assessment of Specific Leaf Area and Leaf Nitrogen in Peanut (*Arachis hypogaea* L.) using a Chlorophyll Meter. J Agronomy Crop Science 186(3):175–182. doi: 10.1046/j.1439-037X.2001.00472.x

Nielsen LR, McKinney LV, Hietala AM, Kjær ED (2017) The susceptibility of Asian, European and North American *Fraxinus* species to the ash dieback pathogen *Hymenoscyphus fraxineus* reflects their phylogenetic history. Eur J Forest Res 136(1):59–73. doi: 10.1007/s10342-016-1009-0

Nigam SN, Aruna R (2008) Stability of soil plant analytical development (SPAD) chlorophyll meter reading (SCMR) and specific leaf area (SLA) and their association across varying soil moisture stress conditions in groundnut (*Arachis hypogaea* L.). Euphytica 160(1):111–117. doi: 10.1007/s10681-007-9581-5

Ortiz-Bustos CM, Pérez-Bueno ML, Barón M, Molinero-Ruiz L (2017) Use of Blue-Green Fluorescence and Thermal Imaging in the Early Detection of Sunflower Infection by the Root Parasitic Weed *Orobanche cumana* Wallr. Frontiers in plant science 8:833. doi: 10.3389/fpls.2017.00833

Palmer AR, Strobeck C (1986) Fluctuating Asymmetry: Measurement, Analysis, Patterns. Ann. Rev. Ecol. Syst.(17):391–421. doi: 10.1146/annurev.es.17.110186.002135

Palmer RR, Strobeck C (2003) Fluctuating Asymmetry Analyses Revisited. In: Polak M (ed) Developmental instability. Causes and consequences. Oxford University Press, Oxford, pp 279–319

Pautasso M, Aas G, Queloz V, Holdenrieder O (2013) European ash (*Fraxinus excelsior*) dieback – A conservation biology challenge. Biological Conservation 158:37–49. doi: 10.1016/j.biocon.2012.08.026

Perfect SE, Green JR (2001) Infection structures of biotrophic and hemibiotrophic fungal plant pathogens. Molecular plant pathology 2(2):101–108. doi: 10.1046/j.1364-3703.2001.00055.x

Peters S, Langer G, Kätzel R (eds) (2021) Eschentriebsterben. Kriterien zur Schadensbonitur an Eschen, 1. Auflage. Fachagentur Nachwachsende Rohstoffe (FNR), Gülzow-Prüzen

Petriţan AM, Lüpke B von, Petriţan IC (2009) Influence of light availability on growth, leaf morphology and plant architecture of beech (*Fagus sylvatica* L.), maple (*Acer pseudo-platanus* L.) and ash (*Fraxinus excelsior* L.) saplings. Eur J Forest Res 128(1):61–74. doi: 10.1007/s10342-008-0239-1

Pliura A, Lygis V, Marčiulyniene D, Suchockas V, Bakys R (2016) Genetic variation of *Fraxinus excelsior* half-sib families in response to ash dieback disease following simulated spring frost and summer drought treatments. iForest 9(1):12–22. doi: 10.3832/ifor1514-008

Poblete T, Camino C, Beck P, Hornero A, Kattenborn T, Saponari M, Boscia D, Navas-Cortes JA, Zarco-Tejada PJ (2020) Detection of *Xylella fastidiosa* infection symptoms with airborne multispectral and thermal imagery: Assessing bandset reduction performance from hyperspectral analysis. ISPRS Journal of Photogrammetry and Remote Sensing 162:27–40. doi: 10.1016/j.isprsjprs.2020.02.010

Polk SL, Chan AHY, Cui K, Plemmons RJ, Coomes DA, Murphy JM (2022) Unsupervised detection of ash dieback disease (*Hymenoscyphus fraxineus*) using diffusion-based hyperspectral image clustering. IGARSS 2022 - 2022 IEEE Int. Geosci. Remote Sens. Symp.:2287–2290. doi: 10.1109/ IGARSS46834.2022.9883429

Ponce JM, Aquino A, Tejada D, Al-Hadithi BM, Andújar JM (2022) A Methodology for the Automated Delineation of Crop Tree Crowns from UAV-Based Aerial Imagery by Means of Morphological Image Analysis. Agronomy 12(1):43. doi: 10.3390/agronomy12010043

Pontius J, Hanavan RP, Hallett RA, Cook BD, Corp LA (2017) High spatial resolution spectral unmixing for mapping ash species across a complex urban environment. Remote Sensing of Environment 199:360–369. doi: 10.1016/j.rse.2017.07.027

Przybylski P, Mohytych V, Sikora K (2025) Spring's Signal: Can Bud Burst Timing Enhance Resistance to Ash Dieback in Europe? Forests 16(1):141. doi: 10.3390/f16010141

Qiu L, Jing L, Hu B, Li H, Tang Y (2020) A New Individual Tree Crown Delineation Method for High Resolution Multispectral Imagery. Remote Sensing 12(3):585. doi: 10.3390/rs12030585

Raza S-A, Prince G, Clarkson JP, Rajpoot NM (2015) Automatic detection of diseased tomato plants using thermal and stereo visible light images. PloS one 10(4):e0123262. doi: 10.1371/journal.pone.0123262

Rodrigues FA, Einhardt AM, Oliveira LM, Dias CS (2018) Physiological and biochemical changes in plants infected by pathogens. In: VIII Simpósio Sobre Atualidades em Fitopatologia (ed) Ferramentas Moleculares Aplicadas à Fitopatologia

Rosyara UR, Subedi S, Duveiller E, Sharma RC (2010) The effect of spot blotch and heat stress on variation of canopy temperature depression, chlorophyll fluorescence and chlorophyll content of hexaploid wheat genotypes. Euphytica 174(3):377–390. doi: 10.1007/s10681-010-0136-9

Sapkota BB, Liang L (2020) High-resolution mapping of ash (*Fraxinus* spp.) in bottomland hardwoods to slow Emerald Ash Borer infestation. Science of Remote Sensing 1:100004. doi: 10.1016/j.srs.2020.100004

Sarabia R, Aquino A, Ponce JM, López G, Andújar JM (2020) Automated Identification of Crop Tree Crowns from UAV Multispectral Imagery by Means of Morphological Image Analysis. Remote Sensing 12(5):748. doi: 10.3390/rs12050748

Seidel H, Šeho M, Fussi B (2025) Hope for ash conservation and propagation—single individuals can be highly resistant to an invasive pathogen. J Plant Dis Prot 132(1). doi: 10.1007/s41348-024-01034-5

Semizer-Cuming D, Finkeldey R, Nielsen LR, Kjær ED (2019) Negative correlation between ash dieback susceptibility and reproductive success: good news for European ash forests. Annals of Forest Science 76(1). doi: 10.1007/s13595-019-0799-x

Skovsgaard JP, Wilhelm GJ, Thomsen IM, Metzler B, Kirisits T, Havrdová L, Enderle R, Dobrowolska D, Cleary M, Clark J (2017) Silvicultural strategies for *Fraxinus excelsior* in response to dieback caused by *Hymenoscyphus fraxineus*. Forestry: An International Journal of Forest Research 90(4):455–472. doi: 10.1093/forestry/cpx012

Smigaj M, Gaulton R, Barr SL, Suárez JC (2015) UAV-borne Thermal Imaging for Forest Health Monitoring: Detection of Disease-Induced Canopy Temperature Increase. Int. Arch. Photogramm. Remote Sens. Spatial Inf. Sci. XL-3/W3:349–354. doi: 10.5194/isprsarchives-XL-3-W3-349-2015

Stener L-G (2013) Clonal differences in susceptibility to the dieback of *Fraxinus excelsior* in southern Sweden. Scandinavian Journal of Forest Research 28(3):205–216. doi: 10.1080/02827581.2012.735699

Tahar KN, Asmadin MA, Sulaiman SAH, Khalid N, Idris AN, Razali HM (2021) Individual Tree Crown Detection Using UAV Orthomosaic. Engineering, Technology & Applied Science Research(11(2)):7047–7053. doi: 10.48084/etasr.4093

Timmermann V, Børja I, Hietala AM, Kirisits T, Solheim H (2011) Ash dieback: pathogen spread and diurnal patterns of ascospore dispersal, with special emphasis on Norway. Bulletin OEPP/EPPO(41):14–20. doi: 10.1111/j.1365-2338.2010.02429.x

Timmermann V, Nagy NE, Hietala AM, Borja I, Solheim H (2017) Progression of Ash Dieback in Norway Related to Tree Age, Disease History and Regional Aspects. Baltic Forestry(23(1)):150–158

Toome M, Heinsoo K, Luik A (2010) Relation between leaf rust (*Melampsora epitea*) severity and the specific leaf area in short rotation coppice willows. Eur J Plant Pathol 126(4):583–588. doi: 10.1007/s10658-009-9566-4

Torresan C, Berton A, Carotenuto F, Di Gennaro SF, Gioli B, Matese A, Miglietta F, Vagnoli C, Zaldei A, Wallace L (2017) Forestry applications of UAVs in Europe: a review. International Journal of Remote Sensing 38(8-10):2427–2447. doi: 10.1080/01431161.2016.1252477

Uddling J, Gelang-Alfredsson J, Piikki K, Pleijel H (2007) Evaluating the relationship between leaf chlorophyll concentration and SPAD-502 chlorophyll meter readings. Photosynthesis research 91(1):37–46. doi: 10.1007/s11120-006-9077-5

Waser L, Küchler M, Jütte K, Stampfer T (2014) Evaluating the Potential of WorldView-2 Data to Classify Tree Species and Different Levels of Ash Mortality. Remote Sensing 6(5):4515–4545. doi: 10.3390/rs6054515

White JW, Montes-R C (2005) Variation in parameters related to leaf thickness in common bean (*Phaseolus vulgaris* L.). Field Crops Research 91(1):7–21. doi: 10.1016/j.fcr.2004.05.001

Wohlmuth A, Essl F, Heinze B (2018) Genetic analysis of inherited reduced susceptibility of *Fraxinus excelsior* L. seedlings in Austria to ash dieback. Forestry: An International Journal of Forest Research 91(4):514–525. doi: 10.1093/forestry/cpy012

Yadav S, Shukla S (2016) Analysis of k-Fold Cross-Validation over Hold-Out Validation on Colossal Datasets for Quality Classification. 2016 IEEE 6th International Conference on Advanced Computing (IACC):78–83. doi: 10.1109/IACC.2016.25

Yahya M, Saeed NA, Nadeem S, Hamed M, Saleem K (2020) Effect of leaf rust disease on photosynthetic rate, chlorophyll contents and grain yield of wheat. Archives of Phytopathology and Plant Protection 53(9-10):425–439. doi: 10.1080/03235408.2020.1748369

Ye H, Huang W, Huang S, Cui B, Dong Y, Guo A, Ren Y, Jin Y (2020) Recognition of Banana Fusarium Wilt Based on UAV Remote Sensing. Remote Sensing 12(6):938. doi: 10.3390/rs12060938

Yu K, Leufen G, Hunsche M, Noga G, Chen X, Bareth G (2014) Investigation of Leaf Diseases and Estimation of Chlorophyll Concentration in Seven Barley Varieties Using Fluorescence and Hyperspectral Indices. Remote Sensing 6(1):64–86. doi: 10.3390/rs6010064

Zhao D, Glynn NC, Glaz B, Comstock JC, Sood S (2011) Orange Rust Effects on Leaf Photosynthesis and Related Characters of Sugarcane. Plant disease(95):640–647. doi: 10.1094/PDIS-10-10-0762

Zheng J, Yuan S, Li W, Fu H, Le Yu, Huang J (2025) A Review of Individual Tree Crown Detection and Delineation From Optical Remote Sensing Images: Current progress and future. IEEE Geosci. Remote Sens. Mag. 13(1):209–236. doi: 10.1109/MGRS.2024.3479871